DTIC FILE COPY

AD-A199 756

DTIC ACCESSION NUMBER

PHOTOGRAPH THIS SHEET

LEVEL

INVENTORY 1

Research On The STATISTICS OF GRAIN LATTICS Echo

DOCUMENT IDENTIFICATION

Dec 1985

This document has been approved for public release and sale; its distribution is unlimited.

DISTRIBUTION STATEMENT

ACCESSION FOR	
NTIS GRA&I	X
DTIC TAB	
UNANNOUNCED	
JUSTIFICATION per ltr	
BY	
DISTRIBUTION /	
AVAILABILITY CODES	
DIST	AVAIL AND/OR SPECIAL
A-1	

DISTRIBUTION STAMP

DTIC ELECTE S D OCT 25 1988 E

DATE ACCESSIONED

DATE RETURNED

DATE RECEIVED IN DTIC

REGISTERED OR CERTIFIED NO.

PHOTOGRAPH THIS SHEET AND RETURN TO DTIC-FDAC

DTIC FORM 70A MAR 86

DOCUMENT PROCESSING SHEET

PREVIOUS EDITION MAY BE USED UNTIL STOCK IS EXHAUSTED.

Contract AFOSR-84-0125

Annual Report to AFOSR

Research on the Statistics of Grain Lattice Echoes and their use in Grain Size Estimation and Grain Echo Suppression

by

Israel Amir, Ph.D.
Department of Electrical and Computer Engineering
Drexel University

and

V.L. Newhouse, Ph.D.
Robert C. Disque Professor of
Electrical and Computer Engineering
Drexel University

December 1985

SECURITY CLASSIFICATION OF THIS PAGE

REPORT DOCUMENTATION PAGE

1a REPORT SECURITY CLASSIFICATION	1b RESTRICTIVE MARKINGS
2a SECURITY CLASSIFICATION AUTHORITY	3 DISTRIBUTION/AVAILABILITY OF REPORT
2b DECLASSIFICATION/DOWNGRADING SCHEDULE	
4 PERFORMING ORGANIZATION REPORT NUMBER(S)	5. MONITORING ORGANIZATION REPORT NUMBER(S)
6a NAME OF PERFORMING ORGANIZATION: DREXEL UNIVERSITY ECE DEPARTMENT; 6b. OFFICE SYMBOL (If applicable)	7a. NAME OF MONITORING ORGANIZATION
6c. ADDRESS (City, State and ZIP Code): PHILADELPHIA, PA 19104	7b. ADDRESS (City, State and ZIP Code)
8a. NAME OF FUNDING/SPONSORING ORGANIZATION: AFOSR; 8b. OFFICE SYMBOL (If applicable)	9. PROCUREMENT INSTRUMENT IDENTIFICATION NUMBER
8c ADDRESS (City, State and ZIP Code): Bolling Air Force Base, D.C. 20332	10. SOURCE OF FUNDING NOS.

PROGRAM ELEMENT NO.	PROJECT NO.	TASK NO.	WORK UNIT NO.
	AFOSR 84-0125		

11 TITLE (Include Security Classification): RESEARCH ON THE STATISTICS OF GRAIN LATTICE ECHOES

12. PERSONAL AUTHOR(S): I. AMIR — Project Director: V.L.Newhouse

13a. TYPE OF REPORT	13b. TIME COVERED	14. DATE OF REPORT (Yr., Mo., Day)	15. PAGE COUNT
Yearly	FROM 6.1.84 TO 9.29.85	85/12/15	150

16. SUPPLEMENTARY NOTATION

17 COSATI CODES			18. SUBJECT TERMS (Continue on reverse if necessary and identify by block number)
FIELD	GROUP	SUB. GR.	

19 ABSTRACT (Continue on reverse if necessary and identify by block number)

Two topics dealing with the reflection of ultrasound bursts from random media are discussed in this work.

In chapter 2 we develop a general formulation of the echo received from a random scatterer ensemble illuminated by a short electromagnetic or sonic signal. We show theoretically that a gradient in either scatterer concentration or in the field function of the transmitter/receiver will return an echo which is partially spatially coherent i.e. specular). Furthermore we show that from the degree of coherency, i.e. from the ratio of the random part to the non-random part of the reflected signal, the scatterer concentration and scattering cross-section can be calculated. We also show experimentally that scattering concentration gradient creates a coherent reflection from whose degree of coherency the scattering concentration can be estimated.

20 DISTRIBUTION/AVAILABILITY OF ABSTRACT	21. ABSTRACT SECURITY CLASSIFICATION	
UNCLASSIFIED/UNLIMITED ☐ SAME AS RPT ☐ DTIC USERS ☐		
22a NAME OF RESPONSIBLE INDIVIDUAL	22b TELEPHONE NUMBER (Include Area Code)	22c. OFFICE SYMBOL

DD FORM 1473, 83 APR — EDITION OF 1 JAN 73 IS OBSOLETE.

SECURITY CLASSIFICATION OF THIS PAGE

19. Abstract

In chapter 3 and 4 we deal with signal processing techniques for the reduction of clutter noise created by random media composed of a high concentration of point scatterers. The problem is to enhance a target embedded in a random medium when the clutter noise variance and the target echo location and amplitude are unknown. In chapter 3 we analyze theoretically a technique that was first proposed by Newhouse et al (3) the so called Minimization algorithm. In this technique we split the received signal spectrum into n frequency windows. The minimum of the squared signals at each range delay is then chosen. The calculated SNRE (signal-to-noise-ratio enhancement) of this technique agrees well with experiments performed by N.M.Bilgutay (4). We calculate also the Receiver Operating Characteristics (ROC) and find out that the improved SNRE of Minimization is negated by loss in detection properties.

In chapter 4 we describe a method for clutter reduction that also uses the split spectrum principle. In this technique we construct the optimum receiver for each range delay from the n outputs of the frequency windows. We calculate the ROC for this technique and find it to be superior to minimization for most cases. We show experimentally the effectiveness of this algorithm in clutter reduction.

In chapter 5 we summarize the results of this research work and show the flexibility and versatility of the techniques by introducing improvements and applications to the described methods.

TABLE OF CONTENTS

LIST OF FIGURES

Page

Page

Page

Page

ABSTRACT

Two topics dealing with the reflection of ultrasound bursts from random media are discussed in this work.

In chapter 2 we develop a general formulation of the echo received from a random scatterer ensemble illuminated by a short electromagnetic or sonic signal. We show theoretically that a gradient in either scatterer concentration or in the field function of the transmitter/receiver will return an echo which is partially spatially coherent (i.e. specular). Furthermore we show that from the degree of coherency, i.e. from the ratio of the random part to the nonrandom part of the reflected signal, the scatterer concentration and scattering cross-section can be calculated. We also show experimentally that scattering concentration gradient creates a coherent reflection from whose degree of coherency the scattering concentration can be estimated.

In chapter 3 and 4 we deal with signal processing techniques for the reduction of clutter noise created by random media composed of a high concentration of point scatterers. The problem is to enhance a target embedded in a random medium when the clutter noise variance and the target echo location and amplitude are unknown. In chapter 3 we analyze theoretically a technique that was first proposed by Newhouse et al [3] the so called Minimization algorithm. In this technique we split the received signal spectrum into n frequency windows. The minimum of the squared signals at each range delay is then chosen. The calculated SNRE (signal-to-noise-ratio enhancement) of this technique agrees well with

experiments performed by N.M. Bilgulay [4]. We calculate also the Receiver Operating Characteristics (ROC) and find out that the improved SNRE of Minimization is negated by loss in detection properties.

In chapter 4 we describe a method for clutter reduction that also uses the split spectrum principle. In this technique we construct the optimum receiver for each range delay from the n outputs of the frequency windows. We calculate the ROC for this technique and find it to be superior to minimization for most cases. We show experimentally the effectiveness of this algorithm in clutter reduction.

In chapter 5 we summarize the results of this research work and show the flexibility and versatility of the techniques by introducing improvements and applications to the described methods.

CHAPTER 1

INTRODUCTION

CLUTTER PROBLEMS IN IMAGING SYSTEMS

One of the most important limitations of Ultrasonic Imaging Systems using pulse echo techniques is imposed by clutter noise at the system output. This clutter noise is usually caused by relatively small, highly dense, randomly positioned scatterers. In one type of clutter problem the target to be detected can be modelled as a strong reflector. Even though the target echo is significantly larger than each of the individual small random scatterers around it, the target is sometimes difficult to detect due to the high density of the interfering scatterers. Such problems exist in almost every field associated with imaging. In Ultrasound Nondestructive Testing the large grain boundary echoes makes it difficult to detect relatively large flaws [1,2,3,4]. In medical imaging the fine tissue microstructure echoes sometimes makes it hard to outline the organ boundary [5,6], and in Radar Systems, rain drops, chaff or sea clutter [7,8,9,10,11,12,13,14] are often strong enough to mask the target. Time averaging or correlation techniques, which reduce random thermal noise significantly, are not suitable for reducing coherent noise resulting from echoes due to the stationary interfering scatterers.

In another type of clutter problem the targets are composed of a high density of point scatterers. The reflected signal is accompanied by a speckle pattern (spatial brightness fluctuations) which is due to

the random interference pattern of the reflectors composing the target. This type of problem appear often in coherent optical imaging [15] when the object (that can be modelled by a high density of small random reflectors) is imaged by a highly coherent illumination. In Ultrasound Medical Imaging the echo from the tissue microstructure which can be modelled in a similar way, is an important part of the image and helps to diferentiate and characterize the different organs [16,17,18,5,6,19-21, 22-25].

In the text we refer to the first problem in which we wish to suppress the clutter echo and enhance a large target echo as a problem in "clutter reduction", and we refer to the second problem in which we wish to reduce the speckle pattern of targets composed of a large sum of point reflectors as a problem in "speckle reduction".

Some conventional techniques to reduce clutter and speckle are described below.

GENERAL LITERATURE REVIEW

Scattering from Random Media

Ultrasonic signal processing techniques have developed dramatically in the last decade mainly due to the introduction of low cost powerful computers. But before reviewing the recent literature on modern signal processing techniques in Ultrasound we should pay some attention to the basic understanding of the scattering from random media as the modelling of random media is the basis on which most of the signal processing techniques base their approach.

The theory covering the propagation of waves in random media is vast. In [26,27,28] one can find the description of the basic acoustical models for wave propagation and in [29,30] a discussion on some of the

theories when applied to biological tissues is given.

The scattering from bodies with simple geometry can be calculated by methods introduced in [26,27,31]. In the limit, for reflectors which are much smaller than the wave length the solutions are explicit. These solutions can be extended to complex elements by assuming a combination of several individual centers.

The scattering is described through the definition of scattering cross section. The total cross section is defined as [26,32]

$$\sigma = \frac{P}{I} \qquad 1.1$$

where I is the incident wave and P is the scattered signal. Of more practical importance is the definition of differential scattering cross section which is related to σ by

$$\sigma = \int_{4\pi} \sigma' d\Lambda \qquad 1.2$$

where Λ is the solid angle. In general $\sigma'=\sigma'(\Lambda)$. For the important case of a small sphere (smaller than the wave length [26])

$$\sigma' = \frac{1}{9} \left[\frac{2\pi}{\lambda}\right]^4 a^6 \left[\frac{K_s - K}{K} + \frac{3\rho - 3\rho}{2\rho_s + \rho} \cos\theta\right]^2 \qquad \text{if} \quad \lambda >> a$$

where

λ = wavelength

a = radius of the scatterer

θ = angle between the incident wave and the direction of scattering.

ρ_s = density of the sphere.

ρ = density of the medium.

K_s = compressability of the sphere.

K = compressability of the medium.

For practical cases isotropic scattering can be assumed only if either $\rho_s=\rho$ or if the range of angles in eq. 3 is small enough and σ is such that $\sigma=\sigma'\Lambda_o$.

The structure of biological tissue is very complex and it exhibits nonhomogeneities in almost any scale. So the assumption of discrete, weak scattering which is often used is clearly a simplified assumption as the scattering bodies range from much smaller than the wave length up to much larger than the range cell [32]. Theoretical results based on these assumptions should be constantly challenged and verified to be considered reliable.

The statistical properties of the backscattered clutter echo play a major role in the optimal signal processing to be chosen for clutter or speckle reduction. It can be shown that if the scatterers are uniformly distributed and the number of scatterers in the range cell is high enough, the backscattered echo amplitude assuming the plane or spherical wave approximation, can be considered Gaussian with zero mean [33]. In [34] the average power backscattered from random media with a density profile is given for continuous wave propagation. In this publication Siegert and Goldstein show that a medium which exhibits a density profile gives rise to a coherent term which translates to an echo with non-zero mean. In [35,36] Glotov calculates the average backscattered power from a slab filled with nonuniform size scatterers illuminated by a burst. The echo again contains a coherent term which resembles specular reflection. If the slab is much smaller than the wave length the reflection is mostly coherent and the random component becomes insignificant. In chapter 2 we will develop a general formulation for the backscattered echo from random media on which our signal processing approaches will be based.

Signal Processing Techniques for Clutter Reduction

One of the most popular techniques used in radar systems to overcome clutter noise is the use of frequency diversity (agility). In this technique the Radar system possesses a center frequency which is varied between pulses. This is similar to increasing the effective bandwidth of the transmitted signal and thus, the clutter noise power which is inversely proportional to the system bandwidth [7,8,14], is reduced. The other improvements obtained with the use of frequency agile Radars namely, antijamming capabilities, range improvement and tracking are not of any importance in biomedical Ultrasound and non-destructive testing. However, techniques used for processing the frequency diverse signals will be the measure against which the new techniques (to be introduced in chapters 3 and 4) will be compared.

A very good review of the literature on frequency agility is given in [4]. To summarize, we only mention that the two most popular processing schemes are composed of either direct summation of the successive echoes before demodulation (which is equivalent to operation with a wide bandwidth or transmitting and receiving with all the frequency windows simultaneously) or summing the different frequency windows after demodulation (envelope detection). This is done when the target echo phase is lost between pulses (due to fast fluctuation of the target position between pulses).

After processing the frequency diverse signals a threshold is set to enable a decision whether a target exists in a prespecified range cell. In the technique which is most often used and called "CELL AVERAGING" we evaluate the clutter noise power [9,37,38,10,11,12,13] from some "test cells". Then assuming that the same clutter noise power exists in the

range cell of interest a CFAR (constant false alarm rate) detector can be designed. This technique provides a noise riding threshold and only cells assumed to contain targets are presented. The detector design depends on the statistics of the clutter echo. Usually the assumption of Gaussian distribution for the clutter noise amplitude is used which is true only if the number of scattering centers in the range cell is high enough. A good review of clutter properties (in Radar applications) is given in [39].

In 1981 "Split Spectrum Processing" was introduced by Newhouse et al [3,4] for the improvement of flaw visibility in the presence of grain noise. In this technique the received echo is split into several frequency windows (possibly overlapping) and the minimum of the squared windowed signals at each range delay is then chosen. In [3,4] the technique is compared experimentally with other conventional techniques and proved to have an improved flaw to grain noise enhancement. As the 'Optimal Processing' technique introduced in Chapter 4 in this report is partially based on elements in this algorithm and will be compared with it, we analyze the minimization algorithm theoretically in chapter 3.

Signal Processing Techniques for Speckle Reduction in Ultrasonic Imaging

Because the Laser speckle phenomenon is so similar to Ultrasound speckle the Laser literature was the main source for techniques for speckle reduction in Ultrasound. An excellent review of the optical speckle phenomenon is given in [15]. It was only towards the middle of the last decade that techniques for Ultrasound speckle reduction were introduced and a substantial number of signal processing techniques appeared in the open literature especially in the last few years [17,18,5,

20,22-24]. One of the earliest papers [40] uses spatial compound scanning to reduce Ultrasound speckle. In this technique the region of interest is illuminated from different directions and the different gray levels are then compounded to create an image. This technique can be successful only when the interrogated medium can be considered isotropic and non refractive and the region of interest is accessible from different directions. Organs such as the breast are ideal for such compound imaging. In 1978 Burckhardt argued for the first time that Ultrasound speckle should be treated in a similar way to optical speckle. He modelled the tissue as a collection of a high density of point scatterers and he evaluated the signal to noise ratio as the mean of the signal envelope to the envelope standard deviation. From this definition the signal to noise ratio is 1.91. He later introduces a new algorithm "Compound scan with maximum amplitude writing". In this technique the maximum of the different echoes associated with a certain point in space is selected instead of the average. He claims that the difference between averaging which is the optimum processing for this model and "Maximization" is negligible.

In 1979 Abott and Thurstone [19] analyzed the Ultrasound speckle phenomenon based again on the concept of Laser speckle. The paper outlines the ways in which speckle can be reduced i.e variations in time, space or frequency parameters. The first of these, time, involves a phase diffuser which is equivalent to generating a random pattern in phase from burst to burst or image to image. This technique was found to be useless in Ultrasound as it resulted in image degradation due to deterioration in focusing and distortion of the transmitted wave front. The second of these, spatial variation, involves either illuminating the

object from different directions or simply moving the transducer in relation to the object sufficiently to change the phase distribution across the transducer aperture. The third of these is equivalent to frequency agility a concept that was discussed earlier in connection with target detection and will be discussed later in this section in connection with speckle reduction.

In 1983 Wagner et al published a pair of papers on speckle. In the first [16] they calculate the second order statistics of Ultrasound speckle in B images as a function of transducer dimensions and range. Their results seem to fit reasonably with experiment. In the second paper [17] they use the results obtained in the first paper and some known results from statistical decision theory to obtain decision rules for lesion detection. The results turn out to be spatial averaging. Several adjacent cells are summed to create a new cell (or a decision rule). Obviously resolution is sacrificed in this procedure. In 1983 [5] Robinson and Knight checked experimentally the performance of some spatial pulse echo compound scan techniques. The performance of peak detected, minimum detected and averaged reconstruction of point targets is compared. They conclude that averaging is capable of increased range resolution compared to peak detection and that the speckle pattern is smoother. The minimum detected signal has an improved resolution of point targets and "shows promise in location of shadowing structures".

Frequency Compounding

A discussion on frequency compounding in connection with Ultrasonic medical imaging is given in [22]. It is found that the degree of speckle contrast reduction is inversely proportional to the bandwidth of the transmitted acoustic burst. Also, a considerable increase in signal to

noise ratio of the speckle pattern can be achieved. In another paper [23] the received spectrum of the backscattered signal is split into two overlapping frequency windows and the respective channels are then summed after envelope detection. This technique is reported to increase the signal to noise ratio of the speckle pattern with improved resolution. We will show later in the this report that the optimum receiver is somewhat different from the one implemented in [23] and should provide better results.

MOTIVATION FOR RESEARCH

The fact that current techniques are not effective enough in the reduction of clutter and speckle noise in Ultrasonic imaging systems is the driving force for this project. Techniques such as spatial averaging (or spatial compounding) are difficult to implement due to the relatively high refraction of the biological tissue and man-made materials, the high accuracy required from the scanning system, and the fact that many of the regions of interest are not accessible from different directions. Frequency diversity (or frequency averaging) is successful when it is easier to transmit narrow frequency windows one at a time instead of the entire available spectrum. In Ultrasound however it is possible to transmit extremely wide bandwidths.

Extending the frequency range by using several elements with different center frequency raises more problems than it solves. First the propagating medium is highly frequency dependent (i.e frequency attenuation dependence) and secondly the scattering from the microstructure rapidly increases with frequency. The beam pattern of the transducer is also sensitive to frequency. Thus simple frequency compounding is not useful.

In this work we concentrate our effort on a different type of signal processing. We concentrate on clutter and speckle reduction through post reception A scan processing only. By working on individual A scans we eliminate the many practical problems associated with compound scanning and make the problem solely a signal processing one. The techniques to be introduced here require that the signals should be processed at the RF level. Techniques usually described in the literature do not deal with processing at the RF level, but as we see later the hardship of working at the RF level has its rewards.

SYNOPSIS OF THE REMAINING CHAPTERS

In this section we summarize the remaining chapters in this report. In chapter 2 we develop a general formulation for the backscattered echo from a random medium that can be modelled as an ensemble of randomly distributed point scatterers. To simplify the mathematics we assume isotropic scattering. The average backscattered power from the random ensemble is calculated as a function of transducer parameters and the spatial density profile of the scatterers. It is shown that the echo from a random ensemble exhibiting a sharp volume density gradient may resemble specular reflection. This explains for example the "specular" reflection from organ boundaries in medical Ultrasound B scans. It is also shown that the ratio between the power of the "specular" echo, i.e. the spatially coherent portion of the echo amplitude to the echo variance should enable us evaluate the scattering density if there is either a density gradient or a field gradient. The results for the former case are verified qualitatively by experiment.

After studying in chapter 2 the general behavior of the backscattered echo from an ensemble of point scatterers we investigate in chapter 3

theoretically an algorithm for clutter reduction that was first suggested in [3,4]. The technique is called the "Minimization Algorithm" and in fact provided the impetus for this research project. We calculate the improvement in signal to noise ratio of this algorithm and compare it with experimental results obtained in [3,4]. The theoretical results seem to fit well with experiment. Finally we calculate the Receiver Operating Characteristic of this algorithm.

In chapter 4 we pose the problem of clutter reduction under the assumption that the local properties of the clutter echo are unknown, namely the local variance. We describe a technique to estimate the local properties of the signal without a priori knowledge of whether a target exists in the region of interest. We use the results to develop so-called optimum detection algorithms for both additive and multiplicative noise based on some known results in statistical decision theory. For the Optimum Detector algorithm for additive noise, we calculate the probability of detection as a function of signal to noise ratio (for the clutter reduction problem). Some experimental results for this type of processing for the enhancement of flaw to grain echoes in metal are also given. Resolution performance and range bias of the suggested technique are evaluated experimentally. We also compare the performance of the "Minimization Algorithm" with the new technique on the basis of ROC (Receiver Operating Characteristics), resolution, bias, and amplitude dynamic range of the processed data.

Finally In chapter 5 we present conclusions, remarks and some suggestions for future work.

CHAPTER 2

SCATTERING FROM RANDOM MEDIA

INTRODUCTION

In this chapter we investigate the properties of the backscattered echo from random media. The results obtained here suggest new techniques for scatterer density estimation and also form the basis for the clutter reduction algorithms to be discussed in chapter 3 and 4.

The random media throughout this work are assumed to be composed of a high density (concentration) of point scatterers that can have random size (strength) and/or random position. For simplicity we assume that the average distance between the scatterers is much larger than their radius thus allowing the assumption that their volume density is Poisson distributed (if their position is random).

It is well known that under the assumption of plane wave approximation and constant scattering density the backscattered echo from random media can be considered Gaussian with zero mean provided the scatterers concentration is high enough (central limit theorem). However, if the average scattering concentration (or size) is not uniform as a function of range delay, or the sonic field exhibits a gradient the problem becomes more complex. Siegert and Goldstein (34) calculated the backscattered echo from a continuously illuminated time varying random medium, composed of identical size scatterers under the assumption of plane wave illumination. They found out that the backscattered echo should have a non zero

mean (coherent echo) which is proportional to the gradient of the scattering density. Some years later Glotov (36) analyzed the case of a short transmitted signal illuminating a slab filled with discrete inhomogeneities for both the plane wave and spherical wave approximation and again showed that the returned echo should have a non zero mean.

In this chapter we investigate the properties of the backscattered echo from random media for pulsed transmission by extending the existing theories to take into account field fluctuations and the scattering density profile. We start by analyzing the backscattered echo from a regular lattice with equal spacing and random scattering cross-section, later we proceed to evaluate the returned echo from random media with uniform scattering density and finally we analyze the backscattered echo from random medium with non uniform scattering density and arbitrary field structure.

THE REGULAR LATTICE

Let the echo detected by a sonic receiver at time t after transmission of a pulse, due to a single point scatterer at $\vec{r}$ be written as

$$E_s(t) = \rho_i G(\vec{r}_i, t) \tag{2.1}$$

where $G(\vec{r},t)$ is defined as the impulse response of a system composed of a transmitter/receiver illuminating a scatterer located at $\vec{r}_i$ and ρ is a proportionality constant that depends on the scatterer scattering cross section. Suppose that we illuminate a regular lattice for which the scattering cross-section of the particles is a random variable (see Figure 1). The backscattered echo from the lattice can be written (assuming the Born approximation)

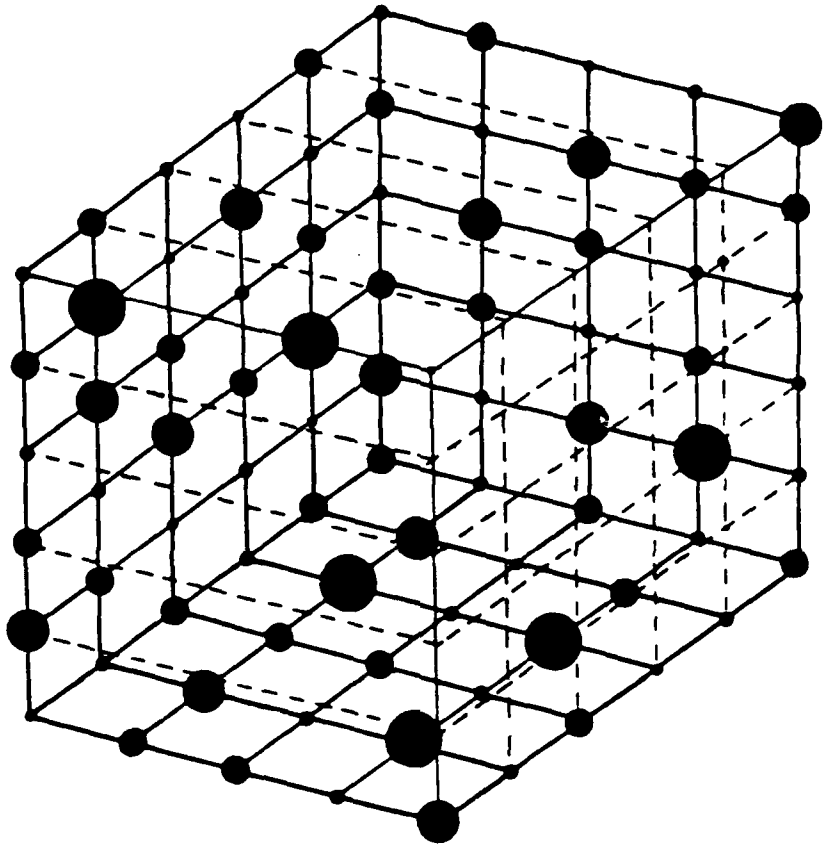

Figure 2.1 The regular lattice. (The scatterers within the lattice were not drawn to retain clarity).

$$E(t) = \sum_{i=1}^{n} \rho_i G(\vec{r}_i, t) \tag{2.2}$$

where n is the number of the scatterers in the range cell, defined as that region in space from which echoes are received at time t after transmission.

The average power of the backscattered echo becomes

$$\overline{P(t)} = \overline{\sum_{i=1}^{n} \sum_{j=1}^{n} \rho_i \rho_j G(\vec{r}_i, t) G(\vec{r}_j, t)} \tag{2.3}$$

Where $\bar{}$ means ensemble average (and not time average). In order to measure this average one would move the transducer with respect to the lattice and average the received power for a given range delay t. Assuming ρ_i to be statistically independent of ρ_j eq. (3) becomes

$$\overline{P(t)} = \overline{\rho^2} \sum_{i=1}^{n} |G(\vec{r}_i, t)|^2 + \bar{\rho}^2 \sum_{\substack{i=1 \\ i \neq j}}^{n} \sum_{j=1}^{n} G(\vec{r}_i, t) G(\vec{r}_j, t) \tag{2.4}$$

Rewriting eq. (4) we obtain

$$\begin{aligned} \overline{P(t)} = \overline{\rho^2} \sum_{i=1}^{n} |G(\vec{r}_i, t)|^2 + \bar{\rho}^2 \{ & G(\vec{r}_1, t)[G(\vec{r}_1, t) + \\ & + G(\vec{r}_2, t) + \ldots + G(\vec{r}_n, t) - G(\vec{r}_1, t)] + + \} \end{aligned} \tag{2.5}$$

Replacing the summations by integrals we obtain

$$\begin{aligned} \overline{P(t)} = & \frac{\overline{\rho^2}}{\Delta v} \int_v |G(\vec{r}, t)|^2 dv + \frac{\bar{\rho}^2}{\Delta v^2} \left| \int_v G(\vec{r}, t) dv \right|^2 \\ & - \frac{\bar{\rho}^2}{\Delta v} \int_v |G(\vec{r}, t)|^2 dv \end{aligned} \tag{2.6}$$

where Δv is the volume of a unit cell of the lattice. but

$$\frac{1}{\Delta v} = \frac{v}{\Delta v v} = \frac{n}{v} = N \tag{2.7}$$

and* eq. (6) becomes

$$\overline{P(t)} = N\overline{\rho^2} \int_V |G(\vec{r},t)|^2 dv + N^2\bar{\rho}^2 \left| \int_V G(\vec{r},t)\right|^2$$

$$- N\bar{\rho}^2 \int_V |G(\vec{r},t)|^2 dv \qquad (2.8)$$

as we see in the next section the second term in eq. (8) very often vanishes. In this case $\overline{P(t)}$ becomes

$$\overline{P(t)} = N\sigma_\rho{}^2 \int |G(\vec{r},t)|^2 dv \qquad (2.9)$$

and the backscattered power is directly proportional to the variance of the scattering cross-section of the lattice particles, σ_ρ^2. It is obvious that if the scatterers are uniform in size no backscattered power is expected.

RANDOM MEDIUM WITH UNIFORM SCATTERING CONCENTRATION

When a random ensemble is illuminated by a transducer the received echo at time t after transmission can be written**

$$E(t|n) = \sum_{i=1}^{n} \rho_i G(\vec{r}_i,t) \qquad (2.10)$$

where n is the number of the scatterers in the range cell. We assume that the range cell has a volume V, and that it contains n randomly positioned scatterers at locations $\vec{r}_1,\vec{r}_2,\vec{r}_3,\ldots,\vec{r}_n$ of strengths $\rho_1,\rho_2,\ldots,\rho_n$. The instantaneous power at time t is

---

*For non cubic unit cell $\frac{V}{\Delta v}$ will be directly proportional to n and not equal to n as is assumed here for a cubic unit cell.

**E(t|n) should be read: E at range delay t given that there are exactly n scatterers in the range cell.

$$P(t|n) = \sum_{i=1}^{n} \sum_{j=1}^{n} \rho_i \rho_j G(\vec{r}_i,t) G(\vec{r}_j,t) \tag{2.11}$$

This can be separated into two parts

$$P(t|n) = \sum_{i=1}^{n} |G(\vec{r}_i,t)|^2 \rho_i^2 + \sum_{\substack{i=1 \\ i\neq j}}^{n} \sum_{j=1}^{n} G(\vec{r}_i,t)G(\vec{r}_j,t)\rho_i\rho_j \tag{2.12}$$

The average power at time t after transmission, for differing locations of the n scatterers in the range cell of volume V can be written

$$\overline{P(t|n)} = n\,\overline{\rho_i^2|G(\vec{r}_i,t)|^2} + n(n-1)\,\overline{\rho_i\,\rho_j\,G(\vec{r}_i,t)\,G(\vec{r}_j,t)} \tag{2.13}$$

Note that $P(t|n)$ is the average over all possible configurations of the scatterer location $\vec{r}_i$ in the range cell. Assuming that $\vec{r}_i$ is uncorrelated with $\vec{r}_j$ for $i\neq j$, we can rewrite eq. (2.13) as

$$\overline{P(t|n)} = n\,\overline{\rho^2} \int_V |G(\vec{r},t)|^2\, p(\vec{r})dv + n(n-1)\,\bar{\rho}^2 \left| \int_V G(\vec{r},t)p(\vec{r})dv \right|^2 \tag{2.14}$$

where $p(\vec{r})$ is the probability of finding one individual scatterer in the volume element at $\vec{r}$, and where the integrals are taken over the volume V of the range cell. We may write

$$p(\vec{r}) = \frac{1}{V} \tag{2.15}$$

Using these two relations we can write the ensemble averaged power $\overline{P(t|n)}$

$$\overline{P(t|n)} = \frac{n}{V}\,\overline{\rho^2} \int_V |G(\vec{r},t)|^2 dv + \frac{n(n-1)\bar{\rho}^2}{V^2} \left| \int_V G(\vec{r},t)dv \right|^2 \tag{2.16}$$

To find the average power $\overline{P(t)}$ we have to evaluate

$$\overline{P(t)} = \sum_{n=0}^{\infty} \overline{P(t|n)}\, p(n) \tag{2.17}$$

from eq. (16) and (17)

$$\overline{P(t)} = \frac{\overline{\rho^2}}{V} \int_V |G(\vec{r},t)|^2 dv \sum_{n=1}^{\infty} np(n) +$$

$$+ \frac{\bar{\rho}^2}{V^2} \left|\int_V G(\vec{r},t)dv\right|^2 \sum_{n=1}^{\infty} n(n-1)p(n) \tag{2.18}$$

where n is Poisson distributed with $\bar{n}$ as its average. Replacing

$$\sum_{n=0}^{\infty} np(n) = \bar{n} \tag{2.19}$$

and (as is known for the Poisson distribution),

$$\sum_{n=0}^{\infty} n(n-1)\, p(n) = \bar{n}^2 \tag{2.20}$$

we obtain

$$\overline{p(t)} = N\, \overline{\rho^2} \int_V |G(\vec{r},t)|^2 dv + N^2\, \bar{\rho}^2 \left|\int_V G(\vec{r},t)dv\right|^2 \tag{2.21}$$

where

$$N = \frac{\bar{n}}{V}$$

Note again that $\overline{P(t)}$ is ensemble average and not time average and that to obtain this average one would have to move the transducer with respect to the medium (if the medium is stationary) and average the received power for a given t. We see that the first term on the right hand side of eq. (21) is proportional to $N\overline{\rho^2}$ i.e. to the average of the sum of the individual backscattered powers. We will therefore refer to it as the incoherent power P_{inc}. The second term is proportional to $(N\bar{\rho})^2$, i.e. to the square of the sum of the backscattered amplitudes. We will therefore describe it as the coherent backscattered power, P_{coh}.

We now show that P_{coh} equals the magnitude squared of the averaged echo, and that P_{inc} equals the variance of this echo.

From eq. (10), (15) and (19)

$$\overline{E(t)} = \sum_{n=0}^{\infty} \overline{E(t|n)}\, p(n) = N\bar{\rho} \int_V G(\vec{r},t)dv \tag{2.22}$$

So that

$$P_{coh} = |\overline{E}|^2 = N^2\, \bar{\rho}^2\, \left|\int_V G(\vec{r},t)dv\right|^2 \tag{2.23}$$

The fact that P_{inc} is the variance of E(t) follows immediately, since

$$\sigma_E^2 = \overline{|E|^2} - |\overline{E}|^2 \tag{2.24}$$

Thus from eqs. (21) and (24),

$$\sigma_E^2 = P_{inc} = N\overline{\rho^2} \int_V |G(\vec{r},t)|^2 dv \tag{2.25}$$

From eq. (21) one can see that the coherent term will be appreciable if either N or $\int_V G(\vec{r},t)dv$ are sufficiently large. Let us examine the integral $\int_V G(\vec{r},t)dv$ for simple beam geometries. For example consider a plane wave travelling along the z axis for which the field function can be written

$$G(\vec{r},t) = I(t - \frac{2z}{c})dz \tag{2.26}$$

The coherent term of eq. (22) becomes

$$\overline{E(t)} = N\rho \int_{-\infty}^{\infty} I(t - \frac{2z}{c})dz \tag{2.27}$$

Changing variables $t' = t-2z/c$ eq. (22) becomes

$$\overline{E(t)} = \frac{cN\rho}{2} \int_{-\infty}^{\infty} I(t')dt' \tag{2.28}$$

The integral and with it the coherent term reduces to zero since the signal cannot contain a dc component. Likewise for a point transmitter/receiver

$$\overline{E(t)} = N\bar{p} \int_0^\infty (I(t-2r/c)/r^2)4\pi r^2 dr \qquad (2.29)$$

which again reduces to zero. Thus we see that both for the case of plane wave approximation as well as for the case of waves emitted from a point transmitter/receiver the coherent term vanishes.

However in a work which is currently performed by Goyao Yu from Drexel University it is shown that for almost any other geometry of transmitter/receiver the integral $\int_V G(\bar{r},t)dv$ does not vanish. For example, Mr. Yu calculated numerically this integral for a point transmitter and a ring shaped receiver and showed that the coherent integral is different from zero in the near field. However in the far field the coherent integral practically vanishes. It is clear that the integral $|\int_V G(\bar{r},t)dv|^2$ is usually much smaller than $\int_V |G(\bar{r},t)|^2 dv$. However the integral $|\int_V G(\bar{r},t)dv|^2$ is multiplied by N^2 while the integral $\int_V |G(\bar{r},t)|^2 dv$ is multiplied only by N (in eq. 2.21) which should make the ratio $|\overline{E}|^2/\sigma^2_E$ measurable.

These results obtained by Mr. Yu give rise to the hope that scatterer concentration and scattering cross section estimation would be possible using coherent reflection caused by field gradients.

RANDOM MEDIUM WITH NONUNIFORM SCATTERING DENSITY

If the scatterers exhibit a certain scattering concentration profile $N(\bar{r})$ the algebra introduced earlier becomes somewhat more involved. Redefining $p(\bar{r})$ to be $N(\bar{r})\frac{1}{\bar{n}}$ the average power at a certain range delay t can be shown to be,

$$\overline{P(t)} = \overline{\rho^2} \int_V N(\vec{r})|G(\vec{r},t)|^2 dv + \bar{\rho}^2 \left|\int_V N(\vec{r})\, G(\vec{r},t)dv\right|^2 \qquad (2.30)$$

with

$$\overline{E(t)} = \bar{\rho} \int_V N(\vec{r})G(\vec{r},t)dv \qquad (2.31)$$

It can be seen by inspection that the integral of eq. (31) will be non-zero provided $N(\vec{r})$ has a gradient in the same direction as that of the function $G(\vec{r},t)$, i.e. in the direction of the sound beam. For the integral to be large the gradient of $N(\vec{r})$ should be sharp compared to the sound wavelength. The value of the integral for a step function in density $N(\vec{r})$ is derived below. Eq. (31) shows that a gradient in scattering density in the direction of propagation of the sound beam will return a spatially coherent echo. The same holds true for the echo from the boundary between two regions with different scattering densities. For simplicity we assume the imaginary boundary to be planar. Replacing $\vec{r}$ by z we can write,

$$\begin{aligned} N(z) &= N_1 \qquad z < z_o = \frac{ct_o}{2} \\ &= N_2 \qquad z > z_o \end{aligned} \qquad (2.32)$$

For a plane wave $G(z,t) = b(t-2z/c)\cos[\omega(t-2z/c) + \theta]$; thus from eq. (31) the returned echo from the boundary becomes

$$\overline{E(t_o)} = \frac{c}{2}\, N_1\, \overline{\rho_1} \int_o^\infty b(t)\cos[\omega t+\theta]dt + \frac{c}{2}\, N_2\, \overline{\rho_2} \int_{-\infty}^o b(t)\cos[\omega t+\theta]dt \qquad (2.33)$$

$\bar{\rho}_1$ and $\bar{\rho}_2$ are the average reflection coefficients of the scatterers in region 1 and 2 respectively. Note that the volume integral in eq. (30) becomes a time integral by change of variables. If the range cell is situated such that the boundary is at its center the variance of $\overline{E(t_o)}$ can be shown to be,

$$\sigma^2 \equiv \frac{1}{2}[\sigma_1^2 + \sigma_2^2] \equiv \frac{c}{4}\,[N_1\overline{\rho_1^2} + N_2\overline{\rho_2^2}] \int_o^\infty |b(t)|^2 dt \tag{2.34}$$

where σ_1^2 and σ_2^2 are the variances of the returned echo from region 1 and region 2 respectively. For $N_2=0$ eqs. (33) and (34) become

$$\overline{E(t_o)} = N_1\,\overline{\rho}_1\,\frac{c}{2}\int_o^\infty b(t)\cos[\omega t+\theta]dt \tag{2.33a}$$

$$\sigma^2 = \frac{1}{2}\sigma_1^2 = N_1\overline{\rho_1^2}\,\frac{c}{4}\int_o^\infty |b(t)|^2 dt \tag{2.34a}$$

Hence the ratio

$$\frac{\overline{E(t_o)}^2}{\sigma^2} \equiv \frac{c}{4}\,N_1\,\frac{\overline{\rho}_1^2}{\overline{\rho_1^2}} \cdot \frac{\int_o^\infty b(t)\cos(\omega t+\theta)dt}{\int_o^\infty |b(t)|^2 dt} \tag{2.35}$$

Measurement of the quantities on the left hand side of this equation, should allow us to estimate the quantity $N\frac{\overline{\rho}^2}{\overline{\rho^2}}$ since the integrals on the right hand side can be computed. For uniform scatterers, $\overline{\rho}^2/\overline{\rho^2}$ is unity, allowing the density N and the scattering cross-section to be estimated independently.

SNELL'S LAW FOR DENSITY GRADIENTS

It is easy to show that the scattered sound from density gradients in a random scatterer ensemble obeys Snell's law. Consider two plane wave transducers used for transmission and reception respectively, oriented at + θ and - θ degrees with repect to the z axis. Then the $\hat{x}$ and $\hat{y}$ components of $\nabla G(\vec{r},t)$ are zero where the function $G(\vec{r},t)$ is as defined in eq. (1) but for separate transmitter and receiver.

Although eq. (31) above was derived for the case of a single transducer used for both transmission and reception, it is equally valid for

the transducer pair described in the previous paragraph. For plane wave transmission and reception it can be shown that the integral in eq. (31) is non zero provided that the gradients of $N(\vec{r})$ and $G(\vec{r},t)$ are parallel. Thus a density gradient in a random scatterer ensemble will scatter a coherent incident beam in the direction given by Snell's law, i.e. in the same direction in which the beam would be reflected by a mirror parallel to the planar constant density. This result is not unexpected and is encountered often (without much excitement) in almost every field of ultrasonic measurement.

EXPERIMENTAL RESULTS

According to eq. (33) we should be able to observe a coherent echo from the boundary between two different regions of differing scattering density.

One of the easiest ways to obtain a sharp boundary for scatterers immersed in water, is to use sponges. A sponge can be cut to produce a sharp boundary and when immersed in water the complex structure of the sponge fibers can be considered as randomly distributed scatterers. Furthermore, one can clamp together two sponges with different scattering properties and thus compose a sharp boundary between two different media, or one can use only one sponge, simulating two media with $N_1=0$ in region 1 and N_2 in region 2. Figures 2(A)-2(D) show pictures of sponges used in such experiments. One can see that sponge A has the finest honeycomb structure. Sponge B has a larger honeycomb structure, sponge C is even more dilute and sponge D is the most dilute in comparison to sponges A,B and C. In Figure 3 we see sponges B and C side by side. One can see that the boundary is sharp in comparison to a wavelength (frequency of

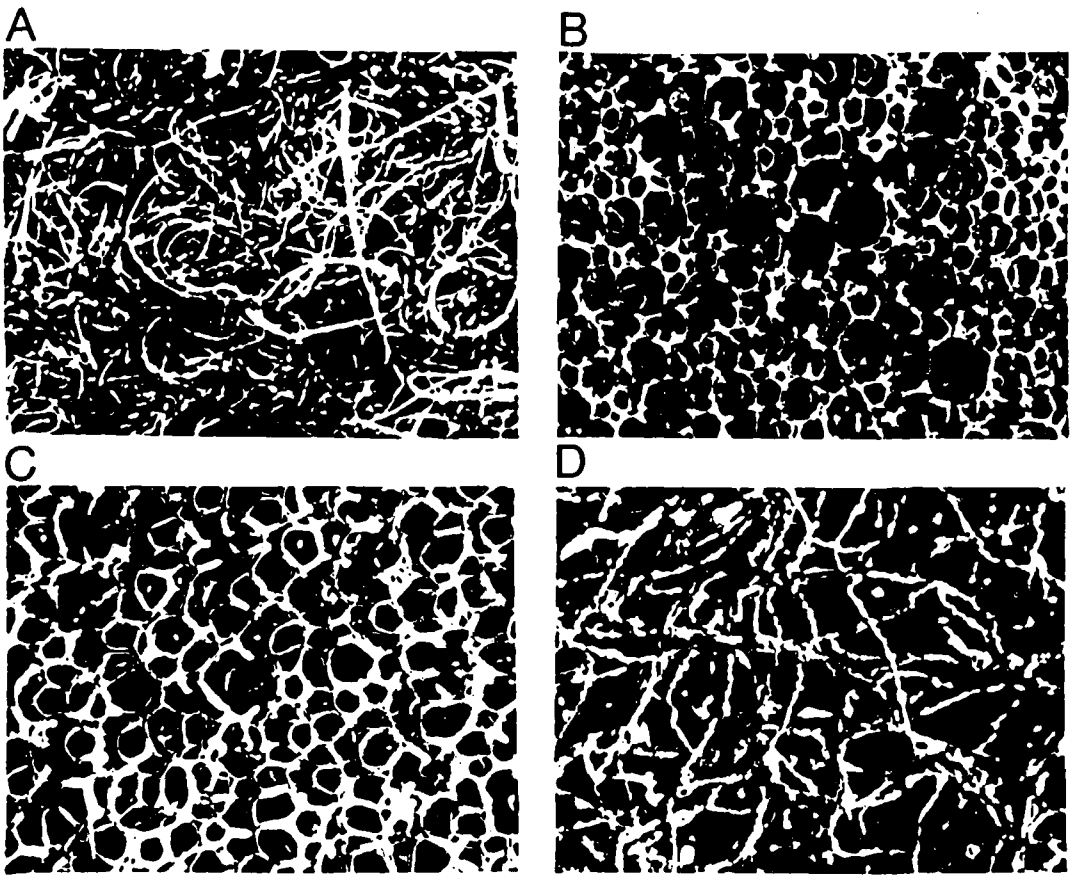

Figure 2.2. A photograph of the surfaces of sponges A,B,C and D. The fine honeycomb structure is visible. (The width of each picture corresponds to 6.5 mm.)

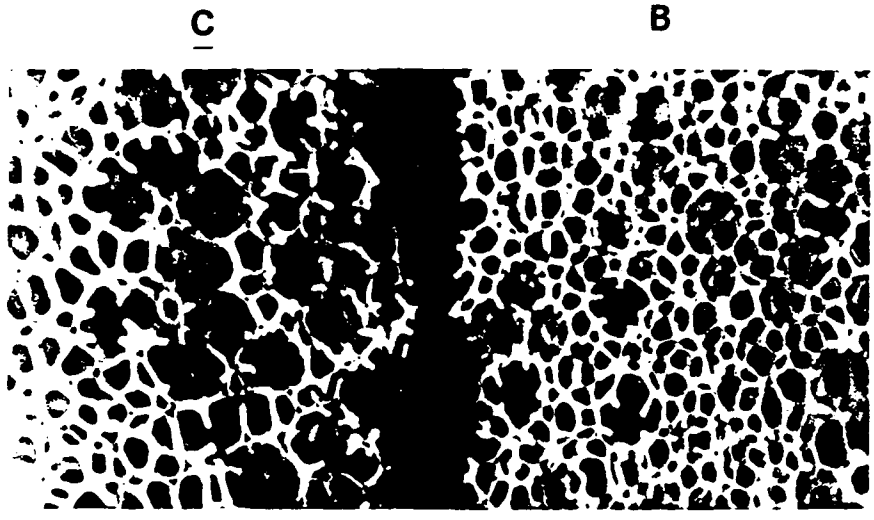

Figure 2.3. Sponges B and C side by side. It is seen that the honeycomb structure of sponge B is finer than that of sponge C.

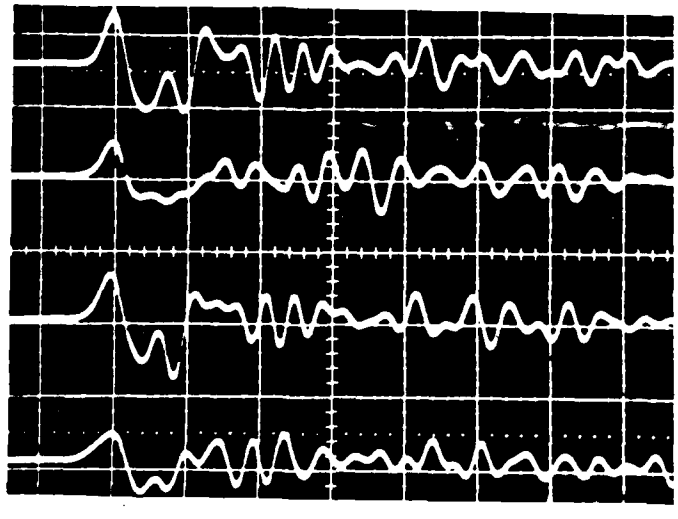

Figure 2.4. Four different echoes from sponge B. Note that the coherent echo component from the sponge boundary and the incoherent component from within the sponge.

2.25 MHz). One can also see again that the honeycomb structure of sponge B is finer than that of sponge C.

Figure 4 shows echoes returned from sponge B. One can see that the echoes from the boundary are highly coherent and exhibit negligible phase change in comparison to the more random echoes from inside the sponge. These echoes are incoherent in the sense that for a certain range delay the amplitude is random with zero mean. Note that the echoes in close vicinity to the first echo seem somewhat weaker than those from deeper inside the sponge (at greater depths the echoes weaken due to attenuation). The reason is probably due to the fact that the transducer surface is not perfectly parallel to the sponge surface and thus it takes more time for the incoherent term to fully develop. This slight misorientation has practically no effect on the coherent term magnitude. However because of this effect, the estimation of the incoherent term should not be done in the immediate vicinity of the first echo.

From eq. (35) we know that the ratio between the square of the average boundary echo and the average power from inside the sponge, neglecting attenuation, is proportional to the scattering density. Thus it should be possible to estimate the sponge density from A-mode echoes of the types obtained. We will not attempt here to estimate the sponge density quantitatively, but will show qualitatively that the experimental results behave according to the theory.

Figures 5(A),(B),(C) and (D) represent the echoes received from sponges A,B,C and D respectively. Each of these pictures is composed of four superimposed traces from four different locations in the sponge, with identical distances between the transducer and the sponge surface. In Figure 5(A) which represents the received echo from sponge A one can

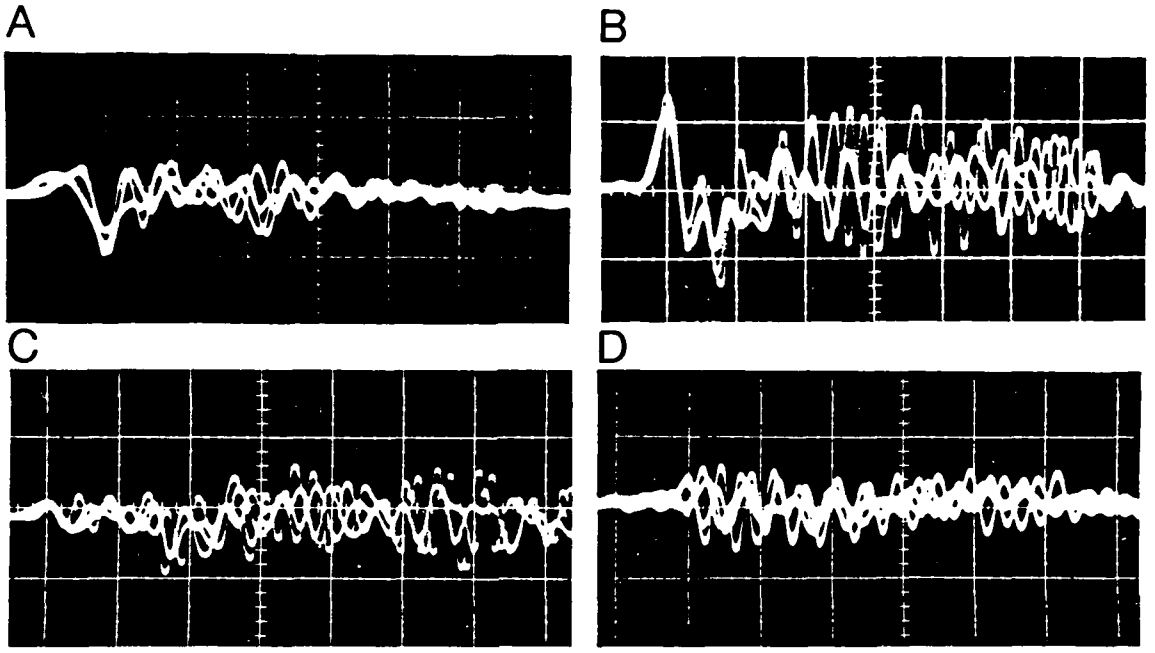

Figure 2.5(A) Four traces (one on top of the other) of the reflected echo from sponge A. Note the large coherent component of the echo from the boundary.

(B) Sponge B. Note that the coherent component is not as large in comparison to the echo from within the sponge as in Figure 4(A)

(C) Sponge C. Note that the coherent component is smaller in comparison to the echo from within the sponge in Figure 4(B)

(D) Sponge D. The coherent component was found to be negligible in repetitive experiments.

see clearly that the coherent echo is large in comparison to the echo returned from within the sponge. Figure 5(A) is similar to Figure 4 but with the traces superimposed. One can see that the coherent component of the echo from the boundary is not as large as that of Figure 5(A) in comparison to the echo returned from within the sponge.

Notice also the great difference in the degree of coherency for sponges B and C. The honeycomb structures of these sponges are similar in shape so that we can assume that $\bar{\rho}^2/\overline{\rho^2}$ is also similar. The integrals in eq. (30) are also similar for the two sponges since they involve only transducer and medium parameters which were the same for all experiments. Thus the ratio between the coherent term and the incoherent term of sponge B and C should be proportional to the scatterer density. Evaluating the coherent term from the ratio of the average of the first echo from the boundary to the power from inside the sponge, (the incoherent term) we find the ratio to be about 2.1 for sponge B and about 0.8 for sponge C which implies a density ratio of about 2.6. The actual scatterer density that can roughly be established from the micrographs is about 2.2 which is in sufficiently close agreement considering the fact that only four sample points were used and that no special arrangements were made for producing extremely smooth surfaces and for keeping the sponge surface parallel to the transducer surface. Figure 5(D) corresponding to sponge D with the largest honeycomb structure has practically zero coherent effect. This is due to the fact that sponge D has much lower density than the other sponges, too low to show a coherent term from only 4 sample points.

Figure 6 shows the echo from sponge D clamped to sponge B. Coherent echoes are clearly seen along the center vertical line of the picture.

The angle dependence of the reflected echo was also investigated,

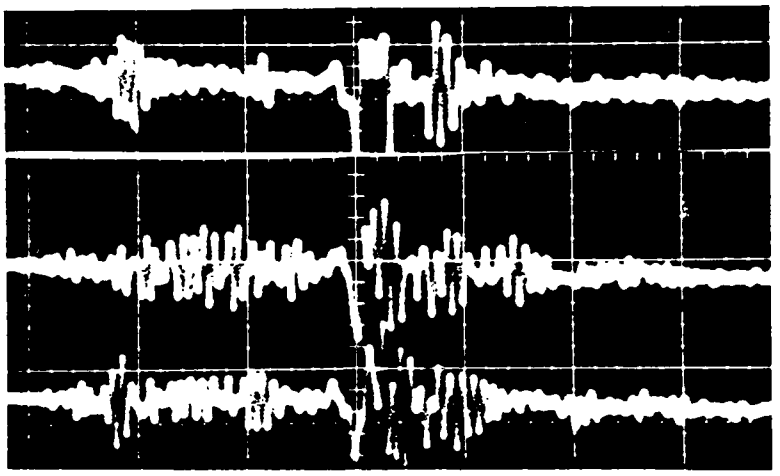

Figure 2.6. The received echo from a 2 layer sponge complex composed of sponges D and B. The coherent component can be seen on the central vertical line. Also note that the power reflected from sponge D is less than that reflected from sponge B.

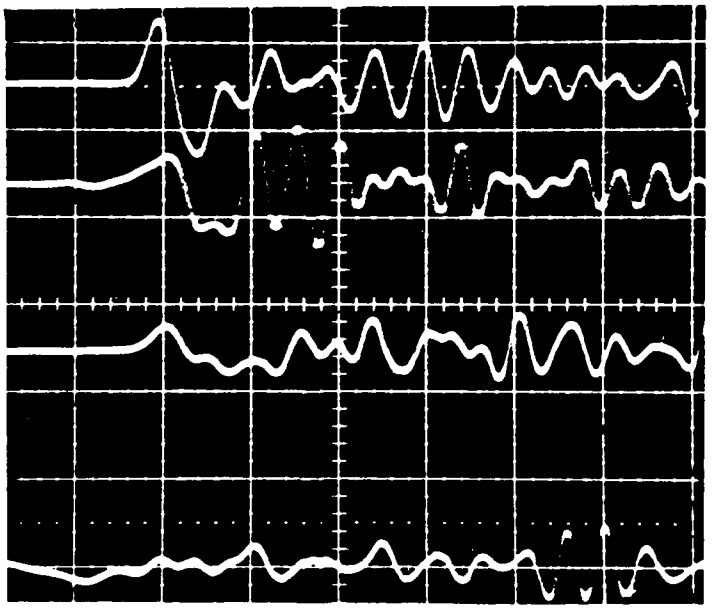

Figure 2.7. Angle dependence of the coherent component (sponge B). Note that while the coherent term is highly sensitive to angle variations, the echo from within the sponge is angle insensitive.

using sponge B as a reflector. One can see from Figure 7 that the coherent effect is highly angle sensitive whereas the echo reflected from within the sponge is not angle dependent. In fact the behavior of the coherent component is very much like that of a specular reflection as predicted by the theory. The reflection from within the sponge is independent of angle since this echo must be independent of boundary region.

It is pertinent to inquire how well the sponges used as test objects in this work fulfill the requirements of the theoretical model. This model places no restriction on the size of the individual scatterers or on the number of the scatterers in the range cell but assumes the Poisson distribution which implies that the scatterers are separated by a distance large compared to their diameter. Weak scattering is also assumed which implies that each scatterer produces no more than one echo. Figure 2 indicates that the size of the sponge unit cells is no larger than that of the sound wavelength of about 0.6 mm., but does not provide information about the size separation of the individual scatterers. The fact that the scatterers echoes from within the sponge are found to be spatially incoherent, shows that the scatterer distribution even in the hexagonal lattice sponges B and C, is at least pseudo-random. To establish the fact that the coherent reflection is not due to a change in acoustic impedance, we measured the sound velocity within the immersed sponges, and found it to be similar to the sound velocity in water.

DISCUSSION

As can be seen in each of the analyzed cases the ratio between the coherent term and the incoherent term for the plane wave approximation is proportional to the scattering density profile and the function $G(\vec{r},t)$ (eq. (35)). In order that the upper integral will be appreciable the

scattering density gradient should be sharp compared to the wavelength. If the gradient is not sharp enough the integral and with it the coherent term become negligible and the backscattered echo can be considered as Gaussian (if the scattering density is high enough) with zero mean and variance which is a function of the range delay. However, if the gradient is sufficiently large the coherent term may be appreciable even if the scattering density is low.

It was shown that the reflection from a sharp boundary separating regions of different scattering density (or scattering cross-section) is characterized by having a non zero mean when spatially averaged and a variance of approximately

$$\sigma^2 = \frac{1}{2}\left[\sigma_1^2 + \sigma_2^2\right] \tag{2.34}$$

The statistics of the boundary echo can be considered Gaussian due again to the central limit theorem with mean $\overline{E(t)}$ (eq. (33)) and variance according to eq. (34). This result states in fact that if the scattering density gradient is sharp enough the reflection from the boundary between regions of different scattering densities resembles specular reflection and it might be appropriate to model the boundary as a strong specular reflector embedded in a high density of point scatterers. We can use this result to incorporate boundary detection in chapters 3 and 4 where we analyze some detection schemes for targets embedded in clutter environments.

We also showed theoretically that the ratio of the coherent signal from the boundary of a scattering region to the incoherent signal from inside the region (if the scattering density is low enough) is proportional to the average spatial density of the scatterers multiplied by a

shape factor. The experimental results suggest that this technique might be useful in nondestructively estimating scatterer size and density even if the scatterers are much too small and much too close to be resolved. It might also be applied to extract more information on the tissue state in biomedical ultrasonic imaging in regions for which the boundary structure is known and is smooth compared to the illuminating wavelength.

Another practical application that this method might provide is in the estimation of the surface grain size of metals. In order for this technique to succeed the metal would have to be polished and immersed in a liquid of similar characteristic impedance.

CHAPTER 3

THE MINIMIZATION ALGORITHM

INTRODUCTION

In chapter 1 we outlined sevaral algorithms and techniques for the reduction of clutter and speckle. We found out that the techniques in most cases do not provide sufficient improvement in clutter reduction. The need for post reception algorithms for the enhancement of target to clutter ratio is evident. In chapters 3 and 4 we will investigate two algorithms for the reduction of clutter using split spectrum processing. This type of processing and the algorithm to be described in chapter 3 was first introduced by Newhouse et al in 1982 (3). N. Bilgutay in his Ph.D. dissertation empirically investigated this algorithm the so-called "Minimization Algorithm", and showed experimentally that it provides an improvement in signal-to-noise ratio over conventional techniques. In this chapter we analyze this algorithm theoretically. We evaluate its signal-to-noise ratio and its Receiver Operating Characteristics and compare its performance to other split-spectrum algorithms.

Chapter 4 introduces a new algorithm which we call "Optimal Processing" (The processing is optimal in the sense that for every range delay the processor maximizes the detection performance).

These two chapters can be read independently. Historically the Minimization Algorithm preceeded the Optimal Processing and was invented "by intuition". So we start with the analysis of the Minimization Algorithm

and procceed in chapter 4 to introduce the Optimal Processor. We compare the two algorithms on the basis of detection properties at the end of chapter 4.

The split spectrum processing was introduced by V. L. Newhouse, N. M. Bilgutay and E. S. Furgason [3] in 1979. In this technique the wideband spectrum of a received signal is split into several frequency windows. The resulting signals are independent provided that these frequency windows do not overlap, and can be compounded in ways similar to those used in frequency agility so as to reduce clutter noise relative to target echo (see Figure 1). Following the nomenclature introduced by Abbot and Thurston [19] for their technique of illumination with different frequencies, we will refer to their technique and to that of reference [3] as "frequency compounding" so as to bring out the similarity between these techniques and that of spatial compounding.

Of the frequency compounding techniques described by Newhouse et al [3], the most powerful used a new procedure, (the so-called Minimization algorithm), in which the signals obtained by frequency splitting the echo spectrum are squared and the minimum value at each delay is chosen. This technique was found to provide a significant improvement in signal-to-noise ratio with respect to the compounding techniques previously used with frequency agility in either radar or ultrasound in which the signals obtained by frequency splitting were either averaged and then squared or were first squared and then averaged. A similar technique has recently been applied to two-dimensional imaging [41].

This chapter is devoted to a theoretical analysis of the Minimization Algorithm and its comparison with the two earlier known frequency agility algorithms. We present expressions for signal to noise ratio, probability

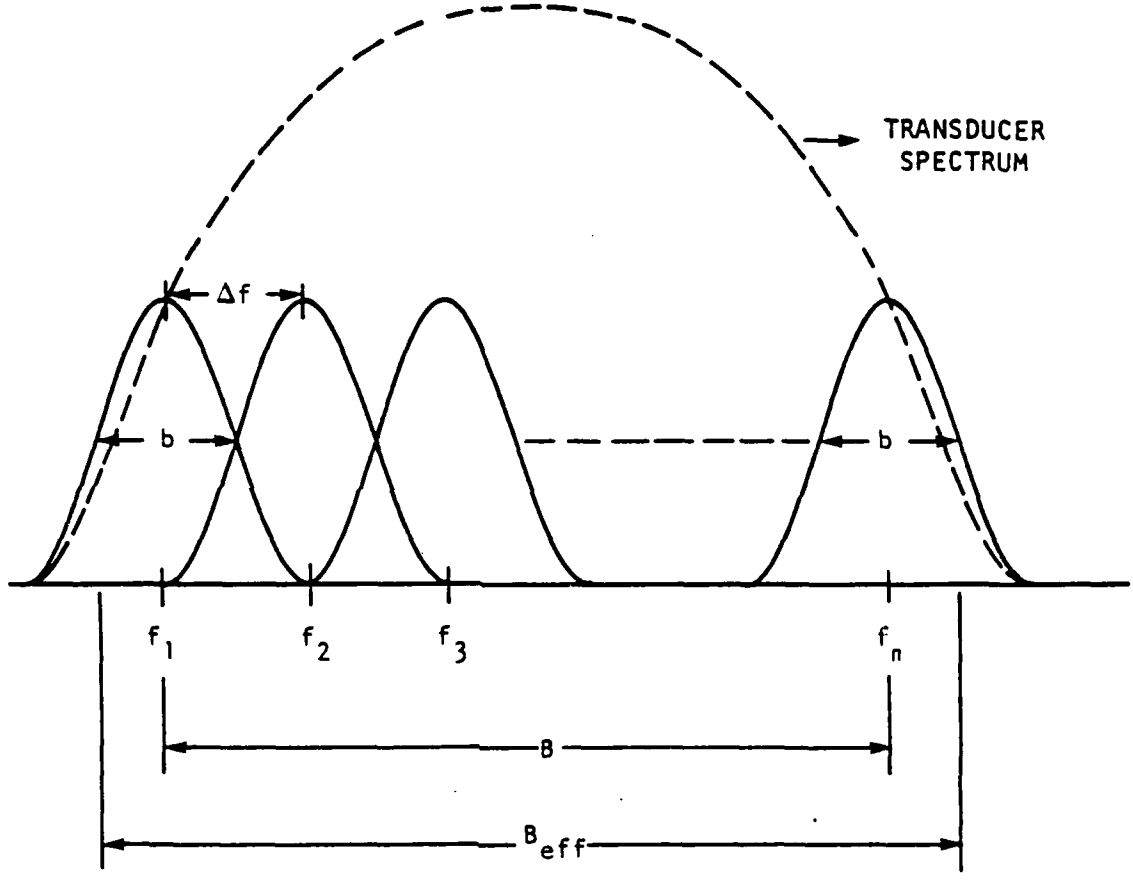

Figure 3.1 The split spectrum process (from 24).

of detection and false alarm as a function of the number of frequency windows, target size and ratio between the clutter variance within and outside the range cell. The analytical results are compared with simulated and experimental data taken from (4). Finally it is shown analytically that, in most cases, the Minimization algorithm provides a much larger signal-to-noise ratio enhancement than the two classical algorithms. However, it is found that this improvement in signal-to-noise ratio enhancement results in a trade-off which increases the probability of error in detection.

Although the algorithms described here could have applications in several different fields, it should be noted, that the assumptions made in the analysis refer only to ultrasonic imaging, in either medical applications or nondestructive evaluation.

ANALYSIS

In this section we perform a comparative analysis of the three frequency compounding algorithms under consideration. We first define our model for the target and its surrounding randomly distributed scatterers, and specify our definition of signal to noise ratio. We then compute the signal to noise ratio enhancement of the three algorithms under consideration, and finally calculate their Receiver Operating Characteristics (ROC).

In all three of the algorithms analyzed here we obtain the frequency diverse signal set used for the frequency compounding, by filtering (or "splitting") the received wide band echo from the target-clutter source complex into different frequency bands or windows which may or may not overlap. For the sake of mathematical simplicity our analysis in this chapter is limited to the case of non-overlapping frequency windows.

Note that the length of the range cell of the frequency compounded image is inversely proportional to the bandwidth of these frequency windows.

Target Model and Signal to Noise Ratio

The model to be analyzed is composed of a strong point reflector (the target) embedded in a high density of smaller scatterers (the clutter). We recognize two differences between the properties of the target and any of the scatterers.

1. The backscattered echo from the target is much larger than that of a point scatterer.
2. There is only one target in the range cell.

In order to determine the statistics of the peak target echo in the presence of the clutter we perform a Gedanken experiment in which we keep the target in its place but change the clutter configuration from experiment to experiment and measure the echo voltage at a range delay corresponding to the peak target echo. The statistics of the clutter without a target in the range cell will be Gaussian (see for example (1)). It follows that the statistics of the echo corresponding to the target range delay will also be Gaussian but with non-zero mean. Thus we could write two hypotheses for this case

H_1: $r = m + n_1$ for the case of the range cell containing noise and a target (3.1)

H_o: $r = n_1$ for the case of the range cell containing noise only

Where r is the value of the received signal at the analyzed delay t, m is defined as the target peak echo and n_1 is the noise voltage which is a superposition of the contribution of the scatterers (clutter) in the range cell. n_1 is a zero mean Gaussian clutter noise with standard deviation

(s.d.) σ_1. If we knew the statistical parameters of the signal, (i.e. σ_1 and m) the statistical decision rule would be trivial. For example setting a threshold level at m/2 would provide the best decision rule for minimum probability of error. In ultrasonic imaging however we do not have a priori information on either m or σ_1. Furthermore these parameters change as a function of distance from the transducer due to attenuation, shadowing or fluctuations in scattering concentration or scattering cross section. In order to evaluate the different techniques (to be presented shortly) we introduce the hypothesis set in the following ways

H_1: $r = m+n_1$

H_0: $r = n_0$

Here n_1 and n_0 are zero mean Gaussian clutter noise echoes with s.d σ_1 and σ_0 respectively; n_0 will be considered always to have equal or larger variance than n_1 (m is as before). The need for introducing different noise levels outside the range-cell is to enable correct evaluation of the minimization algorithm. This algorithm is non-linear and thus treats signal plus noise differently from noise alone (depending on the local signal-to-noise ratio). Therefore with this model we are able to test the effect of algorithms on clutter with unknown parameters that may slowly vary as a function of position. To complete the set we should have added a third hypothesis, H_2

H_2: $r = n_3$

for the case of noise far away from the target which is smaller than that near the target. For simplicity we exclude this hypothesis from the set.

This will be shown to be justified, since Figure 3 demonstrates that the algorithms considered here are monotonic in the sense that if $n_3 < n_o$ then the output of the processed noise n_3 is smaller than the processed noise n_o. Thus enhancement of H_1 over H_o is a sufficient measure of the improvement in the performance of the algorithm.

Since the signal must be squared for two of the three algorithms considered below, we will define the input signal-to-noise ratio in terms of the square of the input signal (unsplit broad band echo). Even this condition, however, is not sufficient to define SNR unambiguously. We therefore select a definition which matches as closely as possible the manner in which SNR is computed in the simulations and experiments with which our analysis is compared below.

We denote Z_{in}^t as the square of the input signal for case H_1 (target in the range cell), and n_{in} as the square of clutter signal amplitude for case H_o. We define the SNR as

$$\left(\frac{S}{N}\right)_{in} = \frac{\overline{Z_{in}^t}}{\sqrt{\overline{n_{in}^2}}} \tag{3.2}$$

The average of the input signal defined as the square of the target echo is:

$$\overline{Z_{in}^t} = E\{Z_{in}^t\} = E\{(m + n_1)^2\} = m^2 + \sigma_1^2 \tag{3.3}$$

and the clutter noise outside the target region is

$$\sqrt{\overline{n_{in}^2}} = [E\{n_o^4\}]^{1/2} = [3\sigma_o^4]^{1/2} = \sqrt{3}\,\sigma_o^2 \tag{3.4}$$

Thus the input SNR becomes:

$$\left(\frac{S}{N}\right)_{in} = \frac{\overline{z_{in}^t}}{\sqrt{\overline{n_{in}^2}}} = \frac{m^2+\sigma_1^2}{\sqrt{3}\ \sigma_0^2} \tag{3.5}$$

Signal to Noise Ratio Enhancement for Non-Linear Averaging

We are now in a position to calculate the signal-to-noise ratio enhancement of the so-called non-linear averaging algorithm, by which, when used in radar frequency agility systems, incoming signals at different frequencies are first squared and then averaged. When used in frequency compounding, as is to be analyzed here, we start by splitting the received wide band echo into n adjacent but not overlapping frequency bands or windows.† This procedure is equivalent to transmitting the frequency bands consecutively as is done in frequency agility. Therefore the results obtained throughout are applicable also for sequential launching of narrow band pulses instead of postreception frequency splitting of a wide band pulse. It is known (see for example - Beasely and Ward (7)) that the signals resulting from this procedure are statistically independent. Since the bandwidths of the signals produced in this way are n times narrower than those of the original signal, the resulting range cells will be n times longer. Hence the noise power, both inside and outside the target range cell, will be n times larger than for the case of the input echo. (It is shown in appendix A, however, that the target peak echo location is unaffected by the frequency splitting process with certain restrictions on the spectra of the transmitted signal. In the appendix we use Gaussian shaped signals. However this restriction that is introduced to simplify the mathematics is not essential as in success-

† Note that the letter n when subscripted stands for noise whereas without subscript it represents the number of frequency splitting channels.

ful experiments we used transducers whose impulse response envelope deviated considerably from Gaussian.) Thus our two conditions to be distinguished for the signals resulting from frequency splitting can be written as:

$$H_1: r_i = m+n_{1i}^* \qquad i = 1,\ldots n$$
$$H_o: r_i = n_{oi}^* \qquad i = 1,\ldots n \tag{3.6}$$

where r_i corresponds to the received signal in the ith window at a certain delay, m is the target amplitude that does not change between windows and n_1^* and n_o^* are the noise components corresponding to the cases H_1 (a target in the range cell) and H_o (no target in the range cell). Both n_1^* and n_o^* are Guassian but with different variances.

The variances of n_{1i}^* and n_{oi}^* are given respectively by

$$\sigma_1^{*2} = n\sigma_1^2$$
$$\sigma_o^{*2} = n\sigma_o^2$$

After squaring each of the channels, the SNR of any one channel can be written

$$\left(\frac{S}{N}\right)_{1CH} = \frac{m^2 + n\sigma_1^2}{n\sigma_o^2\sqrt{3}} \tag{3.7}$$

Summing the frequency windows and averaging we obtain:

$$\overline{Z_{out}^t} = E\left\{\sum_{i=1}^{n} r_i^2\right\} = E\left\{\sum_{i=1}^{n} (m+n_{1i}^*)^2\right\} = n(m^2+\sigma_1^{*2}) \tag{3.8}$$

$$\overline{\sqrt{n_{out}^2}} = \left[\sum_{i=1}^{n} \overline{n_{oi}^{*4}}\right]^{1/2} = [n3\sigma_o^{*4}]^{1/2} = n\sqrt{3n}\,\sigma_o^2 \tag{3.9}$$

and the output signal to noise ratio becomes

$$\left(\frac{S}{N}\right)_o = \frac{m^2 + n\sigma_1^2}{\sqrt{3n}\ \sigma_o^2} \tag{3.10}$$

Combining eqts. (5) and (10) we obtain the signal to noise ratio enhancement (SNRE) for non-linear averaging

$$\text{SNRE} = \frac{\left(\frac{S}{N}\right)_o}{\left(\frac{S}{N}\right)_{in}} = \frac{m^2 + n\sigma_1^2}{\sqrt{n}(m^2 + \sigma_1^2)} = \frac{\sqrt{n}\left[\left(\frac{m}{\sigma_1}\right)^2 \frac{1}{n} + 1\right]}{\left(\frac{m}{\sigma_1}\right)^2 + 1} \tag{3.11}$$

Notice that this enchancement depends only on the clutter noise variance σ_1^2 in the target region, and that it varies from $\sqrt{n}$ at $m<<\sigma_1$ to $1/\sqrt{n}$ at $m>>\sigma_1$. Thus signal to noise ratio enhancement only occurs at small input SNR. There is, however, signal to noise ratio enhancement for the output signal compared to each channel of the split signal as can be seen from eqts. (7) and (10) which give for this case:

$$\frac{\left(\frac{S}{N}\right)_o}{\left(\frac{S}{N}\right)_{1CH}} = \text{SNRE} = \sqrt{n} \tag{3.12}$$

It is this property of the non-linear averaging algorithm which is used in frequency agility radar.

Signal-to-Noise Ratio Enhancement for Linear Averaging

We now analyze the second of the "classical" frequency compounding techniques in which the signals produced by frequency splitting the echo are first linearly averaged and then squared.

It is obvious that splitting the signal and summing the results will merely restore the original signal. Thus this process does not change the relative amplitudes of the signal with respect to clutter. Hence,

the SNRE of linear averaging does not produce any improvement with respect to the original broad band echo. The algorithm does, however, produce enhancement with respect to the individual signals produced by splitting the echo spectrum. Thus one can show that the signal to noise ratio improvement of the linearly averaged and then squared signal with respect to the squared signal of a single channel is

$$\frac{\left(\frac{S}{N}\right)_o}{\left(\frac{S}{N}\right)_{1ch}} = \frac{n\left(\frac{m}{\sigma_1^*}\right)^2 + 1}{\left(\frac{m}{\sigma_1^*}\right)^2 + 1} \tag{3.13}$$

The fact that this signal to noise ratio enhancement approaches n at large input SNR explains why linear averaging is preferred over non-linear averaging in frequency agility radar when the input of the system consists of a set of n frequencies from which a wide band signal can be constructed by linear summation.

Signal-to-Noise Ratio Enhancement for Minimization of Squared Signals

In this section we develop the statistics of the minimized signal and show that the Minimization algorithm provides a much larger improvement in signal to noise ratio than the two techniques analyzed previously. We start as before by splitting the received echo into n non-overlapping frequency bands. The time dependent signal at each of these frequencies is then squared* and the minimum of the squared signals at each delay is chosen, i.e.

---

*In order to allow a fair comparison between the techniques analyzed in this paper, we analyze here the effect of minimizing the square of the signals produced by splitting the echo. This also conforms to the procedure used for the simulated and experimental data which we compare with our analysis.

$$Z(t) = \min[r_1^2(t), \ldots. r_n^2(t)]$$

In order to investigate the statistical properties of the random variable $z = \min[Y_1 \ldots Y_n]$ where Y_i represents the amplitude of the squared signal after a certain time delay for the ith frequency window, we first construct a simple experiment in which we choose the minimum of 2 random variables

$$Z = \min[Y_1, Y_2] \tag{3.14}$$

It is then easy to show (see for instance [2]) that the new distribution function of z is given by

$$F_Z(z) = F_{Y_1}(z) + F_{Y_2}(z) - F_{Y_1 Y_2}(z,z) \tag{3.15}$$

where

$$F_Y(y) = P(Y < y)$$

and

$$F_{Y_1 Y_2}(y_1, y_2) = P(Y_1 < y_1 \text{ and } Y_2 < y_2)$$

If we create a random variable which is the minimum of n random variable

$$Z = \min [Y_1, \ldots, Y_n]$$

Then it can be shown by induction that the probability distribution function $F_z(z)$ will be

$$F_Z(z) = \sum_{i=1}^{n} F_{Y_i}(z) - \sum_{i=1}^{n-1} \sum_{j=i+1}^{n} F_{Y_i Y_j}(z,z) + \sum_{i=1}^{n-2} \sum_{j=i+1}^{n-1} \sum_{k=j+1}^{n} F_{Y_i Y_j Y_k}(z,z,z) - \ldots \tag{3.16}$$

In order to simplify the mathematics we will assume the Y_i's to be independent and identically distributed which corresponds to no overlap between the frequency windows. In this case eq. 16 becomes

$$F_Z(z) = 1 - (1 - F_Y(z))^n \tag{3.17}$$

and the density function of the minimum becomes

$$f_Z(z) = nf_Y(z)[1 - F_Y(z)]^{n-1} \tag{3.18}$$

If we split the received signal echo into n windows, each of the n time signals can be considered to be a Gaussian process.

After squaring the signal containing clutter only the density function of the squared amplitudes for each window becomes

$$f_Y^c(y) = \frac{1}{\sqrt{2\pi y}\ \sigma_o^*} e^{-\frac{y}{2\sigma_o^{*2}}} \qquad y > 0 \tag{3.19}$$

and the distribution function becomes

$$F_Y^c(y) = 2\ \mathrm{erf}\ \sqrt{\frac{y}{\sigma_o^{*2}}} \qquad y > 0 \tag{3.20}$$

where

$$\mathrm{erf}(y) = \frac{1}{\sqrt{2\pi}} \int_o^y e^{-\frac{x^2}{2}}\, dx \tag{3.21}$$

The minimized clutter noise variance can now be evaluated through

$$\sigma_z^2 = \int_o^\infty z^2\ f_Z^c(z)dz - [\int_o^\infty z\ f_Z^c(z)dz]^2 \tag{3.22}$$

where $f_Z^c(z)$ is the density function of the minimized squared clutter signal [eq. 18] with $F_Y(z) = F_Y^c(z)$ and $f_Y(z) = f_Y^c(Z)$.

When a target exists in the range cell the statistics of the returned

echo changes and the signal can no longer be considered as zero mean. In addition the variance of the noise may change if the target occupies a significant part of the range cell thus reducing clutter from this region. The effect on the target echo of passing it through different frequency windows, is analyzed in the appendix and shown schematically in Figure 2 in which we plot the target echo at the output of the different frequency windows. One can see that the maximum of the target signal is unchanged in height and occurs at the same time delay for all the frequency windows and will therefore not disappear due to Minimization. Hence the height of the target signal peak is unchanged by minimizing but its width is reduced. The width is reduced mainly due to the fact that away from the peak region the signals corresponding to the different windows are phase incoherent and for each range delay away from the peak it is highly probable that one of these signals will be very close to zero. The Minimization which chooses the smallest signal for each range delay, will therefore narrow target echoes.

The received target signal after filtering and before squaring will have the following density function for a target in the range cell

$$f_x^t(x) = \frac{1}{\sqrt{2\pi}\,\sigma_1^*}\, e^{-\frac{(x-m)^2}{2\sigma_1^{*2}}} \tag{3.23}$$

where σ_1 is the s.d. of the clutter in the range cell. The density function of the squared signal becomes (for a target in the range cell)

$$f_Y^t(y) = \frac{1}{2\sqrt{2\pi y}\,\sigma_1^*}\left[e^{-\frac{(\sqrt{y}-m)^2}{2\sigma_1^{*2}}} + e^{-\frac{(\sqrt{y}+m)^2}{2\sigma_1^{*2}}}\right] \qquad y > 0 \tag{3.24}$$

the distribution function becomes

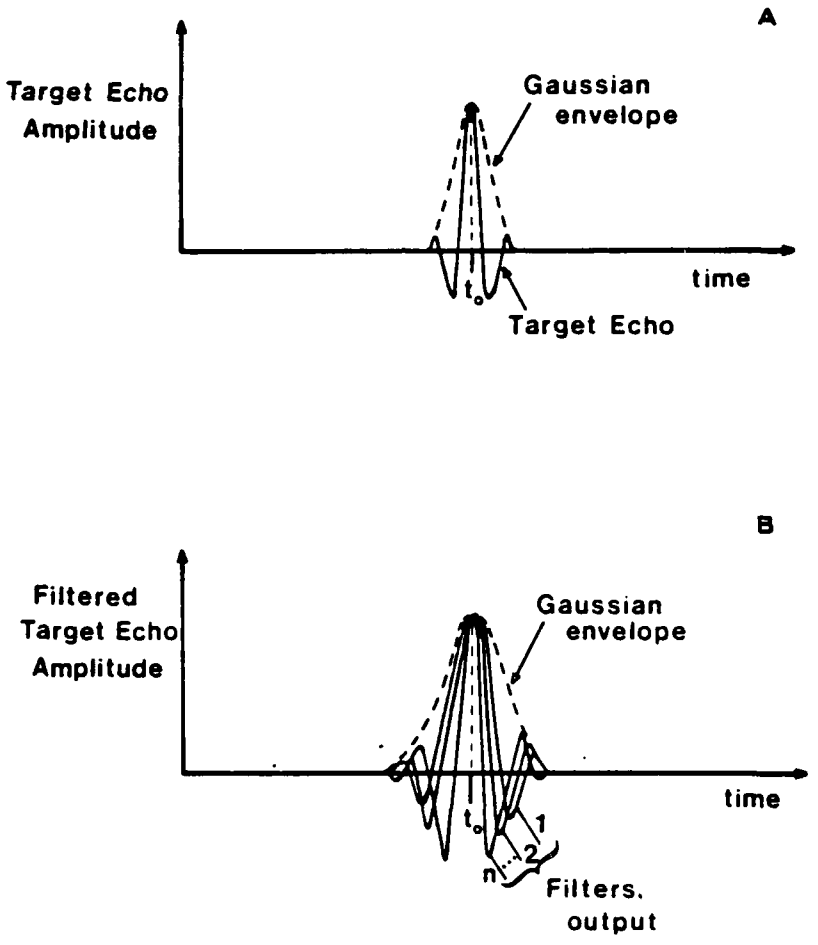

Figure 3.2(A) Target echo with Gaussian envelope before frequency splitting. (B) Target echo after Minimiaztion, showing invariance of peak position.

$$F_Y^t(y) = \left[\text{erf}\left(\frac{m+\sqrt{y}}{\sigma_1^*}\right) - \text{erf}\left(\frac{m-\sqrt{y}}{\sigma_1^*}\right)\right] \qquad y > o \tag{3.25}$$

the mean signal of the target can be evaluated now through

$$\overline{z_{out}^t} = \int_o^\infty z f_Z^t(z)dz \tag{3.26}$$

where as in eq. (17)

$$f_Z^t(z) = n f_Y^t(z)\,[1-F_Y^t(z)]^{n-1} \tag{3.27}$$

likewise the output noise power $\overline{n_{out}^2}$ can be calculated through

$$\overline{n_{out}^2} = \int_o^\infty z^2 f_Z^c(z)dz \tag{3.28}$$

where

$$f_Z^c(z) = n f_Y^c(z)[1-F_y^c(z)]^{n-1}$$

and the signal to noise ratio of the minimized signal is

$$\left(\frac{S}{N}\right)_{out} = \frac{\overline{z_{out}^t}}{\sqrt{\overline{n_{out}^2}}} \tag{3.29}$$

Note that $\overline{z_{out}^t}$ is not merely a function of the target signal but also contains a contribution due to the squared noise.

Using eqts. (26) and (28) the signal to noise ratio enhancement of the Minimization algorithm has been calculated numerically and is shown in Figure 3 as a function of the input SNR for the case of $\sigma_1 = \sigma_o$ i.e. with equal noise near the target and far away from it. Also shown in Figure 3 are the signal-to-noise ratio enhancement provided by the two conventional algorithms as described earlier. It is clear from the figure that the

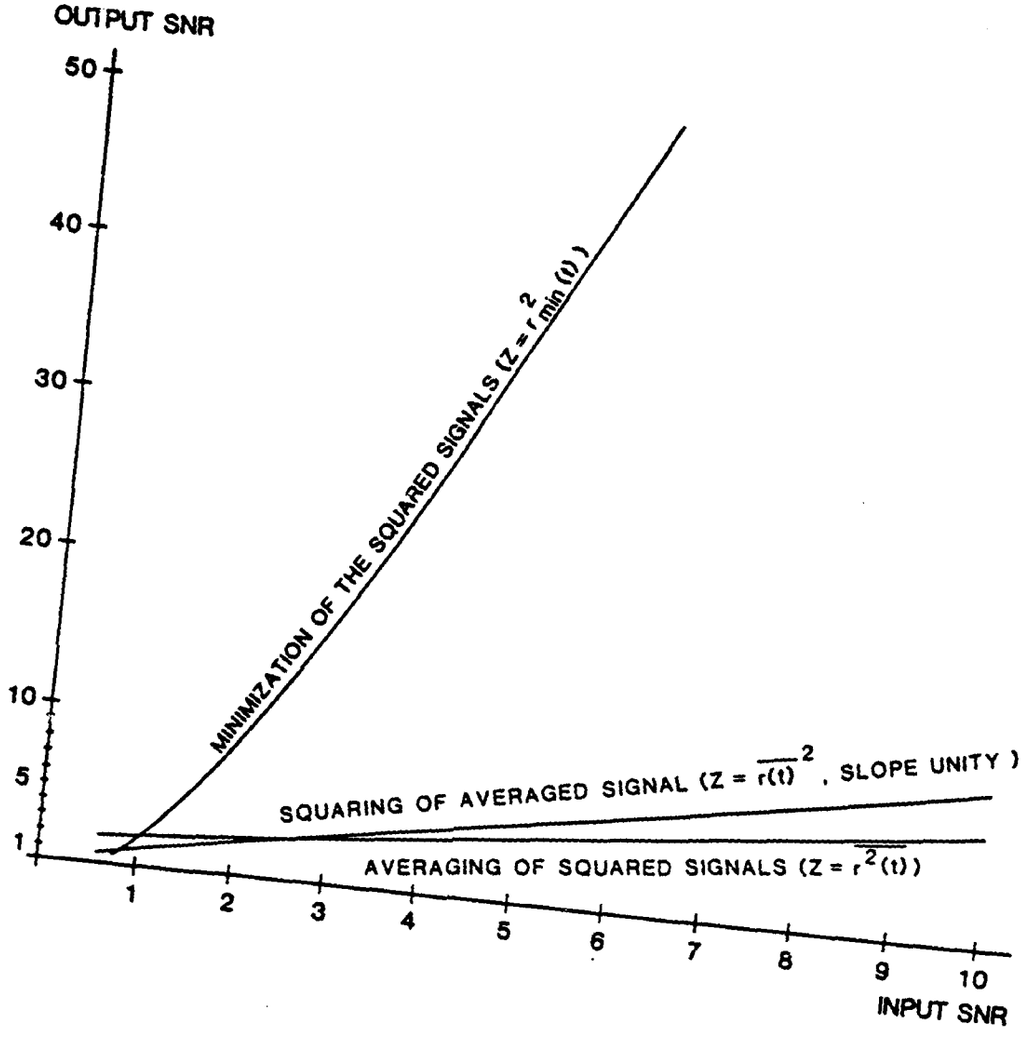

Figure 3.3. A theoretical comparison between different frequency splitting techniques using four independent frequency windows, of SNR enhancement for additive Gaussian noise. (SNR defined in eq. 29). Note that only Minimization produces SNR enhancement.

SNRE for linear averaging is only unity, and that the SNRE for the non-linear averaging algorithm is even worse.

The Minimization algorithm is seen to be highly nonlinear. With high input, SNR the output SNR is significantly higher than for either of the conventional techniques. With low input SNR the improvement is not as strong and its performance actually falls below that of the other techniques.

Receiver Operating Characteristics

The signal to noise ratio enhancement performance is undoubtly an advantage of the Minimization algorithm especially if we intend to display the processed signal without further processing. In this case the ratio between the average signal to the noise power might be taken as a criterion of the visual target enhancement. However, if we are interested in target detection we have to examine the ROC of the proposed algorithms. The fact that the signal to noise ratio obtained by the Minimization algorithm is greater than those obtained by the other algorithms examined does not insure that it will have a better ROC. This is illustrated by Figure 4 which shows the probability density function of the output of a possibly optimum receiver, compared to the output probability density function for Minimization. The density function obtained by using the Minimization can be narrower, providing a lower variance (lower noise power). However, the tail of the probability density function for the minimized signal is broader than that of the optimum receiver, implying a higher probability of high peaks and with it a higher probability of false alarm for Minimization than for the optimum receiver. We assume for illustrative reasons that the target echo size was not significantly reduced (implying a high signal to noise ratio in the input) and the signal

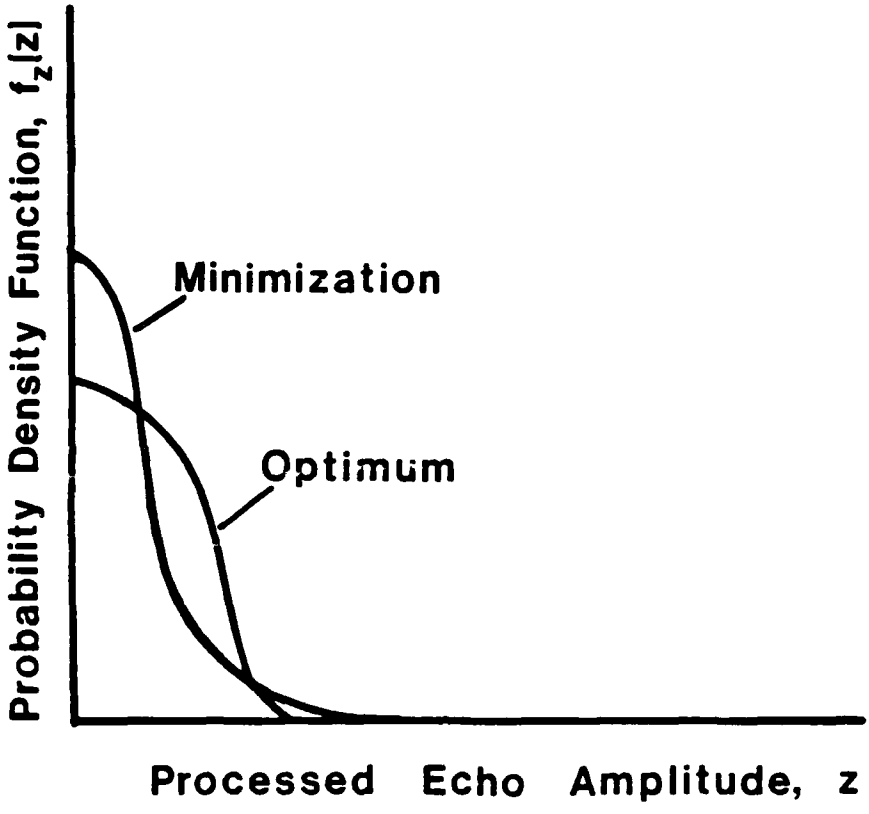

Figure 3.4 Possible probability density unctions for the Minimization process compared to that of an optimum receiver.

to noise ratio at the output is determined by the amount of reduction in the noise variance. The reduction in the peak target echo obviously effects the detection properties adversely.

To calculate the ROC for Minimization we use the model of eq. 6, involving uncorrelated frequency windows. In order to obtain the ROC for the correlated case, one could follow the approach outlined in [42]. However, as stated earlier we restrict ourselves here to the case where the different frequency windows are not correlated. It is clear that squaring the different frequency windows will not change the ROC. Thus it is sufficient to refer to the absolute value of the signal for calculations. It may be seen that for a given threshold z the probability of detection and false alarm for a single frequency window, becomes

$$P_r(D_1) = \frac{1}{\sqrt{2\pi}\,\sigma_1^*}\left[\int_z^{\infty} e^{-\frac{(z-m)^2}{2\sigma_1^{*2}}}\,dz + \int_{-\infty}^{-z} e^{-\frac{(z-m)^2}{2\sigma_1^{*2}}}\,dz\right] \approx \frac{1}{2} + \text{erf}\,\frac{(m-z)}{\sigma_1^*} \tag{3.30}$$

$$P_r(F_1) = \frac{2}{\sqrt{2\pi}\,\sigma_o^*}\cdot\int_z^{\infty} e^{-\frac{z^2}{2\sigma_o^{*2}}}\,dz = 1 - 2\text{erf}\left(\frac{z}{\sigma_o^*}\right) \tag{3.31}$$

where $P_r(D_1)$ is the probability of detection for a single frequency window and $P_r(F_1)$ is the probability of false alarm for a single frequency window for a given threshold z. The probability of detection for the Minimization process equals the probability that the smallest of n target echoes exceeds the threshold, i.e. the probability that all the n echoes are equal or greater than z. Hence for n independent windows, the probability of detection and false alarm for one range delay, are respectively,

$$P_r(D) = [P_r(D_1)]^n = \left[\frac{1}{2} + \text{erf}\,\frac{(m-z)}{\sigma 1^*}\right]^n \tag{3.32}$$

similiarly, the probability of false alarm for Minimization is equal to the probability that independent noise signals all exceed the threshold. Thus

$$P_r(F) = [P_r(F_1)]^n = [1 - 2\text{erf}\,\frac{z}{\sigma_o^*}]^n \qquad (3.33)$$

Note that in general the probability of false alarm P_F of the whole A-line depends on the exact nature of the fluctuations of the clutter scattering density or scattering cross-section and should be defined as

$$P_F = \sum_{i=o}^{\infty} P_r(F|k_i)\, P(k_i) = \sum_{i=o}^{\infty} P_r(F) P(k_i)$$

where k_i is the ratio of the noise std. in a cell without a target to the noise std. of the target cell and $P(k_i)$ is the probability of finding such a ratio along the A-line. $P(k_i)$ depends on the properties of the medium and will change from one type of medium to another. Thus we concentrate our analysis on the first term $P_r(F|k_i)$. In order to calculate P_F for a specific case we require a knowledge of $P(k_i)$ as well as of the function $P_r(F|k_i)$ which are given in Figures 5(A)-(C) below.

The ROC for Minimization obtained in eqs. 32, 33 are plotted in Figure 5((A),(B),(C)) for two, four and six windows respectively. The ratio $R=\sigma_o/\sigma_1$ of noise away from the target to noise near the target, is used as a parameter in these curves. For the sake of comparison the ROC calculated for linear averaging are also shown (Averaging is known to provide the best ROC for the case $\sigma_o = \sigma_1$). One can see that the ROC for Minimization improves with respect to that for averaging as the ratio between σ_o/σ_1 increases. For example, Figure 5(A) shows that for two windows averaging is preferable to Minimization for $R<2$ whereas Minimization

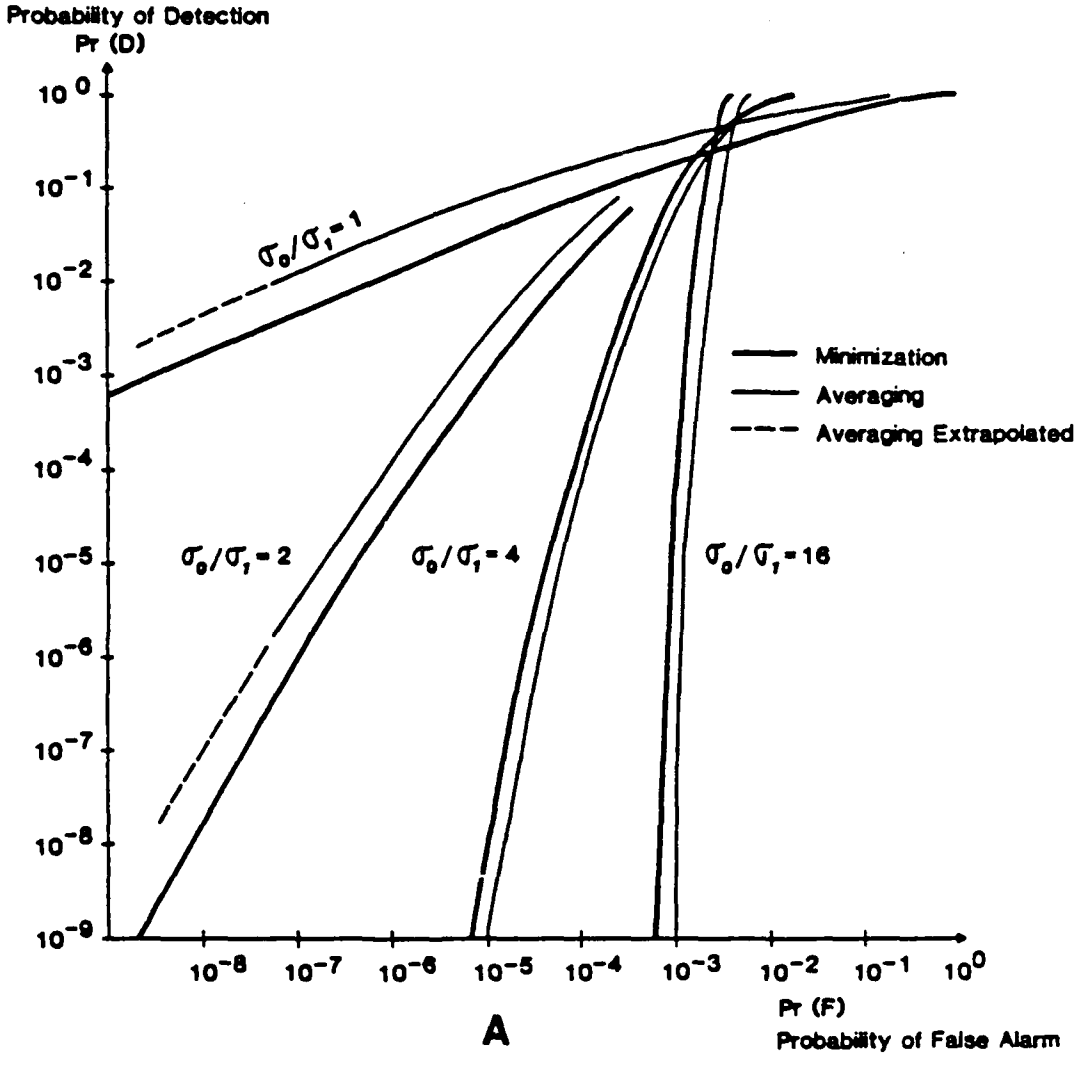

Figure 3.5 Receiver Operating Characteristics for Minimization and averaging using two, four and six frequency windows for various ratios of σ_0 to σ_1, σ_1 is the s.d at the target range delay and σ_0 is the clutter s.d elsewhere (curves thinned-out in the top right-hand corner to retain clarity). m/σ_1 was set to 1.

(A) Two frequency windows.
(B) Four frequency windows.
(C) Six frequency windows.

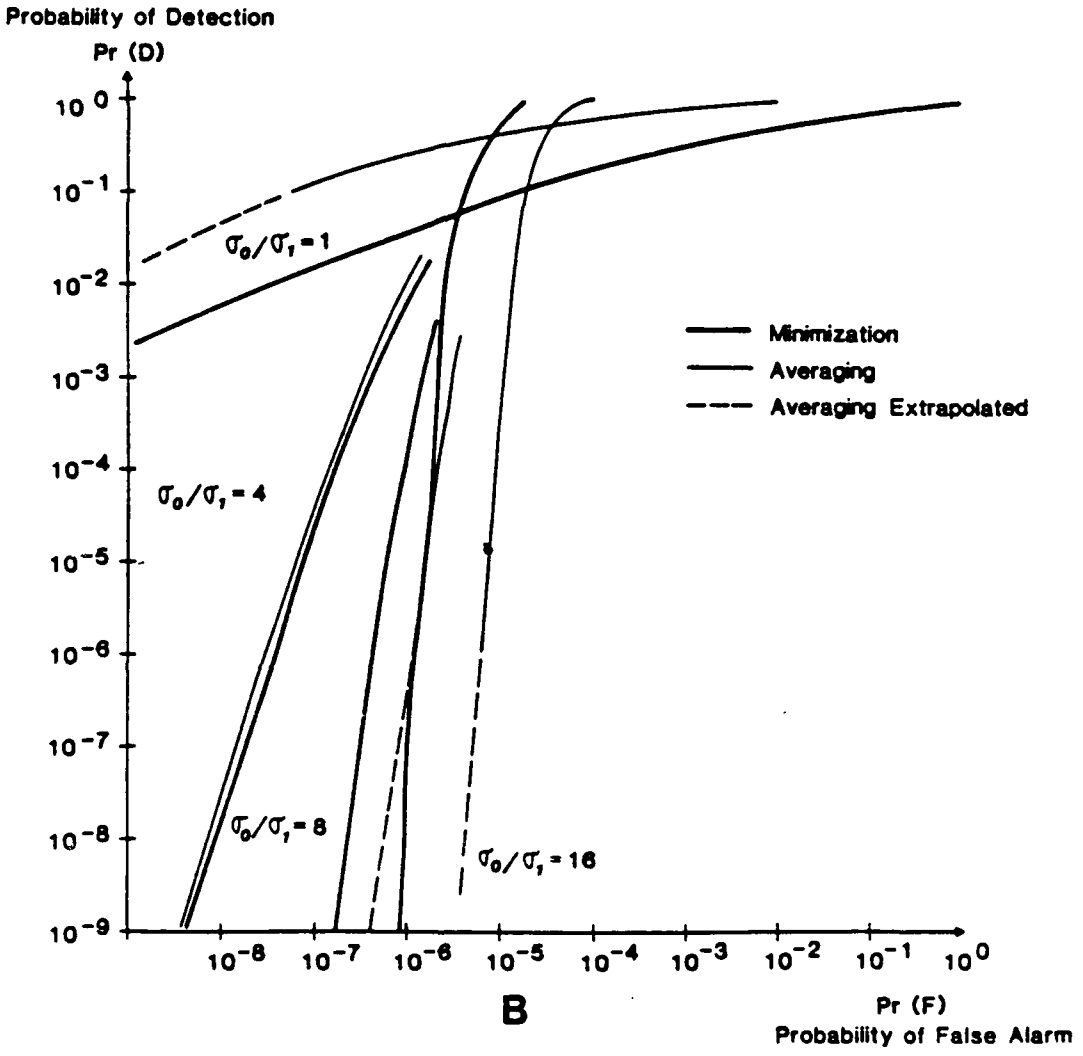

Figure 3.5, cont.

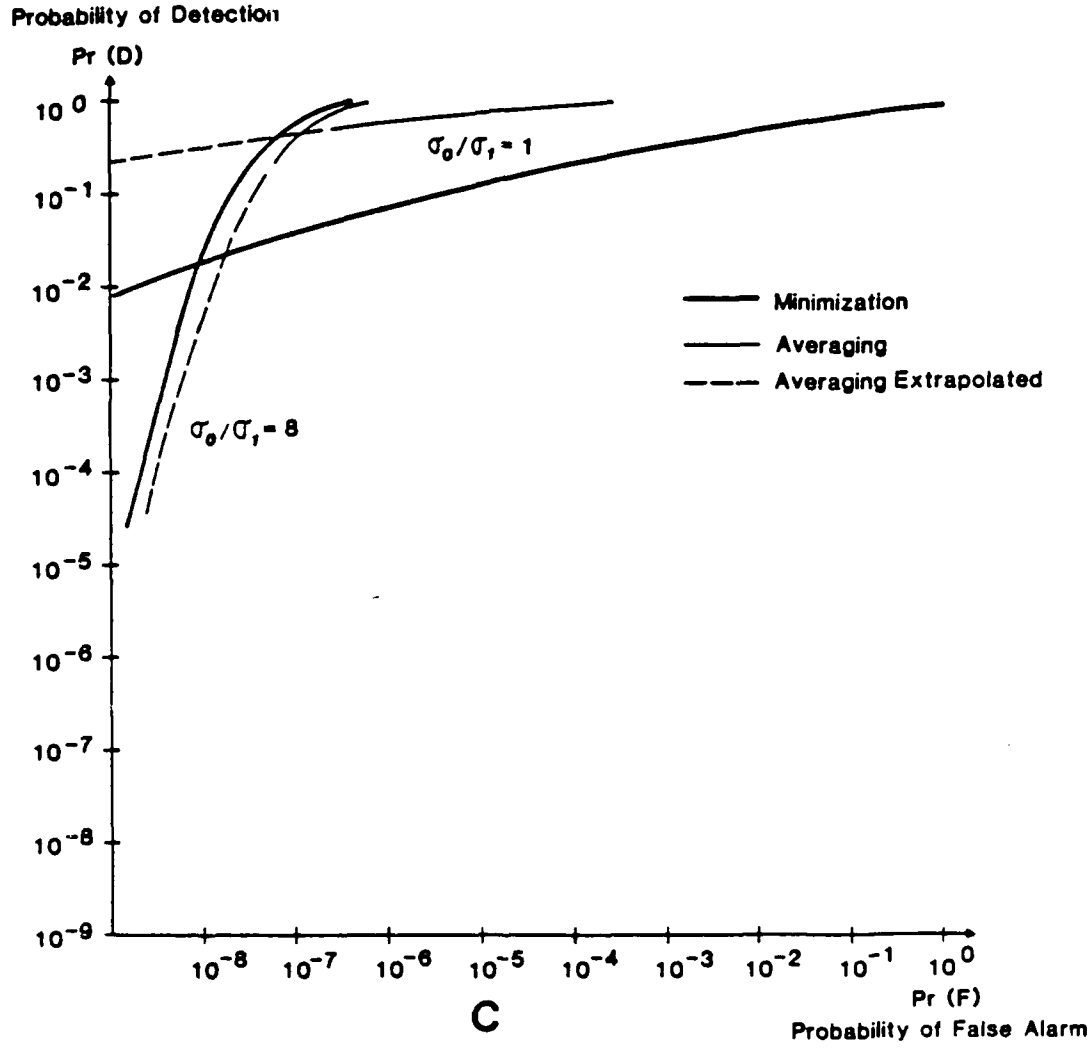

Figure 3.5, cont.

is preferable for R>4. Figure 4(B) shows that the same situation holds for four windows. Figure 5(C) shows that for n=6 Minimization is preferable only for clutter ratios away from the target to that at the target of R > 8. We may therefore conclude that if the ratio of clutter at the target to clutter elsewhere is small enough, Minimization will be preferable to averaging for detection.

EXPERIMENT

The theoretical SNRE plots of Figure 3 which compare Minimization with linear and non-linear averaging are found to agree well with experimental flaw-to-grain echo enhancement curves obtained experimentally in (4). Flaw-to-grain echo ratio is defined as the ratio between the flaw (target) peak echo amplitude and the largest echo amplitude from the clutter present either in the squared backscattered echo signal (i.e. input flaw-to-grain echo ratio) or the processed data (i.e. output flaw-to-grain echo ratio). Therefore, this is an analogous but not quite identical measurement to the SNR definitions defined for the three algorithms defined above.

The experimental data shown in Figure 6 corresponds to a signal which is obtained by summing two separate signals: i) Grain signals obtained from a stainless steel sample with 86 μm average grain size, and ii) A single echo from a flat surface reflector simulating the flaw. The plots in Figure 6 are obtained by varying the amplitude of the simulated flaw signal and measuring the flaw-to-grain echo ratios of the squared received signal and the processed data for all three algorithms.

Although the particular processing parameters selected here are not necessarily optimal for any of the processing algorithms, they result in data representative of the general behavior of each algorithm in enhancing

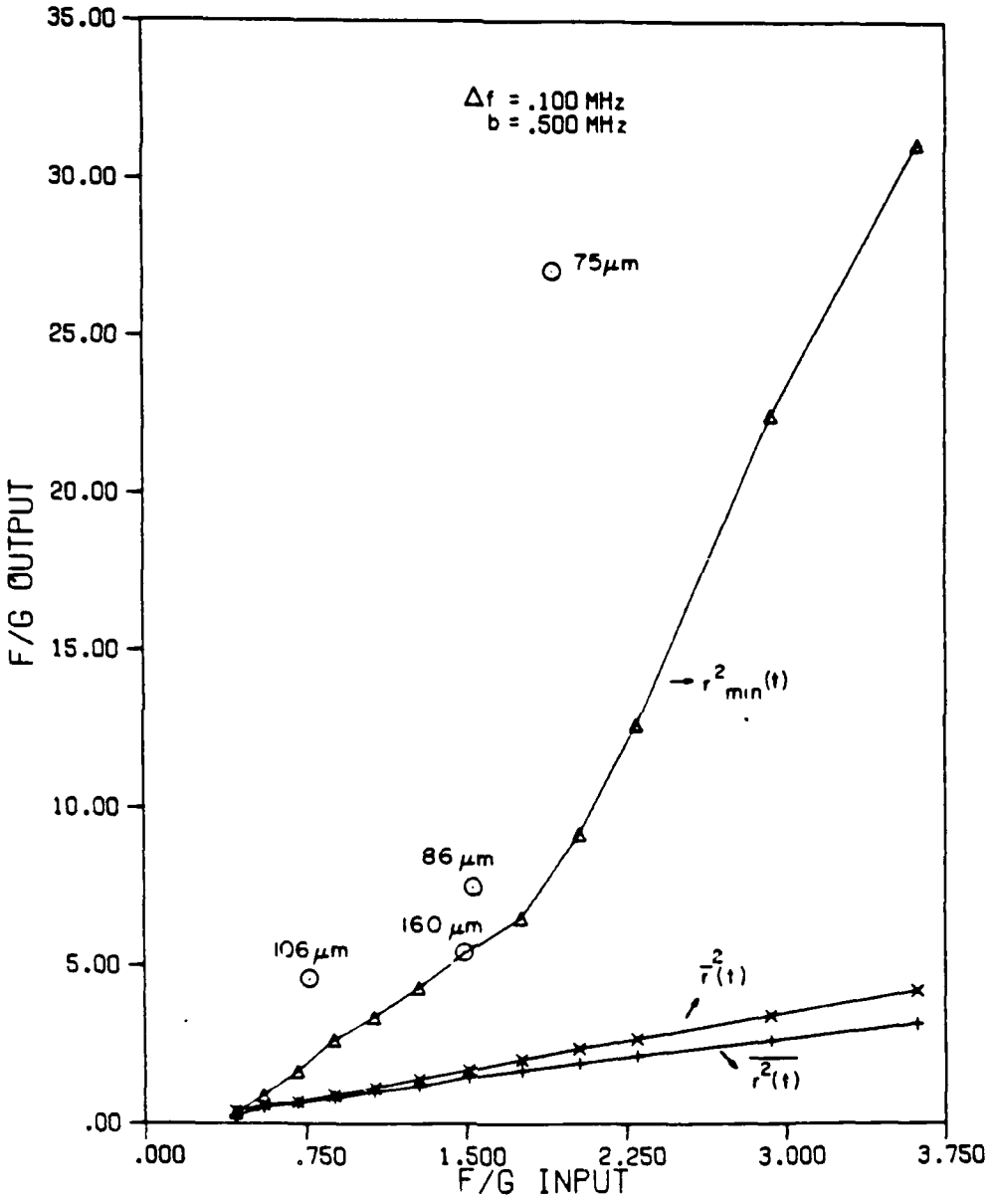

Figure 3.6 (from 24) Input-Output flaw-to-grain echo ratio curves and discrete values for stainless steel samples of indicated grain size. Δf is the spacing between the frequency windows and b is their bandwidth.

the flaw echo. A more detailed description of the experimental techniques used to obtain Figure 6 is presented in (3,4).

Bilgutay in his experiments used at Purdue a noise correlation system as a transmitter/receiver. At Drexel, however, we used a pulser as a transmitter and digitized the received echo with a high speed digitizer. To enhance the signal-to-thermal-noise ratio we averaged the received echo by summing 50 consecutive returned A line echoes. Though the noise correlation system output signal from a single reflector (see (4)) is different from the received signal due to a point reflector illuminated by a pulse, the results, however, are very similar. Experimental results using the new system are shown in Figure 7. In Figure 7(A) we combined the received echo from a stainless steel with average grain size of about 76 μm and the echo reflected from a flat surface. In Figure 7(B) the signal of 7A is squared (to enable comparison with the processed signal which is done on the squared windows) and in Figure 7(C) we can see the signal of Figure 7(A) processed by the Minimization Algorithm. It is easy to see that there is an apparent improvement in a signal-to-clutter-noise ratio. We did not attempt here to optimize the signal-to-noise ratio by changing the number of windows or the amount of overlap between them as was done for example, in (4), as we investigate here a theoretical model and not a particular case. Thus the signal to noise ratio enhancement in our case is less. The advantage of using the new system i.e. using a pulser and a high speed digitizer is in the data acquisition time. The noise correlation system uses a water delay line that employs a motor to control the delay. As a result acquisition of a single A line composed of 512 sample points takes about 20-30 seconds. If the techniques introduced in this research work are to be industrially implemented a high speed acquisition system is clearly a must.

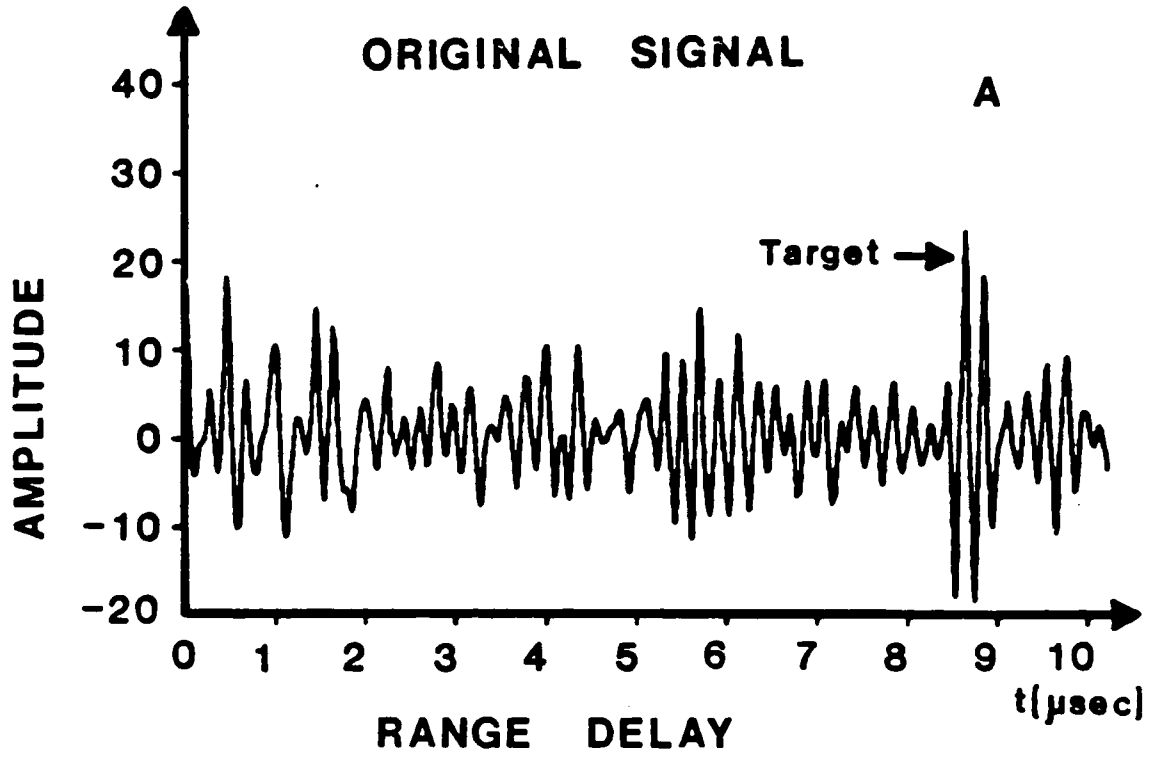

Figure 3.7(A) A signal resulting from the sum of a signal from a stainless steel (with an average grain size of 75 um) and a flat surface reflector target.
(B) The signal of Figure 3.6A squared.
(C) Processed output for the Minimization Algorithm for 10 non-overlapping frequency windows.

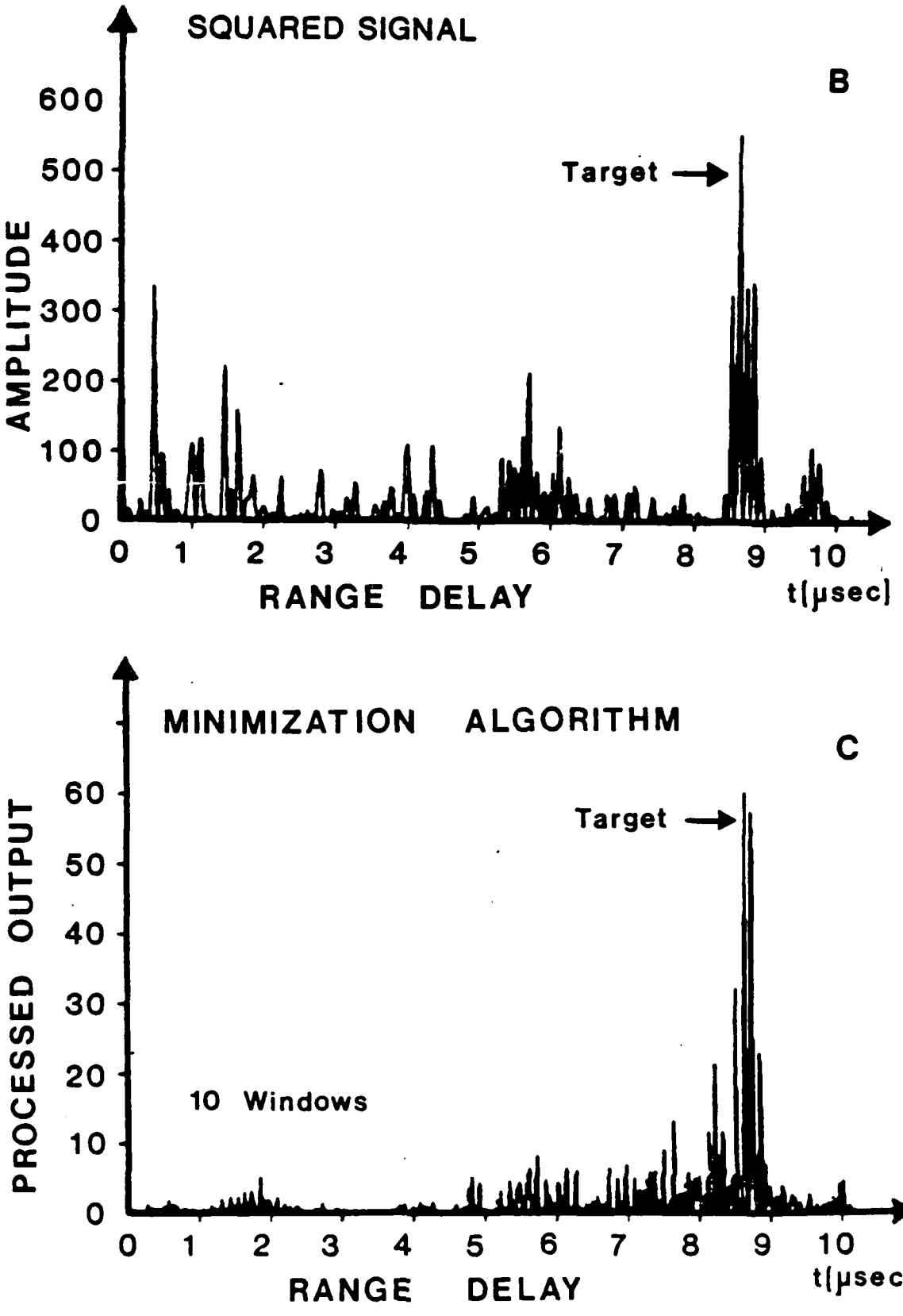

Figure 3.7, cont.

It is clear from Figure 6 that for both averaging algorithms the output flaw-to-grain echo ratio is linearly dependent on the input flaw-to-grain echo ratio, which indicates that the performance of these algorithms is not strongly dependent on the variation in flaw amplitude. These results also indicate that the linear averaging algorithm performs slightly better than the non-linear averaging algorithm, which agrees with the theoretical results shown in Figure 3. However, neither averaging algorithm shows any noticeable enhancement in flaw-to-grain echo ratio experimentally, in agreement with the theoretical derivations.

The Minimization algorithm is seen to show more sensitivity to the flaw amplitude (as is evident from the non-linear nature of the input-output flaw-to-grain echo ratio) than the averaging algorithms. These results are also in close agreement with the theoretical plot shown in Figure 3.

DISCUSSION

In this chapter we analyzed and compared the performance of three frequency compounding algorithms in improving the ultrasound visibility and detectability of targets hidden by additive clutter or speckle, using only the information presented in a single A-scan.

Many criteria need to be considered when comparing algorithms for improving target detectability. These include signal-to-noise ratio or contrast, probability of detection and false alarm (ROC), bias of signal estimates, dynamic range, longitudinal and lateral resolution, and simplicity of implementation. Each of these criteria can be improved, but often only at the expense of increased dynamic range requirements, and the introduction of bias in target amplitude estimation.

In this chapter we analyzed the first two of these criteria for the three algorithms under consideration, namely signal-to-noise ratio and receiver operating characteristic. It was shown theoretically and confirmed by experiment, that the signal-to-noise ratio or contrast enhancement produced by the Minimization algorithm is far greater than that of either linear or nonlinear averaging, provided that the input signal-to-noise ratio is larger than unity. This holds true whatever the ratio between the clutter density in the target region and elsewhere. This advantage of Minimization with respect to linear or nonlinear averaging is however, to some extent illusory, since it may be accompanied by increased probabilities of "target drop-out". In other words even though the contrast and visibility of the target is improved on the average by Minimization, there is also an increased probability that the target echo will be supressed by the subtraction of an awkwardly located noise spike.

These consideration are quantitated by the calculated receiver operating characteristics illustrated in Figure 5 which show that for a given false alarm rate, the probability of detection for Minimization is only improved over that for linear averaging, when the clutter density near the target is at least four times smaller than that elsewhere. This situation is in fact not uncommon, since in attenuative media, the clutter echo from regions close to the transducer is larger than that from deeper lying target regions and so might be the case in fluctuating random media. This situation is not rectified by the use of time-varying gain except in the relatively rare cases where the attenuation and clutter density are known at every point of the medium.

It is in fact ignorance of the local properties of the medium which limits the effectiveness of our procedures. In the forthcoming chapter we derive the optimum receiver for the target model analyzed in this paper,

RESOLUTION: Since Minimization involves filtering the target echo with a narrow bandwidth filter, it reduces the longitudinal resolution in the sense that target echoes may enhance or depress each other over a distance $c/2\Delta F$ where c is the velocity of sound and ΔF the filter bandwidth. Thus a strong target might partially suppress an adjacent smaller target.

However, because of the effect discussed in connection with Figure 2, Minimization narrows the processed target echo to about one wavelength of of the highest center frequency for splitting the spectrum, i.e. produces sharpening in the processed image.

CONCLUSIONS

In this chapter we analyzed the so-called Minimization algorithm and compared its performance in improving the visibility of targets hidden by additive time-invariant clutter or speckle noise, with that of two "classical" algorithms used in frequency agility radar, linear and non-linear averaging. All three algorithms "frequency compound" signals produced by filtering a single A-scan ultrasound echo with a number of non-overlapping spectral "windows". The operation of these frequency compounding algorithms is therefore relatively simple since they operate on only one A-mode echo at a time.

Minimization was shown to be capable of producing significant improvement in SNR and is predicted to produce sharpening in 2-D images. Neither of these effects are produced by the other two algorithms studied.

Linear averaging is known to be the optimum detection algorithm for additive noise and accordingly was found to give the best ROC of the three algorithms tested. However, Minimization is shown to produce better ROC when the clutter near the target has a standard deviation which is at

least four times smaller than that elsewhere. Such cases are often encountered in attenuating media due to shadowing by large targets, and for media which exhibit fluctuations in either scattering concentration or scattering cross-section along the A-line. The analyses in this chapter have been restricted to non-overlapping frequency windows. The conclusions reached should, however, also apply to filtering with overlapping windows, as is shown experimentally in (18) and will be further discussed in chapter 5.

CHAPTER 4

OPTIMAL PROCESSING

INTRODUCTION

Chapter 3 was dedicated to the analysis of the minimization algorithm. We found out that this algorithm provides a significant improvement in signal to noise ratio with a marginal loss in dynamic range. However, the Receiver Operating Characteristic (ROC) was found to be less impressive. Only for a high ratio of variances between a cell containing clutter and the target range cell was the ROC found to be superior to averaging.

In this chapter we introduce a new technique for improving the ROC of the received A-line. This technique which we call "optimal processing" is also based on split spectrum processing. In the first part of this chapter we introduce the theoretical basis and motivation for split spectrum processing. We find that in order to construct the optimum receiver (a receiver that will minimize the probability of error for a given threshold) we should split the spectrum into independent frequency windows whose number is directly proportional to the required range resolution. From the set of random variables that correspond to each range delay we construct the receiver algorithm. For trivial cases i.e. for cases where the noise and signal spectra are white in the frequency range of interest, the algorithm becomes the estimated mean divided by the estimated standard deviation of the spectral decomposition components.

We proceed to evaluate the ROC of the new algorithm for media with fluctuating clutter noise and compare it with the ROC obtained by thresh-

olding the received signal without special processing. Then we introduce a simplified version of the mathematical model for which we replace the matched filters $\sin\pi T(f_n-f)/\pi(f_n-f)$ obtained in the optimum receiver derivation, with Gaussian shaped filters and show that its performance is very close to the performance of the mathematical model. We then implement this simplified algorithm and show experimentally its effectiveness in target enhancement. Finally we evaluate experimentally the resolution performance of the new algorithm in comparison to Minimization.

THEORY

As is known, the received clutter noise power varies as a function of range delay due to changes in scattering density, scattering cross-section, attenuation, beam intensity etc. However if we take a small enough time interval $[T_i,T_f]$ of the received echo e(t) we can assume in most practical cases that the statistical properties of the echo in that interval are constant. We will treat the problem of clutter reduction in this interval $[T_i,T_f]$ as a problem in statistical decision theory. The general Hypothesis set can be written as follows,

$$H_1: r(t) = \mu x(t-\tau_t) + n(t) \qquad T_i < t < T_f \qquad 4.1$$

$$H_0: r(t) = n(t) \qquad T_f - T_i = T$$

where n(t) is a Gaussian random process with variance σ^2, σ, μ and τ_t are unknown and x(t) is a known signal. Though the returned echo $[-\infty, \infty]$ is in general not stationary, we assume that in the interval of analysis $[T_i,T_f]$ the noise process n(t) would be a sample function of a stationary process (a requirement that is met if the interval $[T_i,T_f]$ is sufficiently small). The problem is to find a decision rule as to whether $\mu=0$ or $\mu\neq0$ where σ, μ and τ_t are unknown.

Let us consider first the problem for τ_t known. In this case as we shortly show, the decision rule, can be constructed from the set of random variables obtained by an orthonormal expansion (Karhunen-Loeve expansion, see for example (42)) of the random process r(t). In this technique we transform the problem from a random process problem into a random variables problem (see for example Scharf (43)). These random variables are the r_i's in the expression

$$r(t) = \sum_{i=0}^{n} r_i \, \phi_i(t) \qquad 4.2$$

where the functions $\phi_i(t)$ are orthonormal. To explain the procedure of obtaining the coefficients of the expansion (the random variables) we assume for simplicity that the spectrum of n(t) is rectangular as shown in Figure 1, and that the spectrum of x(t) is no larger than B (There is an apparent contradiction between the time limited interval of the analyzed signal r(t) and the limited bandwidth of the rectangular noise process assumed in the example. However this assumption is often made to simplify an analysis and in most cases is found to be justified).

To find the $\phi_i(t)$ one solves the integral equation,

$$\lambda_i \phi_i(t) = \int_{-\frac{T}{2}}^{\frac{T}{2}} R_{nn}(t-\tau) \, \phi_i(\tau) d\tau \qquad 4.3$$

where λ_i is both the eigenvalue and noise power associated with the i-th orthonormal function, and $R_{nn}(\tau)$ is te autocorrelation function of the noise process. One can show that

$$\phi_i(t) \cong \frac{1}{\sqrt{T}} e^{j2\pi f_i t} \qquad \text{for} \quad f_i = if_o \; ; \; f_o = \frac{1}{T} \qquad -\frac{T}{2} < t < \frac{T}{2} \qquad 4.4$$

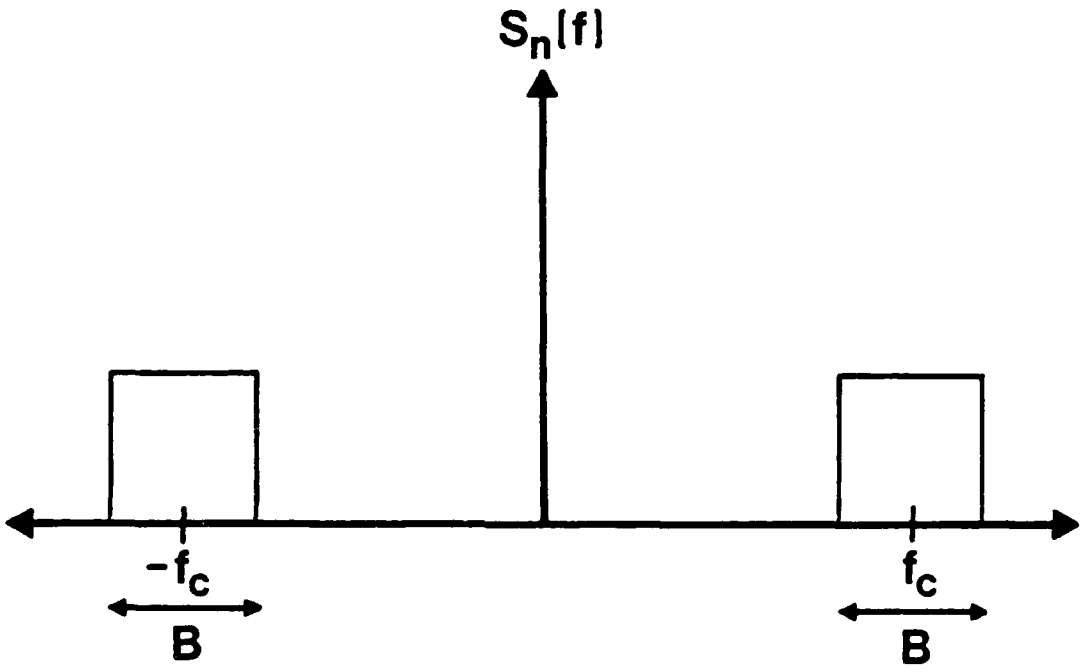

Figure 4.1 The rectangular noise spectrum in the example.

and that

$$\lambda_i \equiv S_n(f_i) \qquad 4.5$$

For our choice of spectrum (shown in Figure 1), all the λ_i's and thus the variances of all the orthonormal coordinates are identical. This makes them identically distributed (if we have only clutter noise in the input). Naturally we are not interested in the orthonormal functions outside the frequency band B of the clutter noise since they carry no information. (We assume that the spectrum of x(t) is no broader than that of n(t) so that there is no energy outside of the frequency band of width B). Note that for the general case where $S_n(f)$ is not white in the frequency range of interest the r_i's will not be identically distributed. The assumption of a white spectrum in the example is therefore merely used to provide an insight to the general solution of the problem.

In order to obtain the set r_i's of the random variables associated with the K.L expansion we have to perform the process shown in Figure 2. Since $f_i - f_{i-1} = f_o = \frac{1}{T}$, the number of filters $\phi_i(\tau - t)$ and the number of independent random variables $r_1, \ldots r_n$ is directly proportional to the observed time T and equals,

$$n = B\ T \qquad 4.6$$

The chosen time window $[T_i, T_f]$ determines the resolution because we must assume that only a single target exists in this window, since otherwise the assumption that the target signal x(t) is known would no longer be valid.

Now for the assumption that the target location in r(t) is known we construct the likelihood ratio test (LRT) (The LRT gives a decision criterion subject to a certain risk function to determine which of two

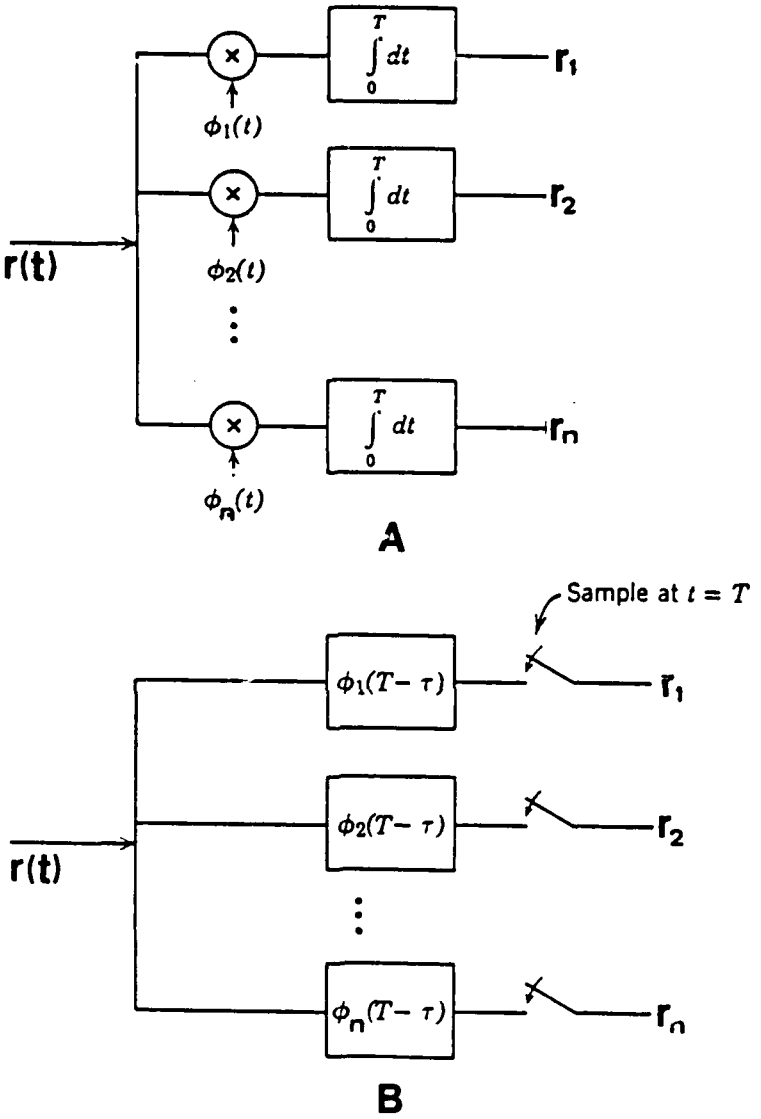

Figure 4.2 Generation of expansion coefficients,
(A) Correlation operation.
(B) Filter operation.

possible hypotheses is true. It is composed of the ratio of the probability density functions of the observables of the two hypotheses.) from the set of random variables r_i's. The random process problem set in eq. (1) can now be restated as a random variables problem

$$H_1: r_i = \mu x_i + n_i$$
$$H_o: r_i = n_i \qquad 4.7$$

where the x_i's are the spectral decomposition components r_i of the signal x(t) fed into the system shown in Figure 2. Instead of solving directly the problem for which the noise spectrum is white in the frequency range of interest (as in our example) we quote first the general solution to the problem of colored Gausian noise. Later we return to our example as a special case of the general solution.

If the spectrum of the received clutter signal is not white in the frequency range of interest or the signal was not whitened before decomposition (the signal can be also whitened during decomposition by assigning appropriate constant multipliers to the filters $\phi_i(t)$), the likelihood ratio test (LRT) becomes (see for example Scharf and Lyte (43), Helstrom (15)),

$$L(\underline{r}) = \frac{\sum_{i=1}^{n} x_i r_i/\lambda_i}{\{\frac{1}{n-1}(\sum_{i=1}^{n} r_i^2/\lambda_i - [\sum_{i=1}^{n} \frac{r_i x_i}{\lambda_i}]^2)\}^{1/2}} \qquad 4.8$$

where λ_i is the eigenvalue associated with the i-th orthonormal coordinate and x_i is as above. The statistics of $L(\underline{r})$ is the student t distribution and we will discuss some of its properties later in the chapter. For the

processing described here we whiten the clutter spectrum making it similar to the example and assume that the target energy spectrum is similar to the clutter power spectrum, which means that the target is assumed to be a strong point reflector. We can then scale x(t) such that $\sum_{i=1}^{n} \frac{x_i^2}{\lambda_i} = 1$ so that

$$\mu \sum_{i=1}^{n} x_i^2/\lambda_i = \mu \tag{4.9}$$

but $x_j=x$ and $\lambda_j=\lambda$ for a white spectrum within the frequency band B so or $\frac{nx^2}{\lambda}=1$

$$\frac{x^2}{\lambda} = \frac{1}{n} \tag{4.10}$$

and the LRT becomes

$$L(\underline{r}) = \frac{\frac{1}{n} \sum_{i=1}^{n} r_i}{\sigma_r} \tag{4.11}$$

This is nothing else but the estimated mean of the spectral decomposition components r_i's divided by their estimated standard deviation and can be written

$$L(\underline{r}) = \frac{m_r}{\sigma_r} \tag{4.12}$$

To estimate σ^2 which is the noise power after whitening we have to calculate

$$\sigma_r = \{ \frac{1}{n-1} \left(\sum_{i=1}^{n} r_i^2 - \frac{1}{n}[\sum_{i=1}^{n} r_i]^2 \right) \}^{1/2} \tag{4.13}$$

and the LRT becomes

$$L(\underline{r}) = \frac{\frac{1}{n}\sum_{i=1}^{n} r_i}{\left\{\frac{1}{n-1}\left(\sum_{i=1}^{n} r_i^2 - \frac{1}{n}\left[\sum_{i=1}^{n} r_i\right]^2\right)\right\}^{1/2}} \qquad 4.14$$

As the number n of the orthonormal functions increase the performance of the algorithm in estimating σ improves. Note that,

$$\frac{1}{n}\sum_{i=1}^{n} r_i = \frac{1}{n}\sum_{i=1}^{n}\int_{T_i}^{T_f} r(t)\,\phi_i(t)dt = \frac{1}{n}\int_{T_i}^{T_f} r(t)\sum_{i=1}^{n}\phi_i(t)dt \qquad 4.15$$

Recall that for eq. 4.14 to hold $\frac{x^2}{\lambda} = \frac{1}{n}$

$$x(t) = \sum_{i=1}^{n} x_i\phi_i(t) = \sqrt{\frac{\lambda}{n}}\sum_{i=1}^{n}\phi_i(t) \qquad 4.16$$

so

$$\sum_{i=1}^{n}\phi_i(t) = \sqrt{\frac{n}{\lambda}}\,x(t) \qquad 4.17$$

and eq. 4.12 becomes

$$\sum_{i=1}^{n} r_i = \sqrt{\frac{n}{\lambda}}\int_{T_i}^{T_f} r(t)x(t)dt \qquad 4.18$$

which is seen to be an estimate of the energy of x(t) in r(t). So eq.(14) is just the value of the estimated signal energy at the analyzed range delay divided by the estimated standard deviation of the clutter in $[T_i, T_f]$. Naturally as the number of elements in the expansion increases so does the accuracy of the variance estimate and the performance of the LRT.

Now that we have derived an optimum LRT to decide whether an individual range cell does or does not contain a target, we return to the original problem in which we treat the A-line as a collection of m range cells. Each of these corresponds to a certain range delay of length T and produces n spectral decomposition components. Since we assumed n(t) to be Gaussian these n r_i terms for each cell are samples from a Gaussian distribution. It is important to note that the cell statistics can change from cell to cell due to either a change in scatterer density which leads to a change in the variance of r(t) or due to the existence of a target in the analyzed time window which leads to a change in its mean. (In chapter 2 we showed that such a change (gradient) should lead to a coherent reflection. However if the change is slow compared to a wavelength (as is the assumption here) the coherent component is negligible). Recall that we do not have any information on the location of the target. Thus we have to find a LRT for every range. There are three possibilities,

1. The analyzed range delay is such that $\tau=\tau_t$ where τ_t is the target range delay. This case is referred to as H_1 and was analyzed earlier.
2. There is no target in the time window of length T. This case was also analyzed and is referred to as H_0.
3. There is a target in the time window T but $\tau\neq\tau_t$. For now we assume that the resolution cell is no smaller than the analyzed time interval T. In this case multiple targets in the time interval T should be interpreted as a single target. We will return to the resolution performance of this algorithm later in this chapter.

If we presented the likelihood ratio as a function of range delay we would obtain a large signal wherever a target exists in the analyzed range cell. In the absence of a target the estimated mean is expected to be small and the processed output would consequently be small. We would

also be able to set a threshold and reject signals below a prespecified signal to noise ratio.

To maximize the resolution of the algorithm (eq. 14), set the frequency windows should overlap so that they can be as wide as possible. The n random variables corresponding to a certain range delay would then become correlated. If the filters are correlated then the correlation between any two channels containing only clutter can be shown to be (assuming that the signal is whitened before processing so the clutter power in all the channels is identical)

$$\rho_{i,j} = \frac{\int_{-\infty}^{\infty} F_i(f)F_j(f)dt}{\int_{-\infty}^{\infty} |F_i(f)|^2 df} \qquad 4.19$$

For Gaussian windows (see (4))

$$\rho_{i,j} = e^{-\ln 16\left(\frac{f_i - f_i}{b}\right)^2} \qquad 4.20$$

where b is the bandwidth of the windows and f_i, f_j are the center frequencies of windows i and j. The LRT for this case would be (19)

$$L(\underline{r}) = \underline{x}^T K^{-1} \underline{r} \qquad 4.21$$

where K is the covariance matrix which is composed of the above $\rho_{i,j}$'s and $\underline{x}$ is the mean vector of the set. This can be obtained by feeding the system in Figure 1 the signal x(t), with the coefficients $r_1, \ldots r_n$ in the figure interpreted as $x_1, \ldots x_n$. The vector $\underline{r}$ is composed of the set $r_1, \ldots r_n$ obtained by feeding the system in Figure 1 the signal r(t). To construct K we need also to know the variance of the channels

$$\underline{x} = \begin{bmatrix} x_1 \\ x_2 \\ x_3 \\ \cdot \\ x_n \end{bmatrix} \qquad K = \sigma^2 \begin{bmatrix} 1 & \rho_{12} & \cdots & \rho_n \\ \rho_{12} & 1 & & \\ \cdot & & \cdot & \\ \cdot & & & \cdot \\ \cdot & & & 1 \end{bmatrix} \qquad \underline{r} = \begin{bmatrix} r_1 \\ \cdot \\ \cdot \\ \cdot \\ r_n \end{bmatrix}$$

σ can be estimated from the r_i's i=1,....n following the same approach as before (eq. 13), if the noise spectrum is white. For colored noise we should whiten the signal before processing and then apply eq. 14.

It is shown later that the range resolution of the optimum receiver algorithm is not significantly degraded in comparison to the unprocessed signal, even when the frequency windows do not overlap. We will therefore not consider the case of overlapping frequency windows for target enhancement further.

Detection Performance

The next step is to evaluate the performance of the optimal processor which is optimum in the sense that it provides the best probability of detection for a given probability of false alarm for the analyzed range cell as defined in eq. (14).

We recall that in our procedure the original signal is segmented into m cells and then spectrally decomposed to obtain n random variables from which the LRT is calculated as depicted in Figure 2. Now let us assume a target somewhere along the A-line. We define the Probability of Detection, P_d as the probability that the processed data of the cell containing the target will exceed a certain threshold. The probability of false alarm P_f is defined as,

$$P_f = \sum_{i=1}^{\infty} P(f|k_i)p(k_i) \qquad 4.23$$

where $P(f|k_1)$ is the probability that the processed data of the i-th cell having a variance k_i times that of the target containing cell will exceed the threshold set for the k-th cell (the target cell). $p(k_i)$ is just the probability of finding such a ratio along the A-line. Naturally for each scenario of fluctuations appearing along the A line a different P_f will exist. In the next section we will describe the detection performance of the optimal processor for different k_i-s.

It is clear that the performance of an algorithm depends strongly on the distribution of $p(k_i)$. Naturally we cannot construct an algorithm that will be optimal for all possible fluctuations in the clutter variance along the A-line (i.e $p(k_i)$). A rough measure of comparison between algorithms might be to check $P(f|k_i)$ for the worst possible performing cell (the cell with the highest variance) and probability of detection for the cell with the lowest clutter power. In order for this test to be meaningful the algorithm should be monotonic in the sense that for 2 cells with $\sigma_1 > \sigma_2$ the probability of false alarm of the processed data of cell 1 will be equal or greater than the probability of false alarm of the processed data in cell 2.

It is important to note that the best detection procedure will not necessarily provide the best Receiver Operating Characteristics (ROC) for this problem. (Recall that ROC is a plot of the probability of detection as a function of probability of false alarm of a receiver for varying thresholds where usually the signal to noise ratio is a parameter). We will give a simple example for this argument. If all the m cells had the same variance, the optimum algorithm is the sum of the elements in each of the cells. Since the variance in all the cells is the same, the variance in the LRT becomes a proportionality constant and the LRT reduces

to the sum of the elements in each of the cells. The variance now no longer influences the ROC, it merely changes the threshold for which the probability of detection and the probability of false alarm is computed. This example shows that the best detection scheme for each of the cells (Which is composed of the estimated mean divided by the estimated standard deviation) is, in general, not the best algorithm for improving the ROC of the whole A line. The conclusion is that our optimum receiver has to be checked against other algorithms for different ratios of variance in the target range cell and the variance elsewhere. Depending on the actual conditions, an optimum algorithm can then be chosen.

If we knew the ratio k between the variances in the target range cell and the cell for which $P(f|k_i)$ is calculated, then an optimum receiver could be constructed. To derive the LRT for this case we use eq. 327 in chapter 2 vol. 1 of "Detection, Estimation, and Modulation Theory" (42). This equation is the general binary solution for the LRT for Gaussian random variables with different vector mean and covariance matrices. In our case the random variables are independent and the LRT reduces after some algebra to,

$$\frac{1}{2}\sum_{i=1}^{n} r_i^2(1-k) + \frac{k}{n}\left(\sum_{i=1}^{n} r_i\right)^2 = L(\underline{r}) \qquad 4.24$$

where k is the ratio of the variance of the cell containing clutter only to that of the target cell.

In this case the probability of false alarm will be determined by the cell containing only clutter and the probability of detection will be determined by the target size and clutter noise in the target range cell. $p(f|k_i)$ and p_d are calculated through,

$$P_d = \int_{\gamma}^{\infty} f_{L_1}(L_1)dL_1$$

$$P_f = \int_{\gamma}^{\infty} f_{L_o}(L_o)dL_o \qquad 4.25$$

where L_1 and L_0 are $L(\vec{r})$ for H_1 and H_0 respectively

Eq. 24 shows that the LRT can range from the sum of the r_i terms in each cell for k=1 to a close approximation of the variance of r_i for k>>1. Naturally choosing a given k for constructing the receiver would worsen the performance for any ratio which is greatly different from the chosen one.

In general, the probability density $p(k_i)$ of the clutter in the various cells of the A line will vary from one A line to the next, and will usually be unknown. Thus there is usually not enough information to construct an optimum receiver for a whole A line, and even if there were, the form of the algorithm would usually have to be changed for each A line which would be an extremely impractical procedure. We will therefore in most cases be constrained to restrict ourselves to the LRT of eq. 12 which provides the maximum probability of detection for a given probability of false alarms for a target in one single range cell.

Before analyzing the performance of the LRT we point out an important property of the function $L(\vec{r})$ which is identical with the well known Student t distribution. For this distribution

$$f_{L_o}(L_o) = \frac{\Gamma(\frac{n+1}{2})}{(n\pi)^{1/2}\Gamma(n/2)}\left[1 + \frac{L_o^2}{n}\right]^{-(\frac{n+1}{2})} \quad \text{for} \quad \mu = 0 \qquad 4.26$$

$$f_{L_1}(L_1) = \frac{n^{n/2}\, e^{-s^2/2}}{\sqrt{\pi}\,\Gamma(n/2)(n+s^2)^{n+1/2}} \sum_{i=0}^{\infty} \Gamma(\frac{n+i+1}{2})(\frac{s^i}{i!})\left[\frac{2L_1^2}{n+L_1^2}\right]^{1/2} \quad s = \mu/\sigma$$

where $f_{L_1}(L_1)$ is the density function of $L(\underline{r})$ if a target exists in the range cell and $f_{L_o}(L_o)$ is the density function of $L(\underline{r})$ if no target exists in the range cell ($\mu=0$).

This distribution can be seen to have the property that the probability density function $f_{L_o}(L_o)$ is only a function of n, the number of windows. Thus for $\mu=0$, i.e. in the absence of a target the variance of $L(\underline{r})$ is independent of the variance of the spectral decomposition components r_i. One of the consequences of this property is that even though an A line may exhibit strong noise fluctuations in different range cells, its LRT $L(\underline{r})$ will have constant variance in every range cell. Another consequence is that using eq. 12, the false alarm rate for cells not containing targets for a given threshold is independent of the noise in these cells. This is clearly a very useful property.

The number of variables in the LRT equation (eq. 11) is too large to fully demonstrate its detection properties on one graph. We chose therefore to set a constant false alarm probability and plot the probability of detection as a function the input of signal to noise voltage ratio in the target range cell. False alarm probability P_f and probability of detection P_d are determined from eqs. 25 and 26, using tables of the student t distribution. The parameter was chosen to be the number of elements in the expansion (or the number of independent windows). In Figure 3 and 4 we present the theoretical results for several n the number of windows. It is clear that increasing the number of windows improves the ROC. Of course as n increases the width of each spectral window decreases which increases the time window $[T_i,T_f]$ and then worsens the resolution. Figure 3 correspond to a constant probability of false alarm (CFAR) of 0.01 and Figure 4 correspond to a CFAR of 0.05. One can immediately observe that as the number of elements n in the expansion

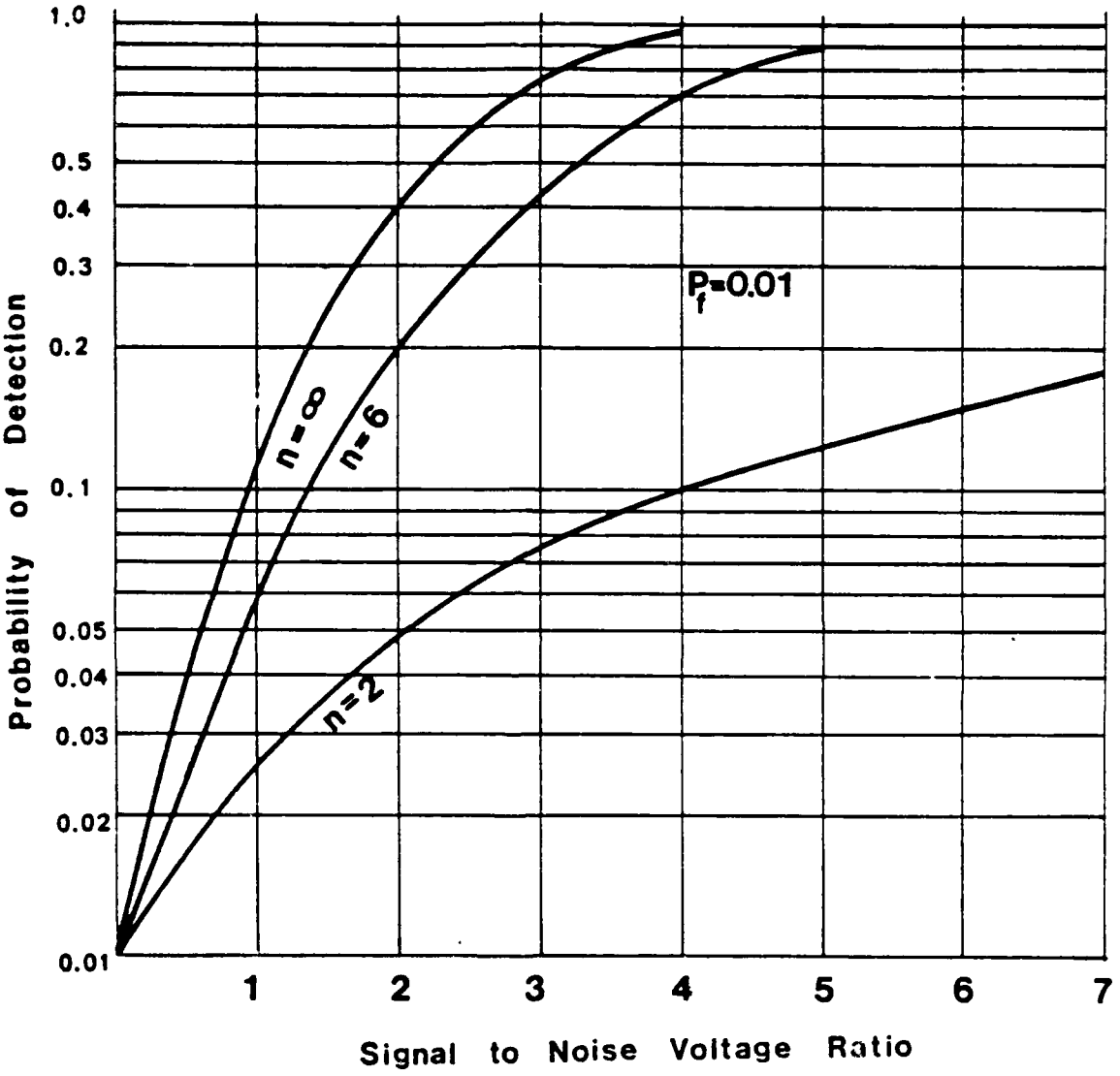

Figure 4.3 Detection probability versus signal-to-noise voltage ratio for optimal processing for various expansion sizes n. The probability of false alarm is set to 0.01. (taken from 36)

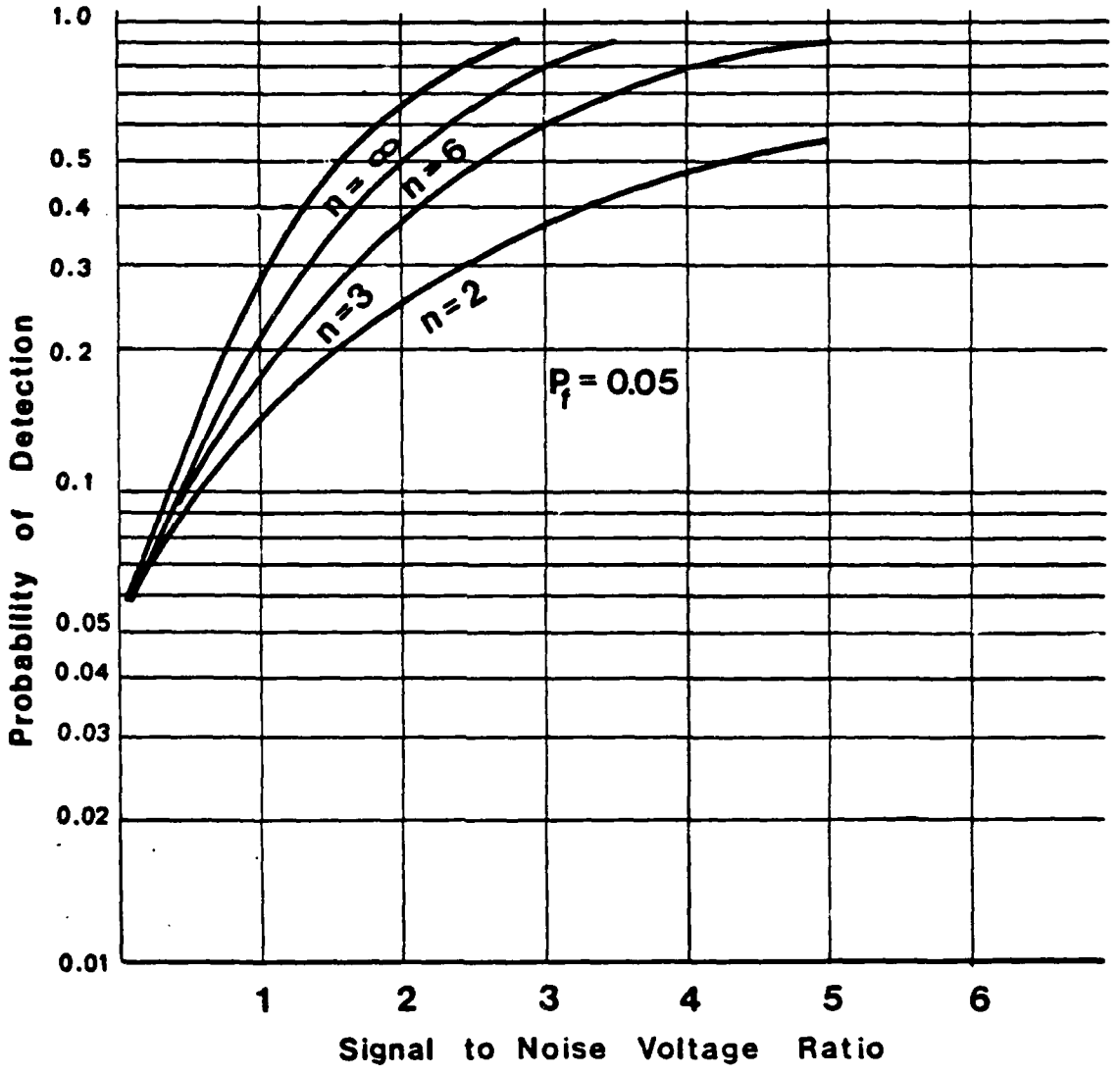

Figure 4.4 Detection probability versus signal-to-noise voltage ratio for optimal processing for various expansion sizes n. The probability of false alarm is set to 0.05. (taken from 36)

increases the performance of the algorithm improves. As mentioned above the performance as shown is also independent of the relative strength of the clutter noise in the different cells but depends only on the signal to noise ratio in the target cell. Thus if we had only clutter with varying parameters along the A line the processed data would have the same statistical properties for all the cells containing only clutter.

In general signal processing algorithms used to reduce clutter do not give results which are independent of the clutter noise in the processed range cell. Thus in the "Minimization" algorithm, analyzed in Chapter 3 the variance of the processed clutter data is a function of the noise variance of the cell before processing and therefore P_f strongly depends on the nature of the fluctuations of the clutter noise $p(k_i)$. Note that for the optimal processing described by eq. 12 P_f is independent of the fluctuations in the clutter noise variance $p(k_i)$ since in this case $P(f|k_i) = P_f' = \text{constant}$ so that $P_f = \sum_{i=1}^{\infty} p(f|k_i)p(k_i) = P_f' \sum_{i=1}^{\infty} p(k_i) = P_f'$.

In figures 5(A)-(D) the performance of the minimization algorithm is compared with that of the optimum receiver on the basis of detection properties for different values of the ratio k of clutter standard deviation σ_0 in the 'worst' cell of the A line to the clutter σ_1 in the target range cell. Each graph corresponds to a certain value of k. We set $p(f|k_i)$ in all the graphs to be 0.05.

In general one can see that the performance of the optimum receiver is independent of k because the 'Student' t distribution variance is independent of the clutter as explained above whereas the performance of the Minimization algorithm is good only for high enough input signal to noise ratio. (However the signal to noise ratio obtained by the Minimization algorithm is much better than the SNR obtained by the optimal processing due to the nonlinear nature of the Minimization algorithm as is shown in

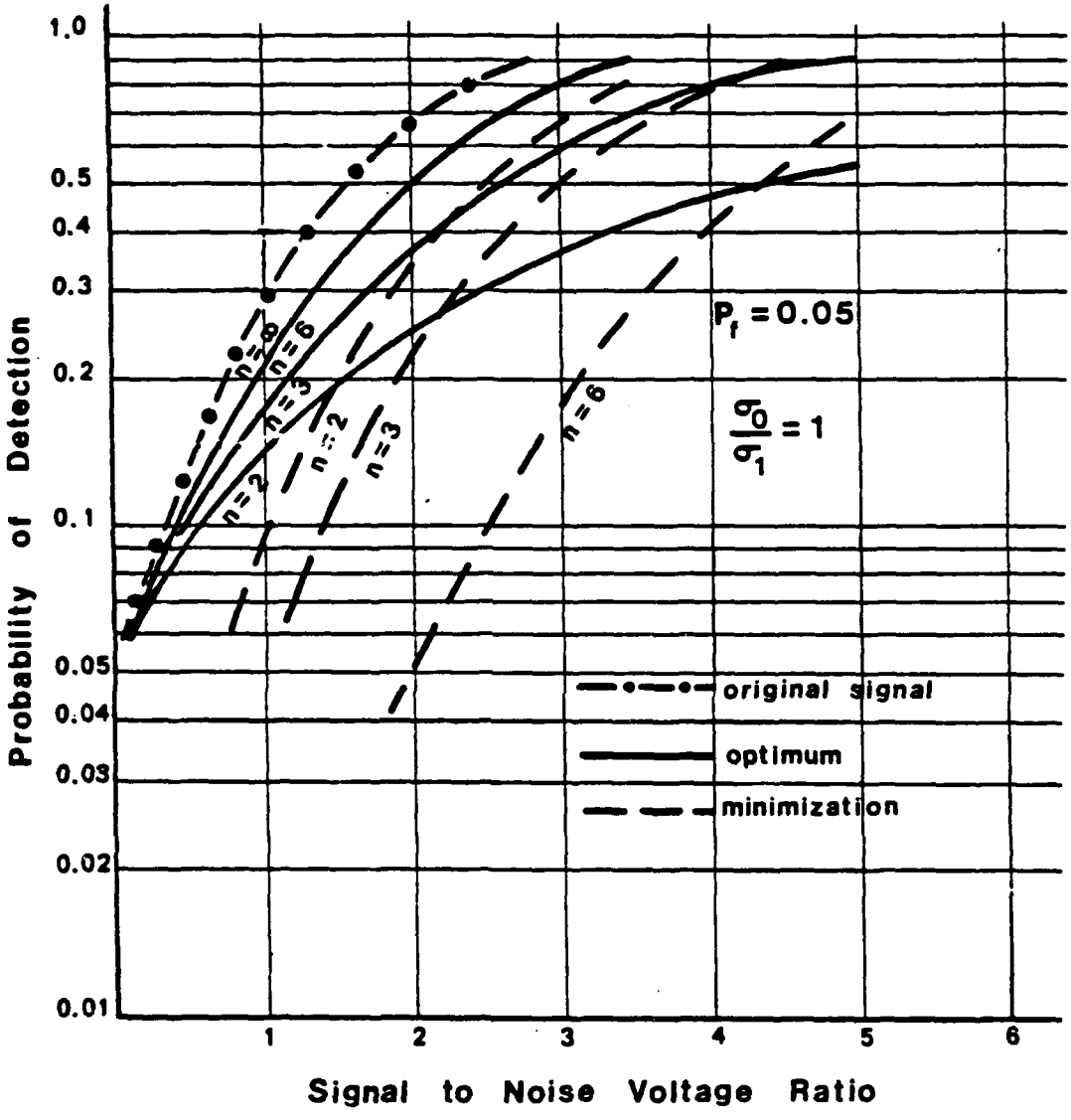

Figure 4.5(A) Detection probability versus signal-to-noise voltage ratio for optimal processing, the original deconvolved signal and the minimization algorithm for $\sigma_0/\sigma_1=1$. σ_0/σ_1 is the ratio between the standard deviation of a cell containing only clutter and the variance in the target range cell.

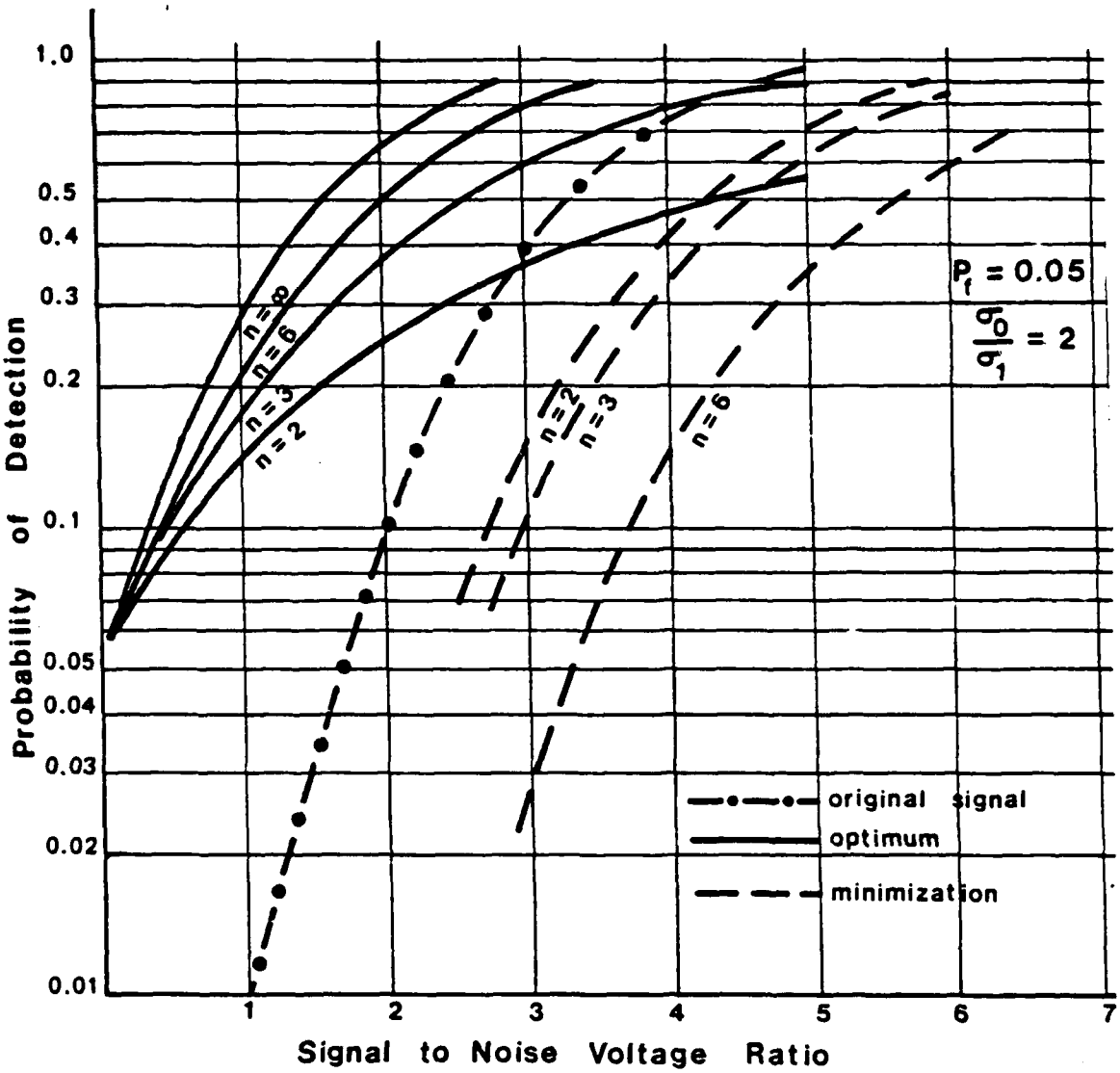

Figure 4.5(B) As in Figure 5(A) but with $\sigma_0/\sigma_1=2$

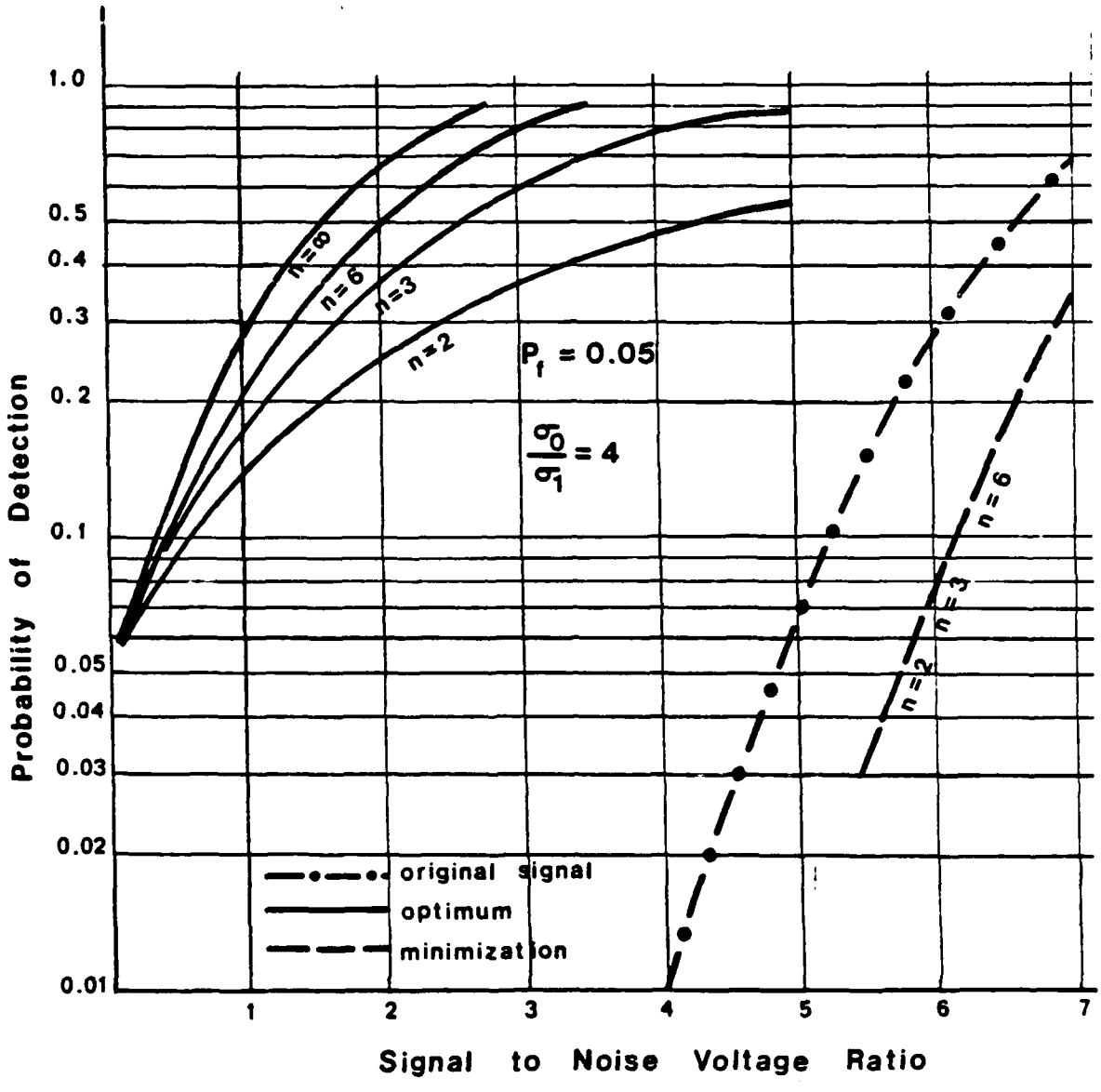

Figure 4.5(C) As in Figure 5(A) but with $\sigma_0/\sigma_1=4$

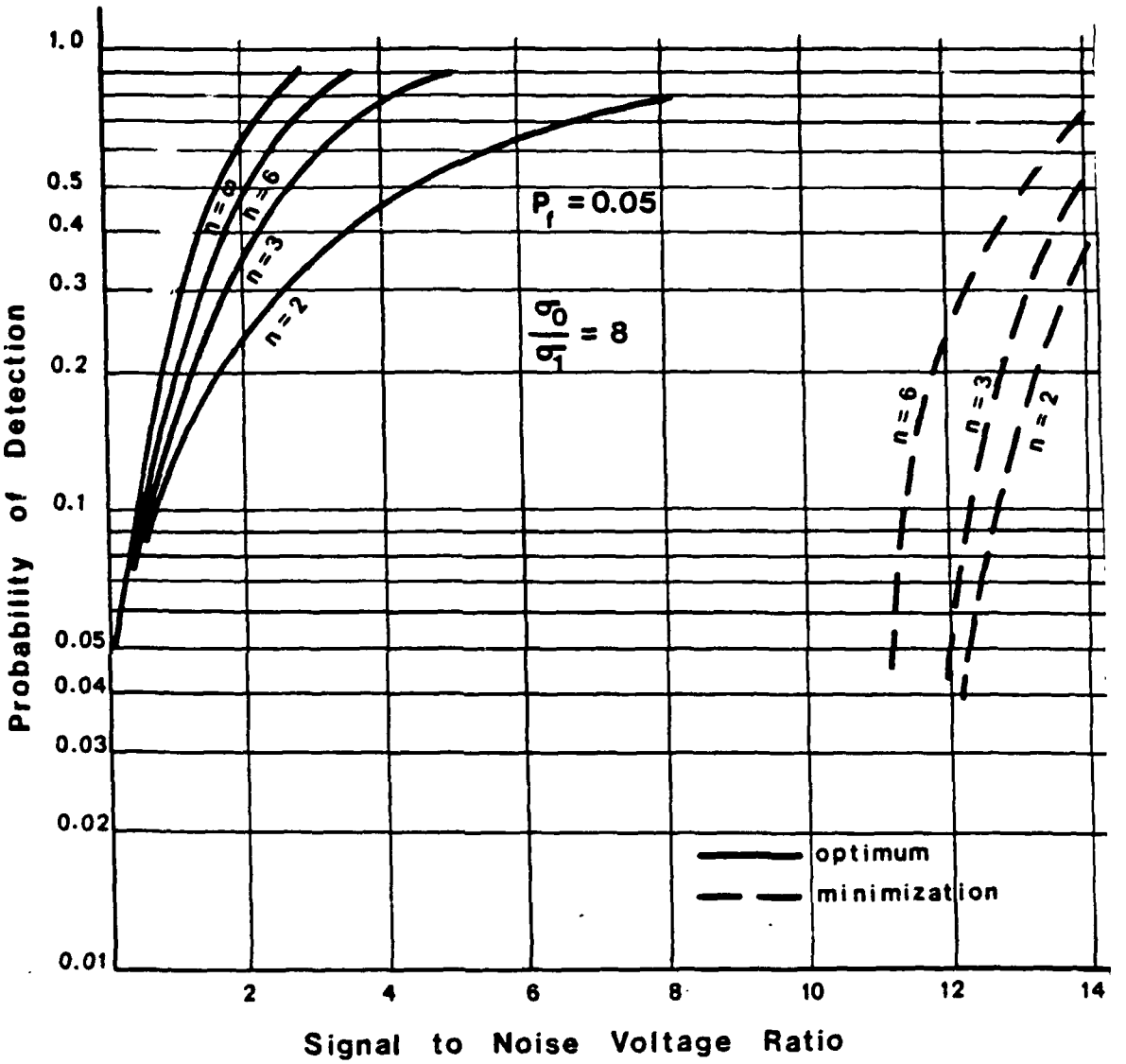

Figure 4.5(D) As in Figure 5(A) but with $\sigma_0/\sigma_1=8$

chapter 3). Figure 5 also shows curves labelled "original signal". For this curve the LRT function used was that obtained by simply summing the outputs of the spectral decomposition components r_i for each range cell (without division by the estimated standard deviation). The use of the sum of r_i's as an algorithm is attractive due to the simplicity in implementation and with the simplifications that we introduce later the optimum processing for $n=\infty$ is equivalent to simply thresholding the original signal deconvolved in the frequency range of interest to obtain P_d and P_f.

These were computed using the equations

$$P_d = \frac{1}{\sqrt{2\pi}\sigma} \int_{\gamma}^{\infty} e^{-\frac{(x-m)^2}{2\sigma^2}} dx$$

$$P_f = \frac{1}{\sqrt{2\pi}\, k\sigma} \int_{\gamma}^{\infty} e^{-\frac{x^2}{2\sigma^2 k^2}} dx \qquad 4.27$$

Figure 5(A) shows that, as was pointed out earlier, this type of processing is also the optimum if the clutter noise power is a constant along the A-line (k=1). It is clear that for higher ratios of k the performance of such an algorithm will deteriorate, as is seen in Figures 5(A)-(D).

The results shown in Figure 5 (A-D) may be summarized as follows. For a finite number of windows the Minimization algorithm, (which is very powerful in enhancing signal to noise ratio) is superior to the optimum receiver scheme in detection performance for large input signal to noise ratio. This is due to the fact that while the optimum processing is insensitive to the variances ratio k the Minimization performs especially well in high signal to noise ratios for which the peak target echo is practically not effected by the low noise power in the target range cell.

However the high noise variance in the worst performing cell is strongly reduced by Minimization in a non linear fashion that provides a superior ROC. As the ratio k increases the apparent advantages of the optimal processor over the Minimization algorithm and the unprocessed signal become more evident. Note also that for high enough ratio (e.g k=8) the Minimization algorithm performance is superior to that of the unprocessed signal. A surprising result is the fact that for low clutter density fluctuations (k=1 and k=2) increasing the number of frequency windows results in deterioration in the ROC of the Minimization algorithm.

EXPERIMENTAL RESULTS

In this section we describe an experimental realization of the optimum detector algorithm. Some simplifications are made that allow easy implementation of the technique in practical applications.

Recall that the filters in the K.L expansion are matched filters with frequency response shape of $\sin\pi\, T(f_n-f)/\pi(f_n-f)$. In our experimental realization Gaussian shape filters were used in order to taper the effect of the sharp edges of the window. This use of non-matched filters will now be justified after clarifying some assumptions and summarizing some known results.

Up to this point we have not concerned ourselves with the transmitted spectrum shape. In ultrasound imaging it can often be assumed, due to the transducer impulse response, that the spectrum shape of the received signal is roughly Gaussian. It is shown in appendix A that filtering such Gaussian signals with Gaussian shape filters result in Gaussian shape outputs. If the frequency spectrum of the input signal is much broader than that of the filters the mean frequency and the standard deviation of

the output signals will be practically unchanged. It is also shown that the peak amplitude of a target echo will appear at the same range delay for all the filters whatever their center frequency. If we normalize each of the filters (an operation which is equivalent to whitening the process within the desired frequency range and practically involves assigning a constant multiplier to the filters so that their output power in the different channels will be identical), then the peak amplitudes appear at the same range delay and have the same amplitude.

We can assume that the clutter noise spectrum in the input of each filter is much wider than the filter bandwidth, thus for the sake of comparison between the matched and non-matched filters we can assume the clutter noise to be white. In this case (see for example (44)) the detection properties of a matched filter at a specific range delay depend as is well known on the parameter $d=\sqrt{\frac{E}{2N_o}}=\frac{m}{2\sigma}$ which is the parameter that defines the ROC performance of a receiver. Where E is the energy of the signal to which the filter is matched, N_o is the one sided spectral density of the clutter noise, m is the mean of the matched filter output for a target plus noise in the filter input and σ is its standard deviation. For the detection of a signal with additive Gaussian noise the distance is a function of the signal strength m and the noise variance. For mathematical simplicity assume that the filter is matched to a burst of duration ΔT instead of a Gaussian shaped signal. In this case

$$E = \frac{A^2 \Delta T}{2}$$

and

$$d = \sqrt{\frac{A^2 \Delta T}{4N_o}} = \sqrt{\frac{A^2}{4N_o B}} = \frac{A}{2\sigma} \quad ; \quad \sigma^2 = N_o B \; ; \quad B \cong \frac{1}{T} \qquad 4.28$$

So the distance $m/2\sigma$ for a filter matched to a burst of length ΔT is $A/2\sqrt{N_0B}$ (see for example 59) but this is the statistics of the range delay corresponding to the expected peak target echo when filtered by a simple filter of bandwidth b. Its mean will be A and the standard deviation will be $\sqrt{N_0B}$ (assuming of course that the peak echo amplitude will not be reduced considerably due to filtering). We conclude therefore that it is possible to use simple filtering instead of matched filtering without a substantial loss of performance. In our realization the maximum likelihood ratio was computed from the estimated mean and variance from the n outputs of the non-matched filters for each range delay.

In the experiments the target echo and the clutter echo were created separately. The clutter signal consisted of the echo received from grainy metal, whereas the target signal consists of the echo reflected from a flat surface. This makes it easy to change the signal to noise ratio of the received echo. The received signal was amplified and digitized at the RF level using a 50 MhZ digitizer (Biomation). The information from the Biomation buffer was read into a PDP 11-23 computer. An FFT was then performed and the spectrum was split into 10 non-overlapping Gaussian windows. Instead of using eq. 8 directly we adjusted the filters gain to obtain a white spectrum in the frequency range of interest and then applied eq. 12.

In Figure 6(A) a typical echo from a target plus clutter echo is shown. In this case the spectrum of the received signal was split into 10 channels with identical bandwidths. Though there was some correlation between the channels the amount of overlap was relatively small and we assumed the channels to be uncorrelated. This assumption simplifies the computations needed to obtain the Likelihood Ratio Test. In Figure 6(B)

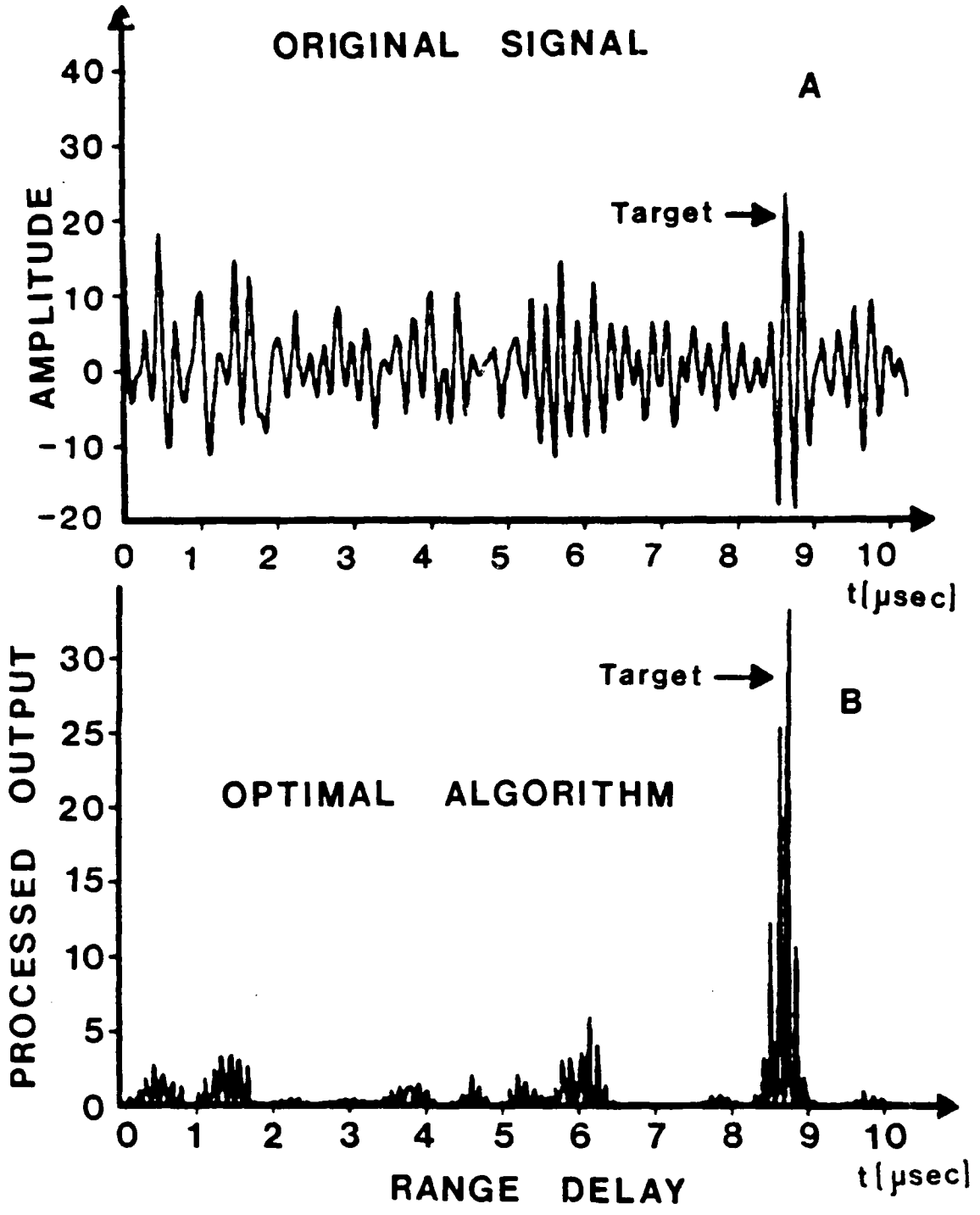

Figure 4.6(A) Simulation of a received signal from a target plus clutter. (B) Processed output for optimal processing b=0.2 MHz and n=10 windows.

the Likelihood Ratio Test is plotted as a function of delay. It is seen that the ratio reaches its peak at the target range delay as is expected.

For target enhancement we might consider using the LRT instead of the original signal. This will eliminate problems of incorrectly presenting target size embedded in homogenous (i.e. uniform) type clutter (such as grains for example) due to attenuation or shadowing. In these cases the local signal to noise ratio is the right measure of the target size.

RESOLUTION AND RANGE BIAS

The theoretical evaluation of the resolution and range bias for both the Minimization algorithm and the optimum receiver present a challange. Though numerical calculation is possible it was found easier to evaluate these properties empirically.

We examined these properties by simulation. Two target echoes at different distances were summed and both types of processing were applied to the signals. These distances were changed from half a wavelength up to several range cells and three parameters were observed. The first was the ability to resolve the signals by eye, the second was the effect of the processing on the amplitude of the processed signal and the third was bias (i.e change) in the distance between the signals due to processing. It is clear that signals in proximity will have an adverse effect on each other. For the Minimization procedure this is due to the increased probability of one echo target reducing the other and for the optimum procedure it is due to increased variance caused by the neighboring target.

It was found that the resolution is phase sensitive. For example for about half a wave length distance between the signals, which means that they were completely unresolved before processing, they were resolved

for the optimal procedure after processing but were very noisy for the Minimization algorithm, as can be seen in Figures 7(A),(B) and (C) for both the suboptimum receiver and the minimization algorithm. However for an initial distance of a full wave length the signals were unresolveable (Figure 8). This behavior was found to be cyclic, i.e for an even number of half wavelengths the signals were not resolveable while for an odd number of half wave lengths the signals were resolveable for optimal processing and noisy and meaningless for minimization. For a distance larger than the original range cell (defined by the bandwidth of the transmitted signal) the signals were always fully resolveable for optimum processing (Figures 9,10). (However for minimization the signals were resolved only for a distanct of 8 wave lengths and above). It is important to note that these empirical results were obtained for a certain system and two processing configurations, namely 5 MHZ transducer and either, 4 or 10 frequency windows.

Further work is needed to establish the general resolution properties of the optimum receiver and the minimization algorithm. However it seems that there is no significant degradation in resolution produced by these types of signal processing for targets positioned by more than one range cell apart.

The above results were obtained without any added noise and it is of importance to investigate these results under noisy conditions. A clue to the behavior under noisy conditions can be learnt from the effect of the processing on the signal amplitude of the two adjacent signals. One can see the amplitude of the processed signals as a function of separation It is seen that in general the amplitude of the processed data is reduced substantially if the separation is smaller than the input range cell. In

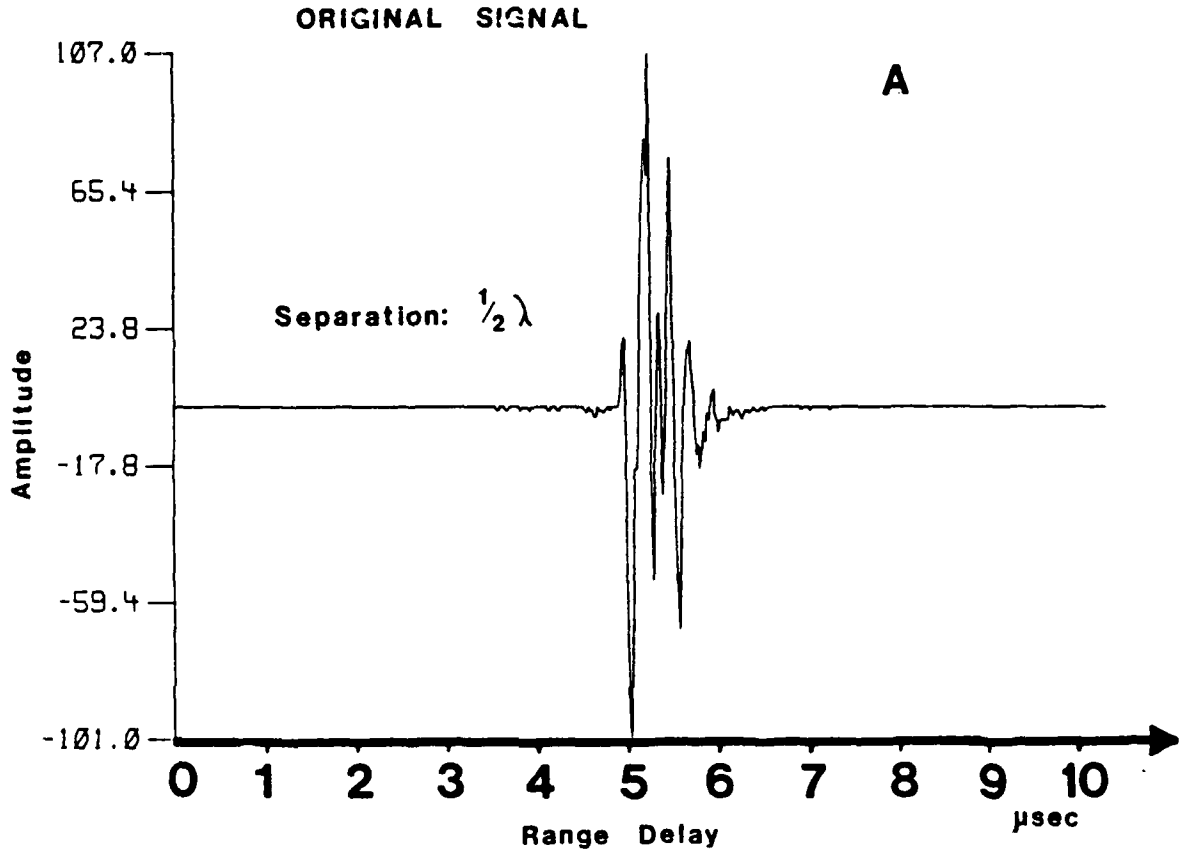

Figure 4.7(A) Simulation of the echo from two targets 1/2 a wavelength apart.

(B) Processed output for optimal processing of the signal in Figure 11(A). Note that the targets are resolved but that there is a bias in the distance between them and that their amplitude is substantially reduced.

(C) Processed output for the minimization algorithm of the signal in Figure 11(A) Note that the signals are not resolved and that the amplitude of the processed data is substantially reduced.

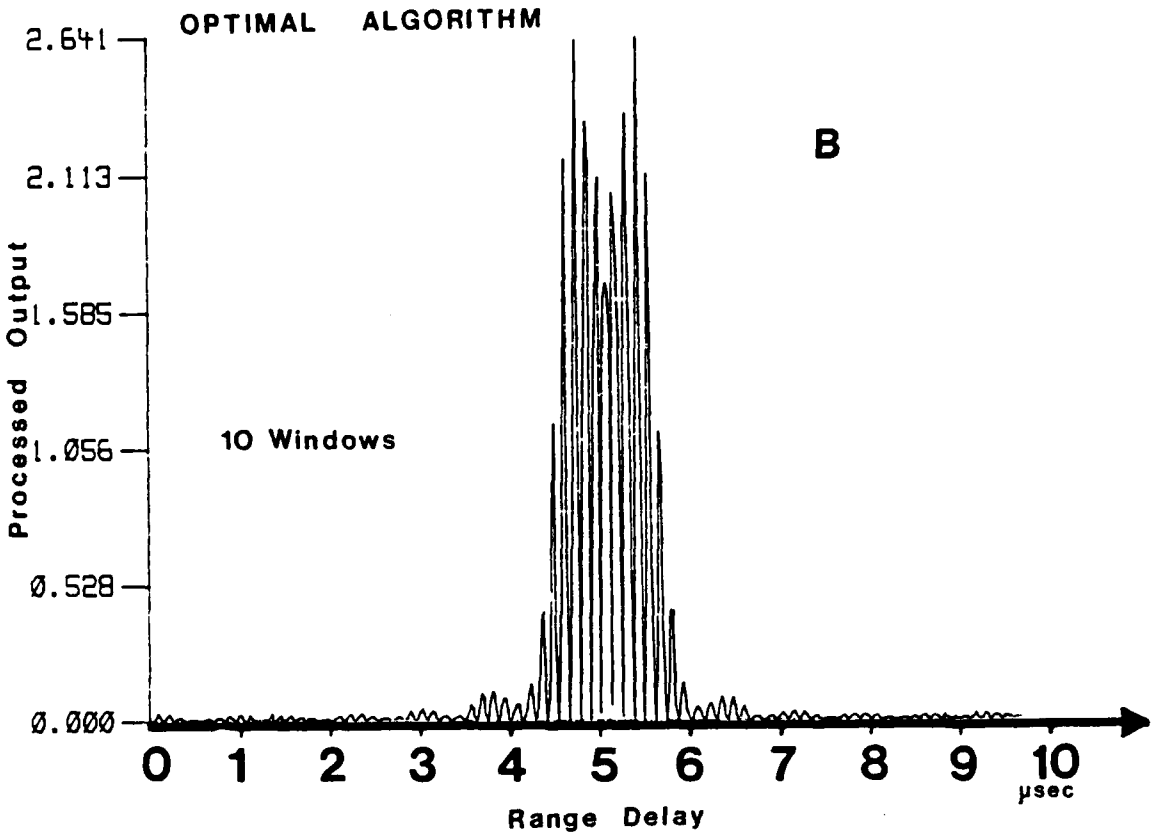
OPTIMAL ALGORITHM
B
2.641
2.113
1.585
1.056
0.528
0.000
Processed Output
10 Windows
0 1 2 3 4 5 6 7 8 9 10
μsec
Range Delay

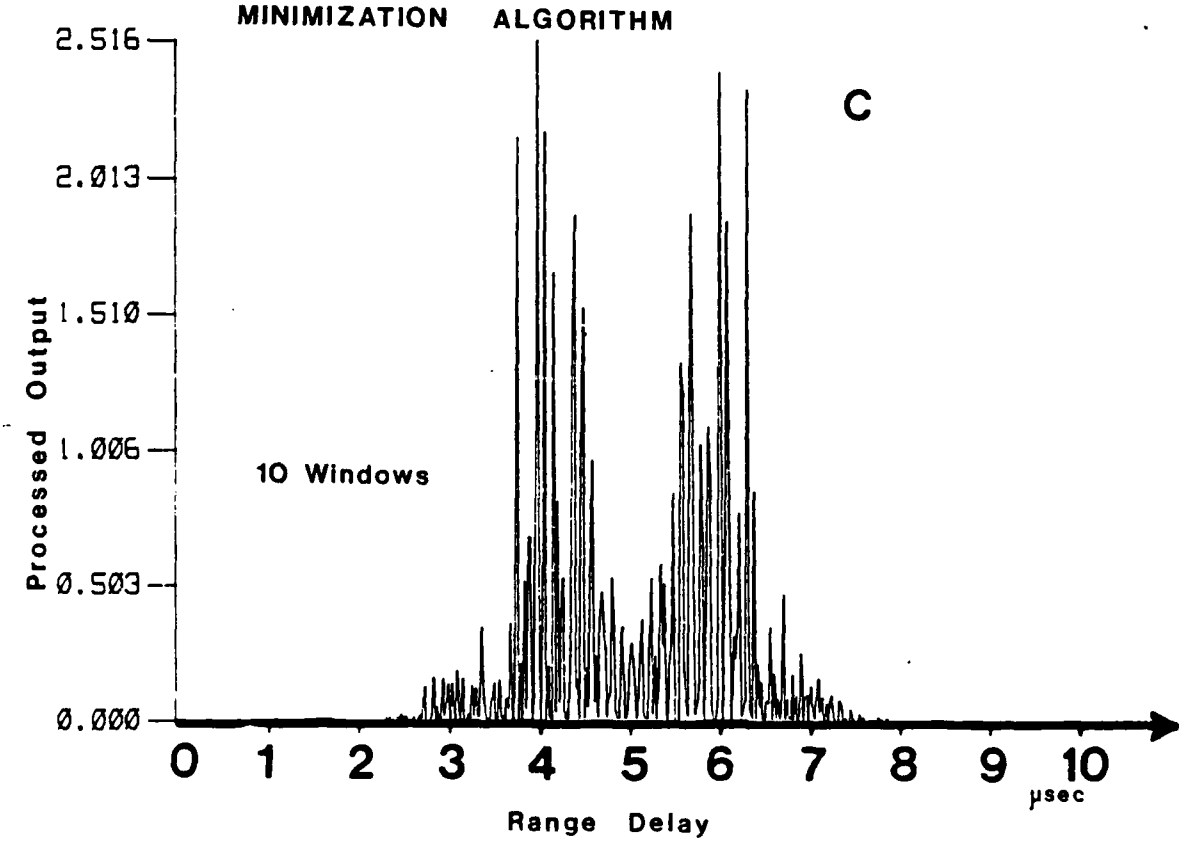
MINIMIZATION ALGORITHM
C
2.516
2.013
1.510
1.006
0.503
0.000
Processed Output
10 Windows
0 1 2 3 4 5 6 7 8 9 10
μsec
Range Delay

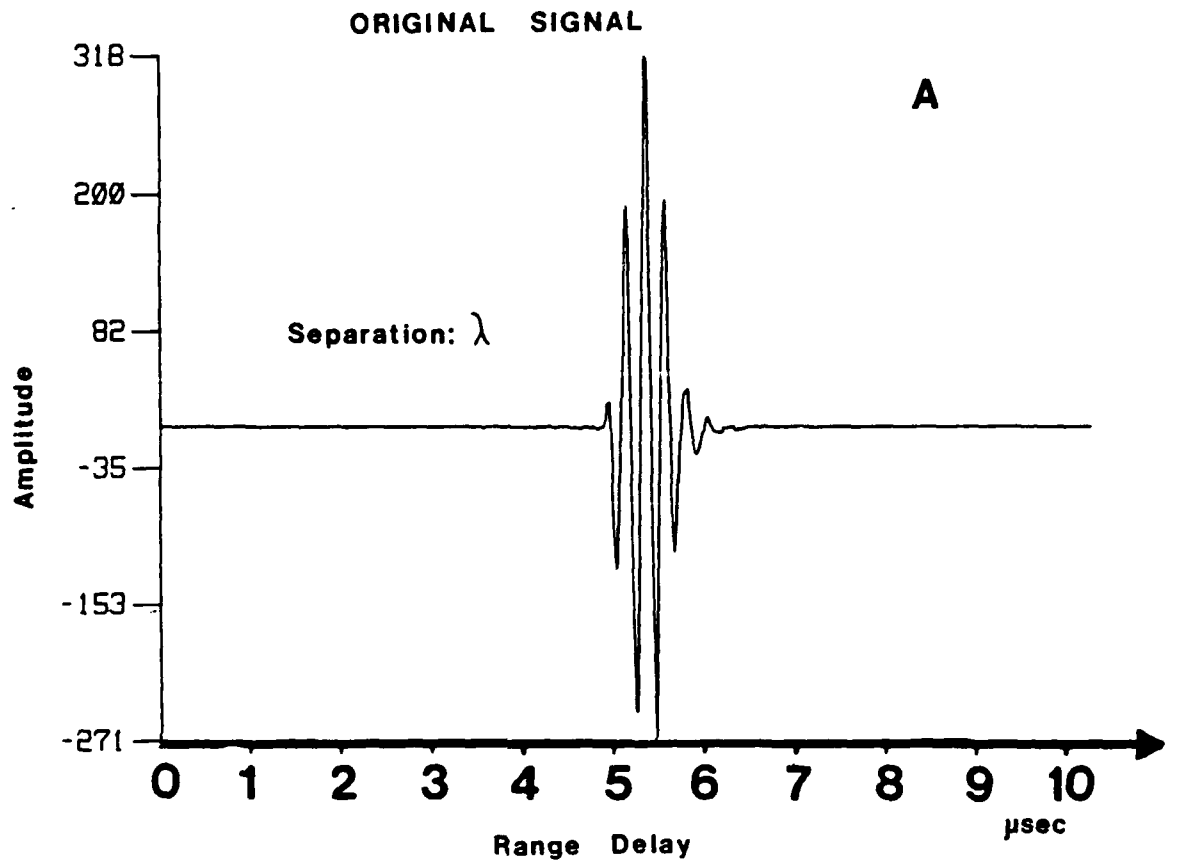

Figure 4.8(A) Simulation of the echo from two targets a full wave length apart.

(B) Processed output for optimal processing for the signal in Figure 12(A). Note that the targets are not resolvable but that the amplitude is large.

(C) Processed output for the minimization algorithm for the signal in Figure 12(A). Note that the targets are not resolvable.

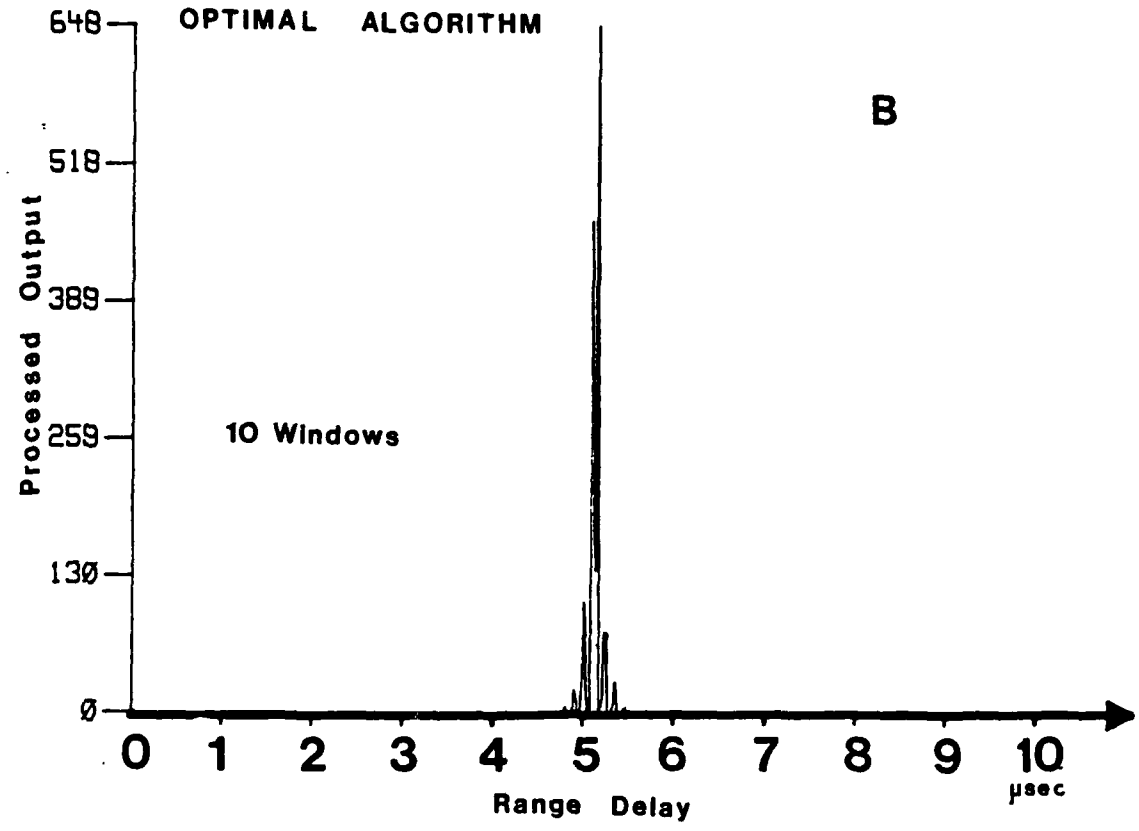
OPTIMAL ALGORITHM
B
648
518
389
259
130
Ø
Processed Output
10 Windows
0 1 2 3 4 5 6 7 8 9 10
μsec
Range Delay

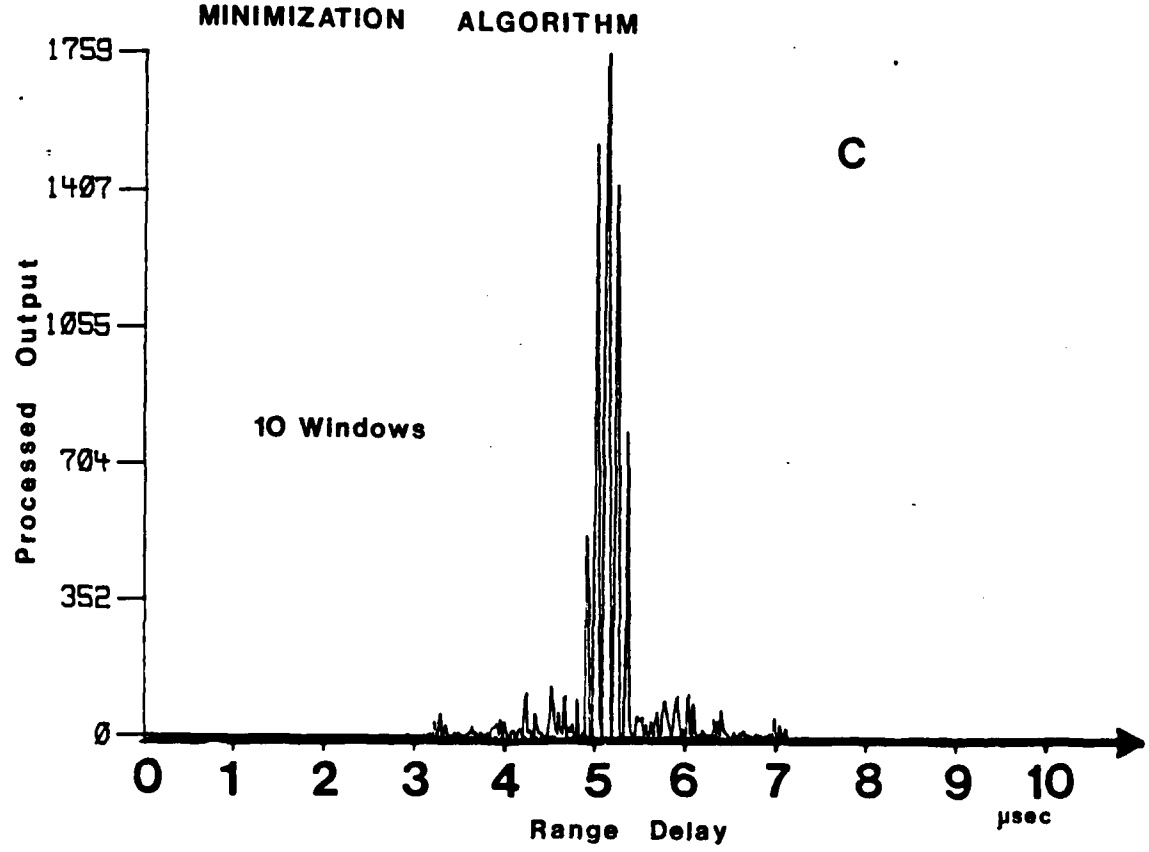
MINIMIZATION ALGORITHM
C
1759
1407
1055
704
352
Ø
Processed Output
10 Windows
0 1 2 3 4 5 6 7 8 9 10
μsec
Range Delay

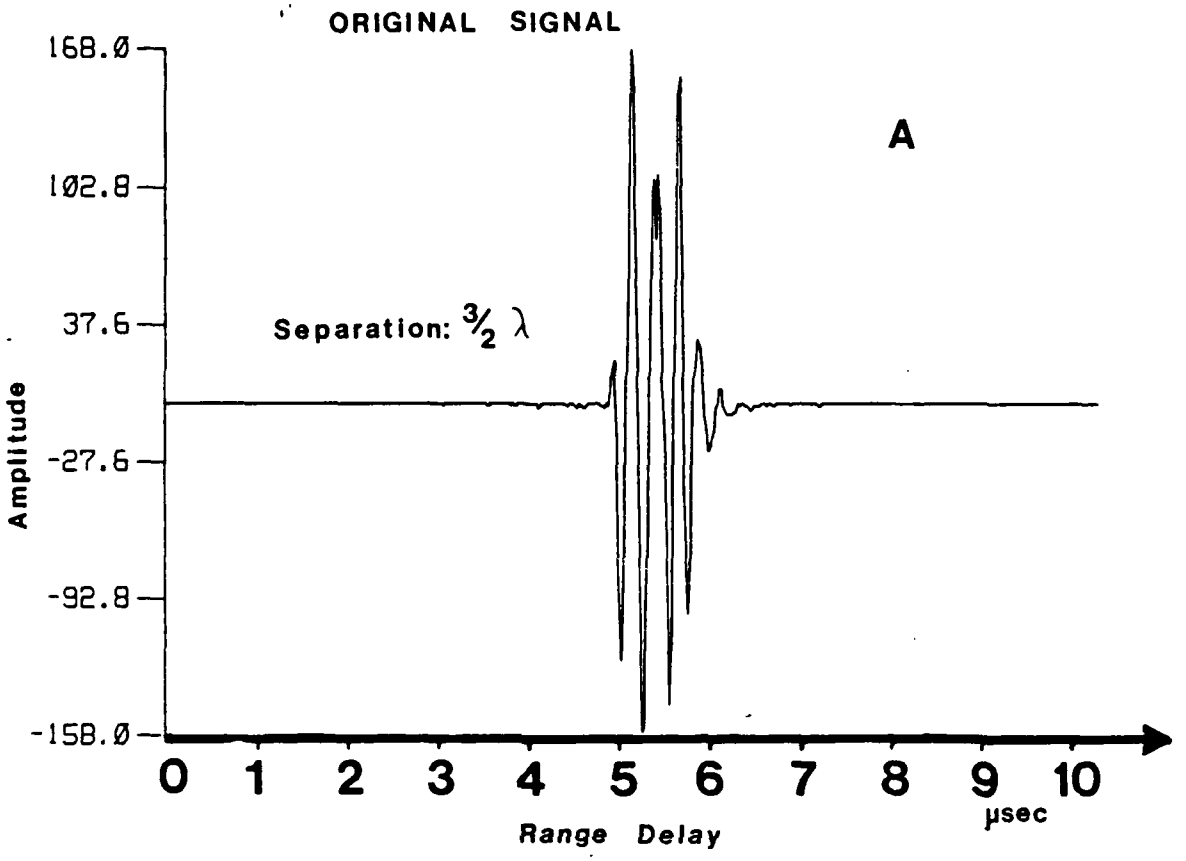

Figure 4.9(A) Targets separated by 3/2 wavelengths.

(B) Processed output for the Optimal Processing. The targets are resolvable and there is a bias in the distance between them.

(C) Processed output for the Minimization Algorithm. The signals are very noisy and not resolvable.

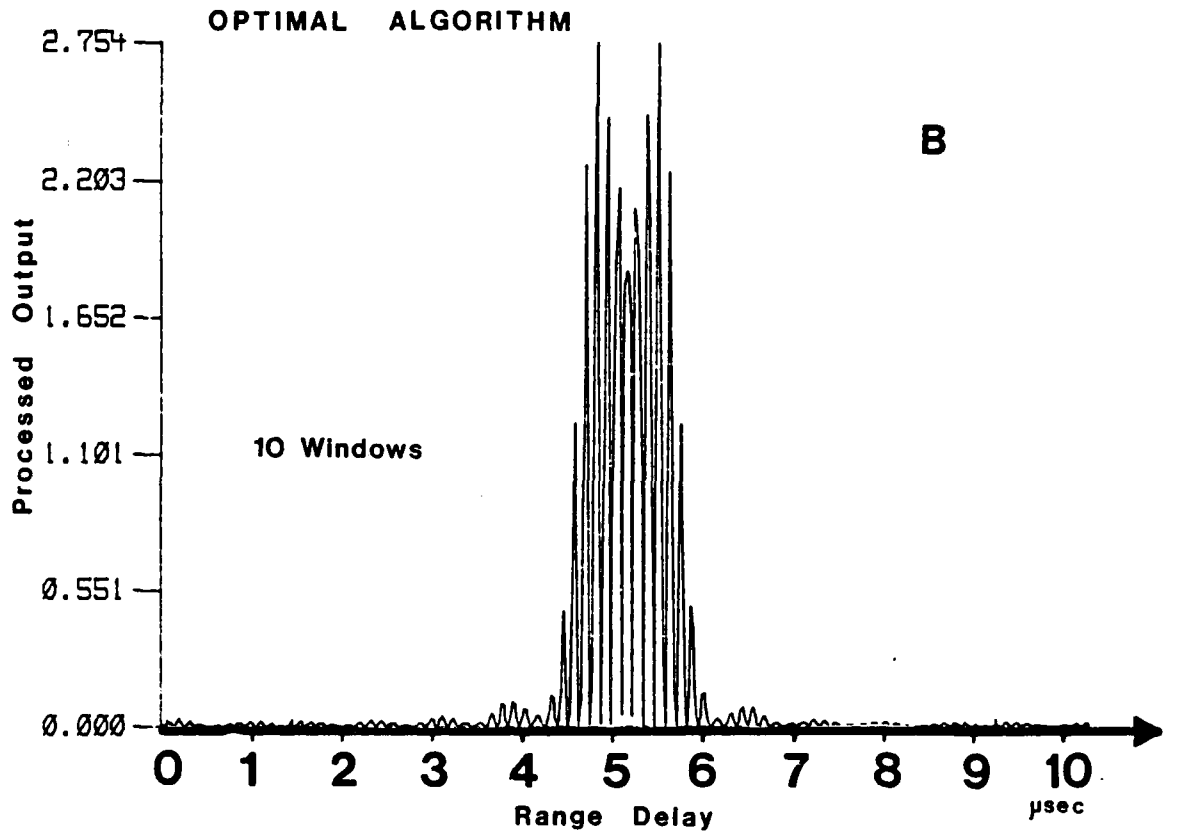
OPTIMAL ALGORITHM
B
2.754
2.203
1.652
1.101
0.551
0.000
Processed Output
10 Windows
0 1 2 3 4 5 6 7 8 9 10
μsec
Range Delay

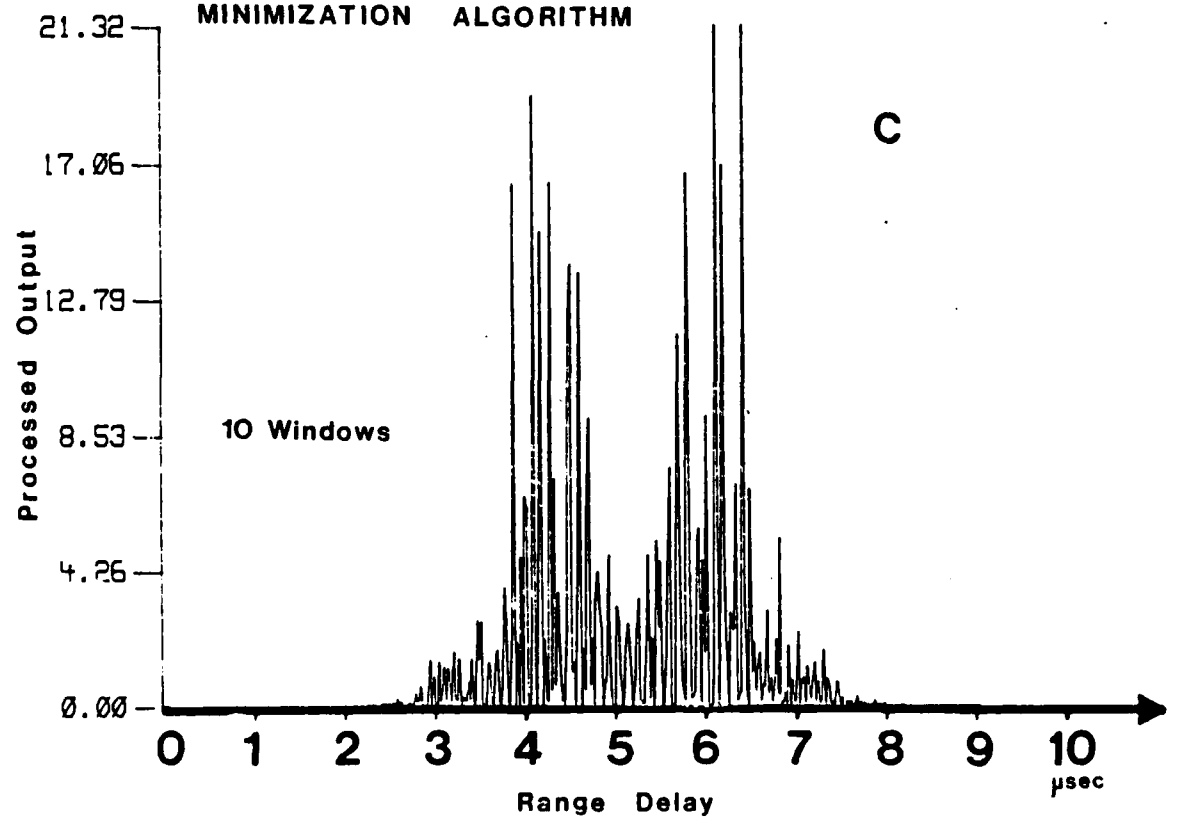
MINIMIZATION ALGORITHM
C
21.32
17.06
12.79
8.53
4.26
0.00
Processed Output
10 Windows
0 1 2 3 4 5 6 7 8 9 10
μsec
Range Delay

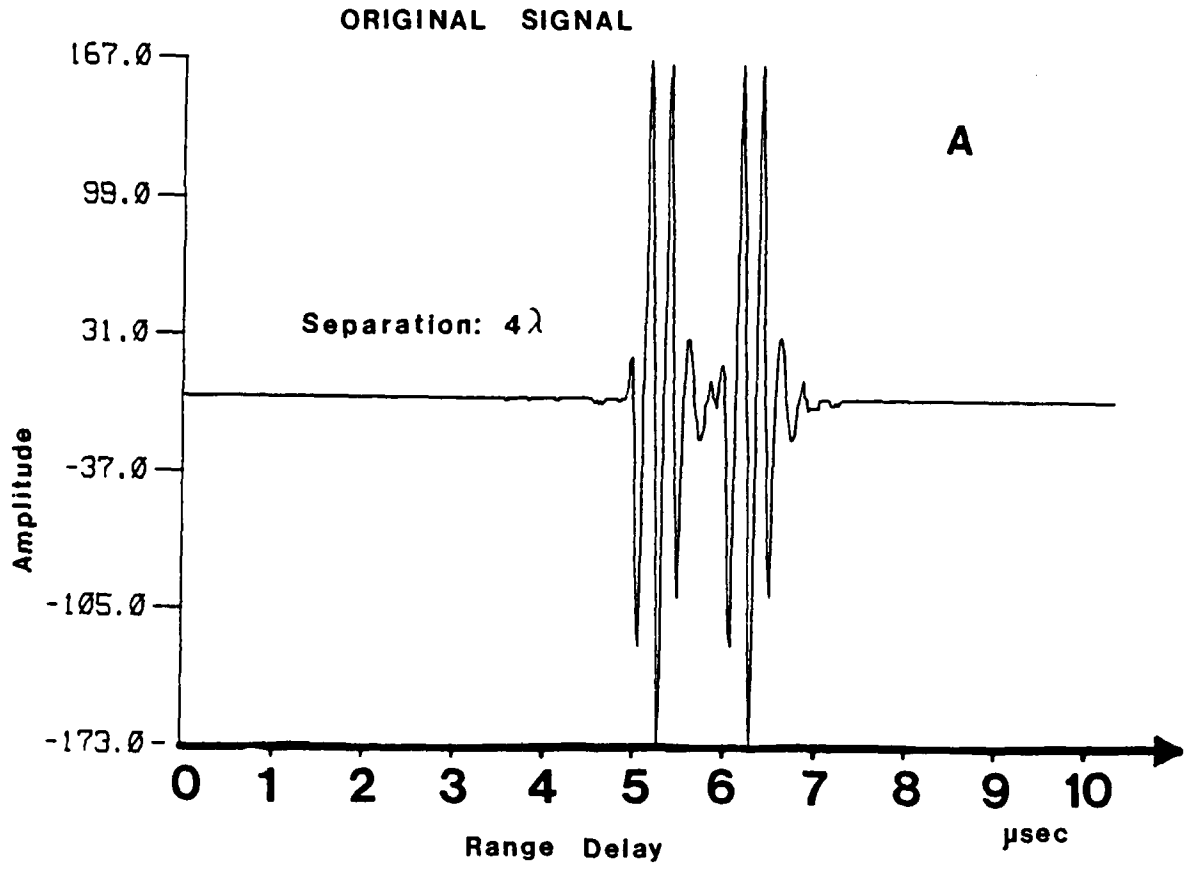

Figure 4.10(A) Targets separated by 4 wavelengths.

(B) Processed output for the Optimal Processing. The signals are fully resolvable and the signal-to-noise ratio is high.

(C) Processed output for the Minimization Algorithm. The output is noisy and the signals are not resolvable.

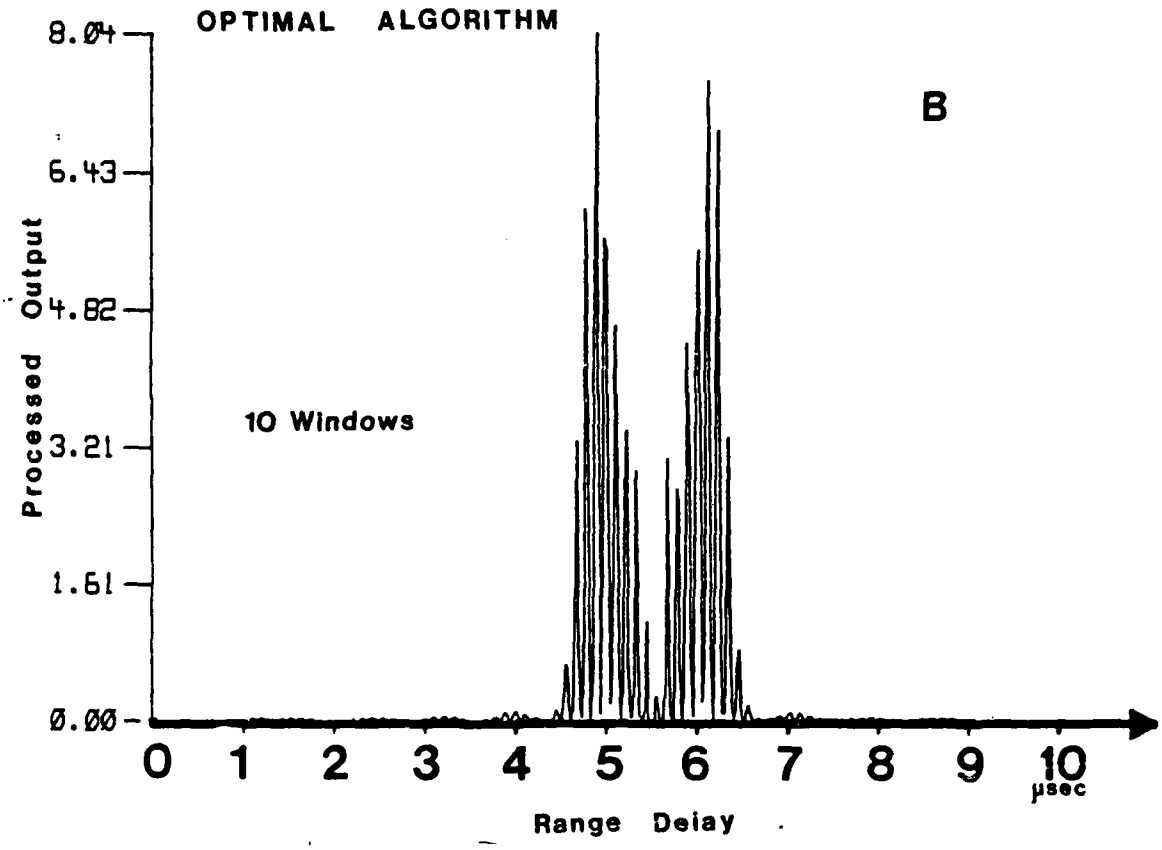
OPTIMAL ALGORITHM
B
8.04
6.43
4.82
3.21
1.61
0.00
Processed Output
10 Windows
0 1 2 3 4 5 6 7 8 9 10
μsec
Range Delay

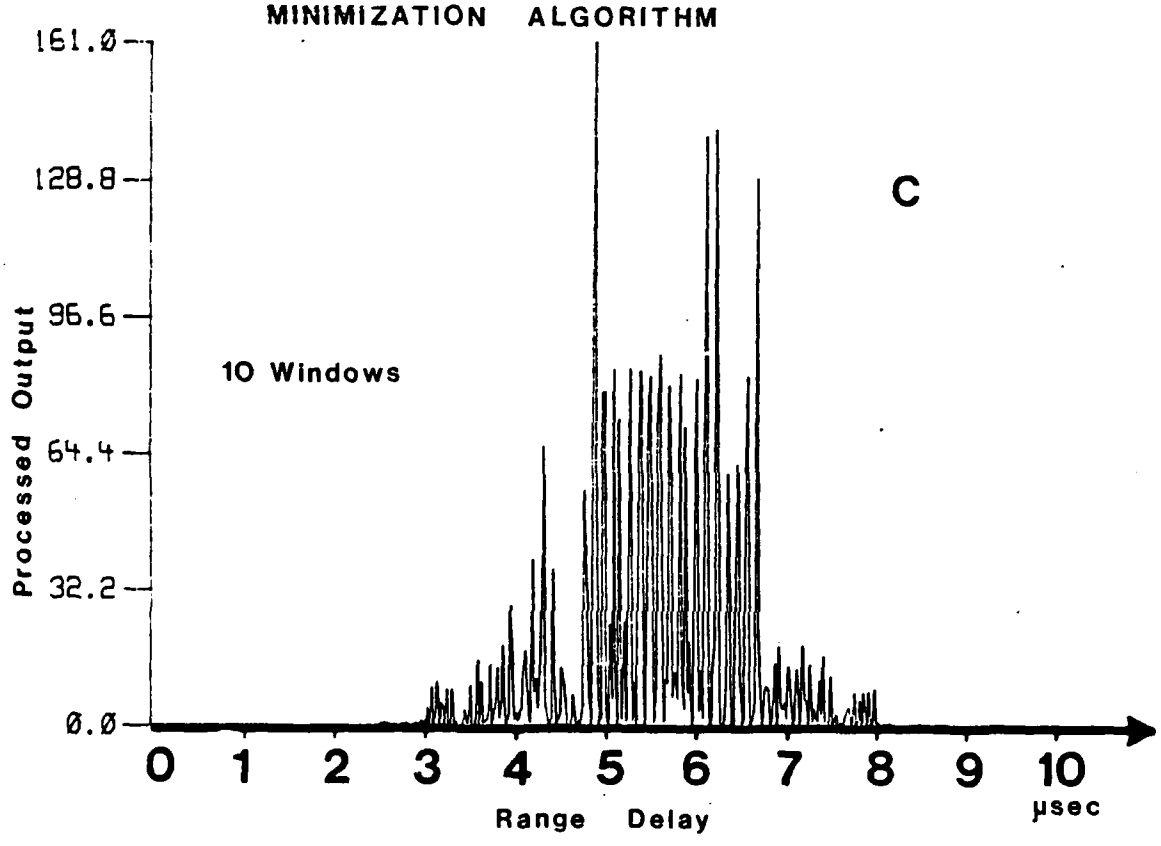
MINIMIZATION ALGORITHM
C
161.0
128.8
96.6
64.4
32.2
0.0
Processed Output
10 Windows
0 1 2 3 4 5 6 7 8 9 10
μsec
Range Delay

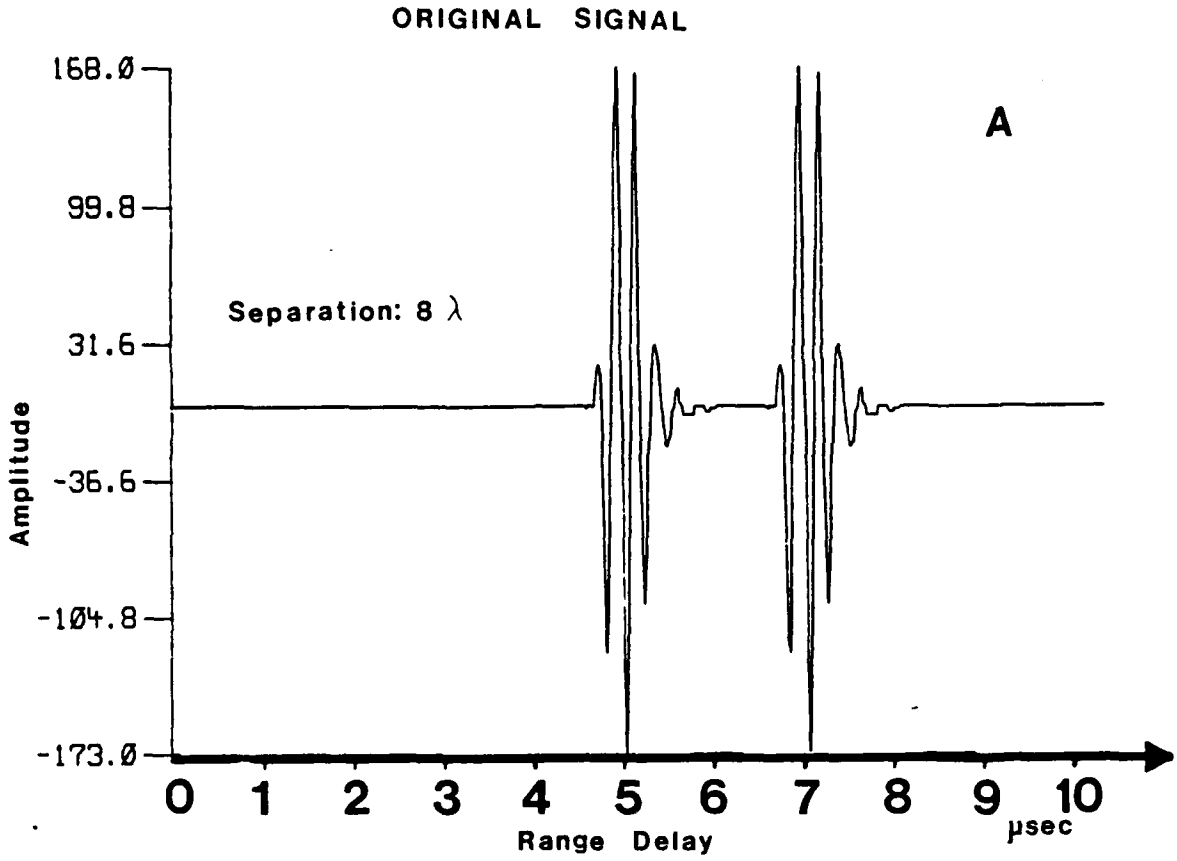

Figure 4.11(A) Targets separated by 8 wavelength.

(B) Processed output for the Optimal Processing. The signals are fully resolvable and there is no bias in the distance between the signals.

(C) Processed output for the Minimization Algorithm. The signals are fully resolvable and there is no bias in the distance between the signals.

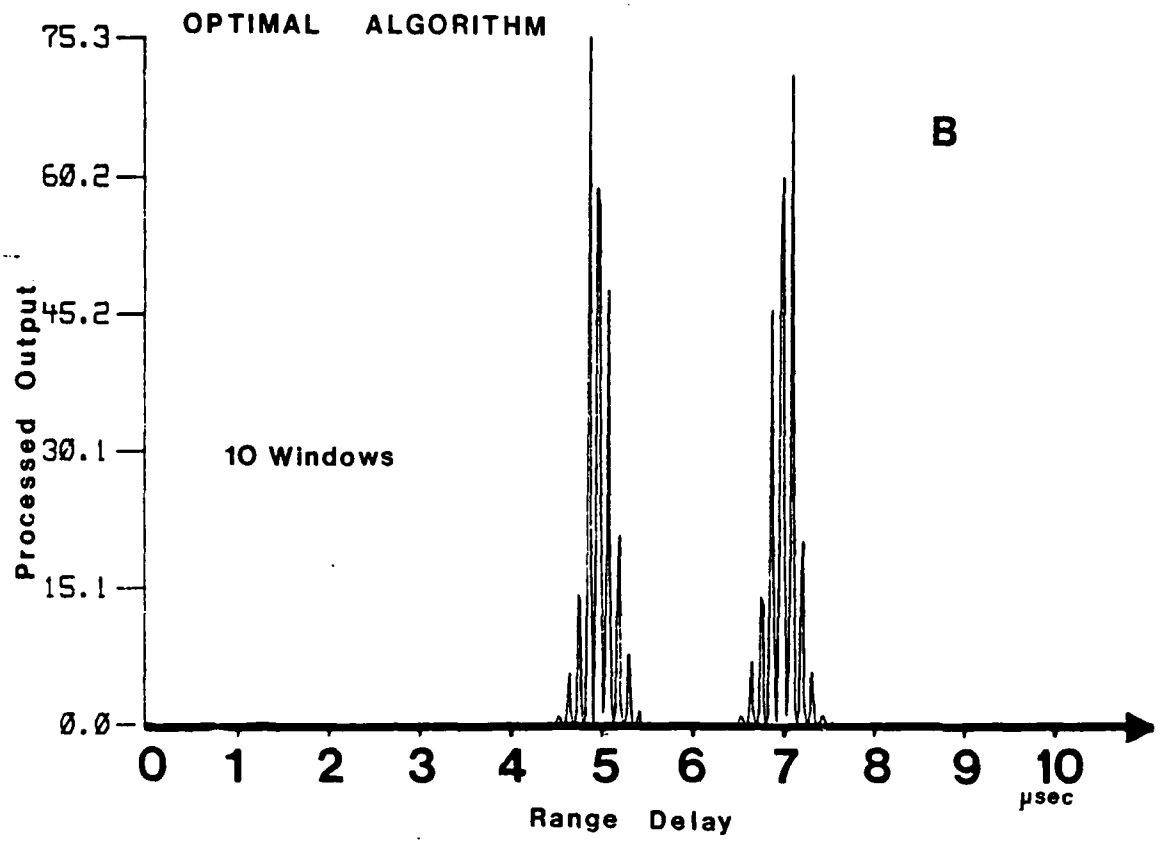
OPTIMAL ALGORITHM
B
75.3
60.2
45.2
30.1
15.1
0.0
Processed Output
10 Windows
0 1 2 3 4 5 6 7 8 9 10
μsec
Range Delay

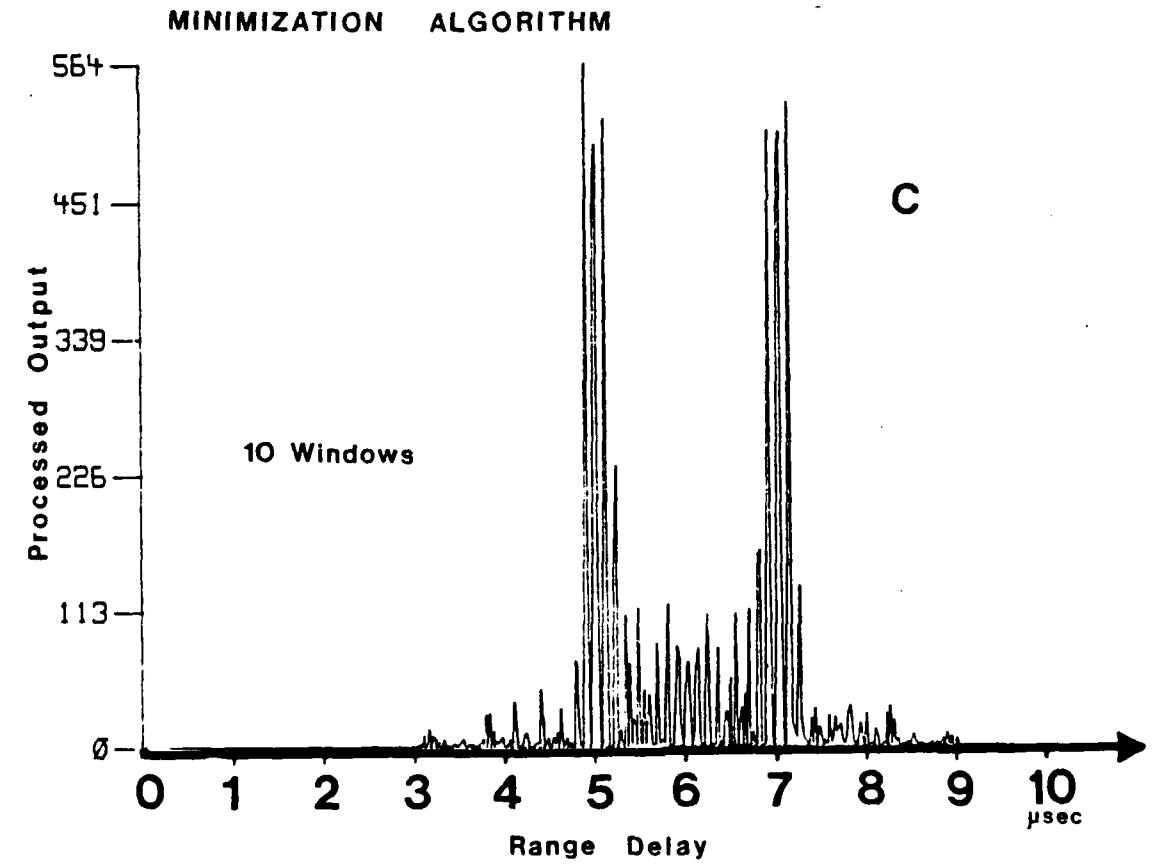
MINIMIZATION ALGORITHM
C
564
451
339
226
113
0
Processed Output
10 Windows
0 1 2 3 4 5 6 7 8 9 10
μsec
Range Delay

order to evaluate the results qualitatively we have to compare the amplitudes of the processed data to the value of signals embedded in noise after processing. For the case of the optimum receiver we can readily conclude that if the signal to noise ratio is higher than 4 or 5 the results would not change considerably because the effect of the signals on each other would be stronger than that of the noise. Minimization does not perform as well for low signal separation. For example for approximately half a wave length separation the signal is reduced from 31,000 to ~ 2.4 which for any reasonable signal to noise ratio in the input is negligble. However for a full wave length separation (the targets are not resolveable) the signal is reduced to only 1747 while for a separation of a wave length and a half the signal again is almost destroyed. For a separation of more than the original range cell the signals will appear with a relatively high signal to noise ratio. (Figures 10, 11).

It is important to note that while under some conditions two adjacent signals will be separated by the processing there will be a bias in the distance between the signals after processing. This bias was experimentally found to be very large for low separation between the signals. For separation larger than the original range cell the bias was found to be negligible. An example of such bias can be seen in Figure 8. One can see that the processed signals are separated by much more than half a wavelength which is approximately the original distance between the signals.

We can conclude that for signals which are separated by less than the original resolution cell the results for both minimization and the suboptimum receiver are not reliable and can result in almost a complete loss of both signals.

The reason for the surprisingly excellent range resolution performance is due to the fact that in practice each of the signals has several peaks. The estimated variance at each of the range delays corresponding to these peaks due to the neighboring signal is clearly phase sensitive. The variance estimate at each peak would be different and will depend on the exact location of the peak in respect to the neighboring signal. It is very likely therefore that in at least one of the peaks range delay, the variance estimate will be low, making the ratio large. This explains also the bias in the range distance when the targets are very close to each other. If the enhanced peak is not the main peak target echo the target range delay of the processed data would seem to be biased.

SUMMARY AND CONCLUSIONS

In this chapter we introduced a technique for clutter reduction which maximizes the ROC performance in each range cell. This technique has the property of a noise riding threshold as its performance is independent of the local properties of the clutter (but is dependent on the local signal to noise ratio). It was pointed out, that determining algorithm for clutter reduction on an A line, requires a knowledge of the fluctuations in the power clutter along that A-line. In general each A line would require a different processor. It is therefore more practical to use a detection algorithm which is optimum for one cell. This gives a likelihood ratio test of m/σ = Student t, independent of clutter. We found out that as the fluctuations in the noise variance increase so does the performance of the optimal algorithm in comparison to minimization and the deconvolved original signal. (Execept for k=1 for which the unprocessed signal is the best). However in contrast to Minimization the

optimum receiver requires a high dynamic range. Depending on the input noise variance the processed output can range from infinity for zero noise power to almost zero for signals embedded in noise. The optimum receiver algorithm obviously provides the best detection procedure for individual cells. However as was pointed out in chapter 3 there are several features that determine the performance of an algorithm as a tool for target enhancement. We discussed already the ROC, dynamic range, resolution and bias of the optimum receiver. However one of the most important features of an algorithm is the improvement in signal-to-noise ratio for which the Minimization is much superior to the optimum receiver. (Note that we did not calculate the signal-to-noise ratio for the optimum receiver as the LRT m/σ is itself a measure of the signal to noise ratio). SNRE is most important when additional information on the target is available. For example if the target is known to have a line structure (for an image composed of A-lines) the contrast of the line target to the background noise is more important than ROC of a single pixle. If several pixles along the A-line are missing due to the processing the picture will still be very clear to the eye if the signal to background noise is high. The eye will complete the missing details and random isolated bright pixles can easily be removed from the image. We showed that we can simplify the system by the use of non-matched filtering instead of matched filtering and exemplified the effectiveness of the algorithm by simulation. We also showed that surprisingly the range resolution is not significantly deteriorated by the processing. However a range bias is introduced for signals separated by less than the original range cell. The current experimental system should be useful for correctly presenting targets embedded in homogenous type clutter as it would automatically

correct for attenuation and shadowing. With some modifications this system can be used for detection of targets with arbitrary spectrum embedded in clutter.

CHAPTER 5

SUMMARY, CONCLUSIONS AND FUTURE WORK

INRODUCTION

As pointed out in the introduction the motivation for this research stemmed from the failure of current techniques to provide sufficient clutter and speckle reduction. In this research work we improve these techniques with post-reception algorithms using the split spectrum principle.

At the outset (chapter 2) an analysis of the backscattered echo from random media is performed. We first calculated the average of the received echo from a regular lattice with random size scatterers and found out that the received echo is proportional to the scatterers size, scatterer variance, scattering density and the function $G(\vec{r},t)$ (which is the impulse response of the system). Later we analyzed the backscattered echo from medium with random scatterer location and size, but uniform average scattering density with results similar to those obtained for the regular lattice case. Then we studied the properties of the reflected signal from a medium with random scatterer location, random size and non-uniform scattering density. We showed that the received echo is strongly dependent on the gradient in scattering density and calculated the echo average for a step function in the scattering density. We confirmed the theoretical results qualitatively by experiment using sponges to simulate an inhomogenious medium.

The results obtained in chapter 2 set the physical basis to the scattering models introduced in chapter 3 and 4.

In chapter 3 we analyze the Minimization Algorithm, a technique that was first introduced in 1979 by Newhouse and Bilgutay and showed a remarkable improvement in flaw-to-grain echo suppression. We showed theoretically that the signal-to-noise ratio of the processed data is much better than that of the two other techniques that it is compared to, without a significant loss of dynamic range (but with an inferior Receiving Operating Characteristic). We demonstrated the effectiveness of the algorithm in the reduction of clutter. (This was of course demonstrated also in Bilgutay's work of 1982) and empirically examined the resolution performance of the algorithm. It was shown that the resolution is not too seriously adversely affected by the processing.

In chapter 4 we developed the theoretical basis for the split spectrum principle. We showed that by this procedure we transform the random process problem into a random variable one. We then constructed the optimum receiver and used a simplified version of the this receiver to construct an experimental system. We analyzed the performance of the rece theoretically and compared it to the performance of the original sign without "special processing". We also investigated the resolution performance of the algorithm empirically for signals separated by less than a single channel range cell as well as for signals separated by less than the original range-cell size. We show experimentally that the resolution is not adversely affected by the processing.

DISCUSSION

Though both of the techniques introduced in chapters 3 and 4 i.e. the Optimal Processing and the Minimization algorithm were developed for the reduction of clutter, there is a significant difference between them. While the optimum receiver scheme allows us automatic detection of targets by introducing a prespecified threshold that determines the minimum signal-to-noise ratio for which the receiver decides that a target exists in the range-cell the Minimization algorithm is a technique to enhance the contrast of the target signal to a background noise.

The split spectrum processing introduces new ways for signal processing. We demonstrate the versatility of this algorithm later in this chapter. The development of new techniques should be easy due to the simplicity in presentation of the problem (a set of finite number of random variables, set to be identically distributed). The technique is attractive also due to the simplicity in implementation if simple filtering instead of matched filtering is used. In practice there is no need to digitize the RF data and apply FFT to filter the signal. The filtering can best be done analogically, which in most cases involves capacitors and inductors only (Fine tuning is needed to control phase and amplitude response). The post filtering process can also be done in hardware (and very cheaply in most cases).

To show the versatility and flexibility of the use of the split spectrum principle we present two simple ways to improve the algorithms described in chapters 3 and 4.

PHASE REVERSALS AND OVERLAPPING FREQUENCY WINDOWS

If one examines the Minimization algorithm carefully one would probably decide that the principle behind the algorithm is the following: If there is no target in the range cell there is a high probability that the random noise phasor is very likely to cross the zero line if we observe its movement as we slowly change the center frequency of a frequency window along the received signal band. According to our approach we do not change the center frequency of the frequency windows continuously but in steps and have n non overlapping windows. In this case instead of obtaining zero for noise only we choose the phasor which is closest to the zero line instead of the zero we wished to "catch". Fortunately we can determine if there would have been a zero crossing had we shifted the center frequency of the windows continuously. Thus, if any of the n random numbers corresponding to a certain range delay changes polarity (or reverses its phase) i.e. if there are both negative and positive numbers among the n random numbers (one is sufficient), then it is clear that there was a zero crossing. So we may decide that if we observe a phase reversal (polarity change) we will set the new processor output at zero instead of the minimum used for the Minimization algorithm and instead of the m/σ for the Optimal Processing. It is clear that if the signal to noise ratio is high enough the effect of the new scheme will not affect the target echo significantly. However for low signal-to-noise ratio it would probably adversely effect the ROC though improvement in signal-to-noise ratio should still be high. (Note that for very low signal-to-noise ratio the basic model we used collapses. The target echo decreases and the assumption that the target echo is much stronger than that of each of the small point reflectors that compose the clutter is

not valid any more). In Figures 1 and 2 we show the same data shown earlier in chapter 3 and 4 but with the addition of polarity changes. The improvement in signal-to-noise ratio is evident for both techniques.

Another concept is the use of overlapping frequency windows. The concept was first introduced by Newhouse et al but was never analyzed theoretically.

Here we use overlapping windows instead of the n orthonormal windows (that the K.L expansion calls for) to increase the probability of catching a zero crossing. The operation becomes somewhat more cumbersome but proves to be very effective as is shown in the theses of Bilgutay (4). The addition of frequency windows should provide also more information to improve the variance estimmate in Optimal Processing. In his thesis Bilgutay investigates empirically the performance of the Minimization Algorithm for different degrees of overlap as a function of grain and flaw size. It is pertinent to investigate the theoretical performance improvement for overlapping channels for both Minimization Algorithm and the Optimal processing. The derivation is not straight forward and probably only Chernoff Bounds can be established for the problem.

SPECKLE REDUCTION

In the introduction to this report we mention speckle reduction as a topic of interest (mainly for applications in Ultrasound Medical Imaging). Up to now we have used split spectrum processing only for the reduction of clutter. We now show that split spectrum processing can be used for speckle suppression (multiplicative type noise) also. Following the same approach used in chapter 4 we obtain for the interval $[T_i, T_f]$ the following hypotheses set,

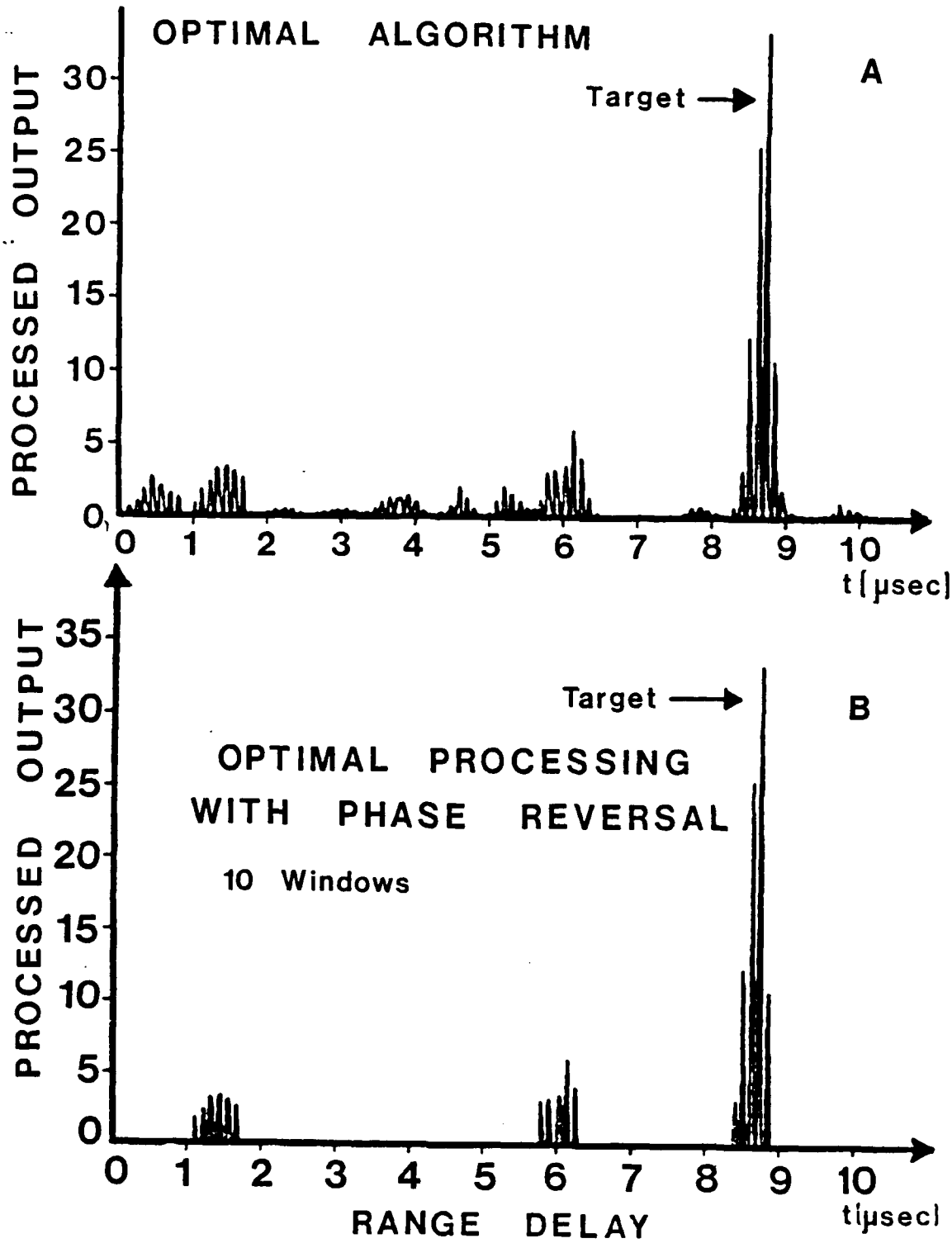

Figure 5.1(A) Processed output for the signal of Figure 4.6(A) for the Minimization Algorithm without phase reversal algorithm using 10 non-overlapping frequency windows. (B) Processed output the Minimization Algorithm with phase reversal algorithm.

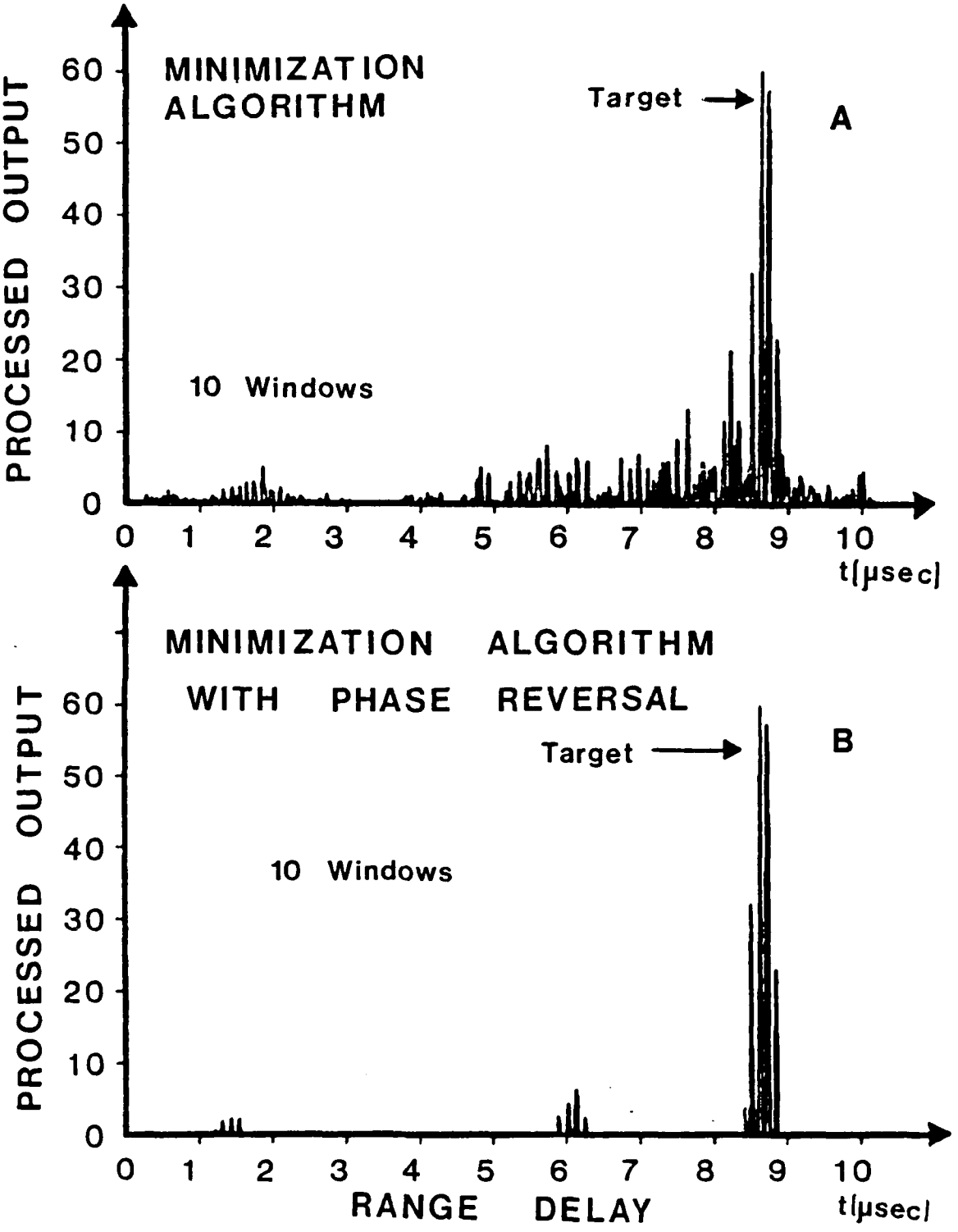

Figure 5.2(A) Processed output for the signal of Figure 4.6(A) for the Optimal Processing without phase reversal using 10 non-overlapping frequency windows. (B) Processed output for Optimal Processing with phase reversal algorithm.

$$H_1: r(t) = n_1(t) \qquad \text{with } \sigma_1$$

$$H_o: r(t) = n_2(t) \qquad \text{with } \sigma_2 \tag{5.1}$$

following the same procedures and arguments, the LRT obtained by n identically distributed Gaussian random variables assuming σ_1 and σ_2 are known is (see for example (42) chapter 2 pp. 107),

$$\left[\frac{1}{\sigma_1^2} - \frac{1}{\sigma_2^2}\right] \sum_{l=1}^{n} r_l^2 \underset{H_o}{\overset{H_1}{\gtrless}} \gamma \tag{5.2}$$

In this case no decision can be made without further information since we cannot estimate σ_2 in region 1 and vice versa. However if we evaluated the variance for a certain region and want to determine if a new region belongs to the same category i.e. has the same variance then a decision rule can be constructed. It is found that in general the sum of the squares constitutes the best detector. The sum of the squares might be a good tool also for image formation of an Ultrasonic image built by A scans if the grey levels are calibrated according to the lowest (or highest) power region (this is of course done in any Ultrasound medical imaging system on the market).

As was previously mentioned it is practically impossible to build nonoverlapping filters that will cover the whole spectrum. Sometimes due to resolution requirements we are forced to use wide bandwidth filters and if the specified number of windows needed for speckle reduction is too large to fit into the available transmitted spectrum we use overlapping windows. In this case if the amount of overlap is substantial we are faced with a set of random variables which are correlated. For this case the general solution is the following (see (42))

$$\underline{r}^t[K_1^{-1} - K_0^{-1}]\,\underline{r} \underset{H_0}{\overset{H_1}{\gtrless}} \gamma \tag{5.3}$$

where K_0 and K_1 are the covariance matrices of H_0 and H_1 respectively defined as,

$$E[(\underline{r}\,\underline{r}^t)|H_1] \overset{\Delta}{=} K_1$$
$$E[(\underline{r}\,\underline{r}^t)|H_0] \overset{\Delta}{=} K_0 \tag{5.4}$$

For example assume that we split the spectrum into two overlapping channels (due to resolution requirements). Let us assume that ρ is their correlation coefficient and that the two channels are assumed to have identical power)

$$\rho = \frac{\int_{-\infty}^{\infty} F_1(f)F_2(f)df}{\int_{-\infty}^{\infty}|F_1(f)|^2 df} \tag{5.5}$$

so

$$K_1 = E[\underline{r}\,\underline{r}^t|H_0] = \sigma_1^2\begin{vmatrix} 1 & \rho \\ \rho & 1 \end{vmatrix} \tag{5.6}$$

likewise

$$K_0 = E[\underline{r}\,\underline{r}^t|H_1] = \sigma_2^2\begin{vmatrix} 1 & \rho \\ \rho & 1 \end{vmatrix} \tag{5.7}$$

and

$$K_{1,0}^{-1} = \frac{1}{\sigma_{1,2}^2(1-\rho^2)}\begin{vmatrix} 1 & -\rho \\ -\rho & 1 \end{vmatrix} \tag{5.8}$$

The optimum receiver becomes,

$$\left[\frac{1}{\sigma_1^2} - \frac{1}{\sigma_2^2}\right] \begin{bmatrix} r_1 & r_2 \end{bmatrix} \begin{bmatrix} 1 & -\rho \\ -\rho & 1 \end{bmatrix} \begin{bmatrix} r_1 \\ r_2 \end{bmatrix} = \left[\frac{1}{\sigma_1^2} - \frac{1}{\sigma_2^2}\right] \frac{1}{1-\rho^2} (r_1^2 + r_2^2 - 2\rho r_1 r_2) \qquad 5.9$$

$\left[\frac{1}{\sigma_0^2} - \frac{1}{\sigma_1^2}\right](1-\rho^2)$ is just a constant multiplier. The receiver should be constructed as shown in Figure 3.

If we assume that N consecutive points on the A line are taken from the same statistics but are independent, the best detection scheme can be shown to be a moving average of the output,

$$z = \sum_{i=1}^{N} z_i \qquad 5.10$$

which is

$$z = \sum_{1=1}^{N} r_{1i}^2 + r_{2i}^2 - 2\rho\, r_{1i} r_{2i} \qquad 5.11$$

The first two terms correspond to envelope detection and the next term to a lowpass version of the correlated signal.

SUGGESTED FUTURE WORK

In this section we outline future work that could evolve from this research.

1. Use of coherent reflection from random media for the estimation of scatterer concentration. As was shown in chapter 2 there are two ways for a coherent reflection to occur, i.e field gradient and average scattering density gradient. The major problem in constructing strong enough field gradient lies in the proper design of a suitable transducer shape that will maximize the field gradient (or the integral of $G(\vec{r},t)$ as defined in chapter 2).

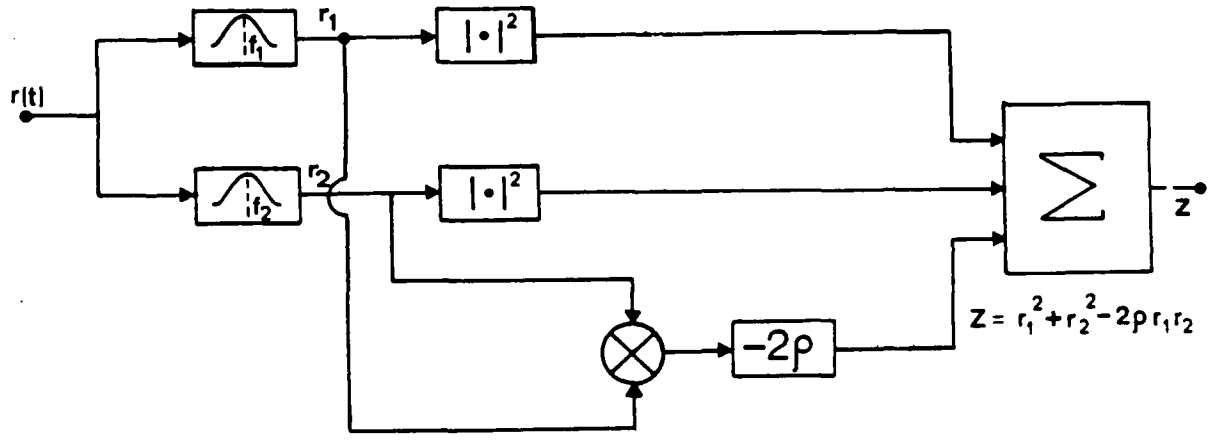

Figure 5.3 A block diagram of the receiver as described in eq. (5.9) for two overlapping frequency windows.

The use of a scattering concentration gradient to estimate the scattering concentration profile should have applications. Thus studies on the behaviour of the reflection from smooth boundaries in the human body in relation to the reflection from within the tissue should provide information on the tissue state if the scattering model introduced in chapter 2 can be assumed (i.e. if the microstructure of the human tissue can be modelled as a collection of point reflectors). For example the echo from the myocardium boundary in relation to the signal from within the myocardium might indicate an abnormality of the myocardium (as the myocardium fibers are often modelled as an ensemble of point reflectors).

As was pointed out at the end of chapter 2 this technique can provide a way to estimate surface grain size in metal if the metal can be immersed in a liquid of similar characteristic impedance.

ANALYSIS OF PHASE REVERSALS AND OVERLAPPING CHANNELS

Phase reversals (or suppression of polarity changes) and overlapping channels belong in some aspects to the same category of signal processing. Both of the techniques use the fact that a cell containing clutter only has a higher probability of a zero-crossing than a cell containing a target. Analysis of the signal-to-noise ratio for both the Minimization algorithm and Optimal Processing with polarity change suppression is needed in order to evaluate the improvement of these additions to the performance of the algorithms. A careful examination of the loss in ROC is also needed to establish possible practical implementation as a tool in Image Processing. In preliminary empirical tests for the evaluation of the resolution performance of this addition to both the Minimization algorithm and the Optimal Processing we found out that the resolution is

improved for both techniques. In Figures 4 to 13 we compare the results of "suppression of polarity changes" applied to both algorithms with the results without "suppression". It is clearly seen that for all cases the signals are much better separated with the suppression than without it. It is necessary to establish the exact impact that the "suppression" has on resolution, signal amplitude, dynamic range and range bias of multiple signals.

AUTOMATIC FLAW DETECTION

The technique in chapter 4, "Optimal Processing", can also be used for automatic flaw detection. We can use the variance estimate to construct a threshold that will determine a constant false alarm rate. It is also possible that flaw characterization in the presence of clutter noise would be possible if different type of flaws would exhibit specific characteristic spectra. In this case a receiver with specific constant multipliers assigned to the different filters would "match" a specific flaw type (and a recognition of flaw type would be possible using some known techniques in pattern recognition).

EDGE SHARPENING

According to the analysis presented in chapter 2 sharp gradients in scattering concentration result in a coherent reflection that resembles a reflection from a flat surface or a large reflector. When a plane wave is illuminating a random medium with a step in its scattering concentration we found out in chapter 2 that the variance at the range delay corresponding to the imaginary boundary separating the two regions of different scattering concentrations is approximately half of the sum of

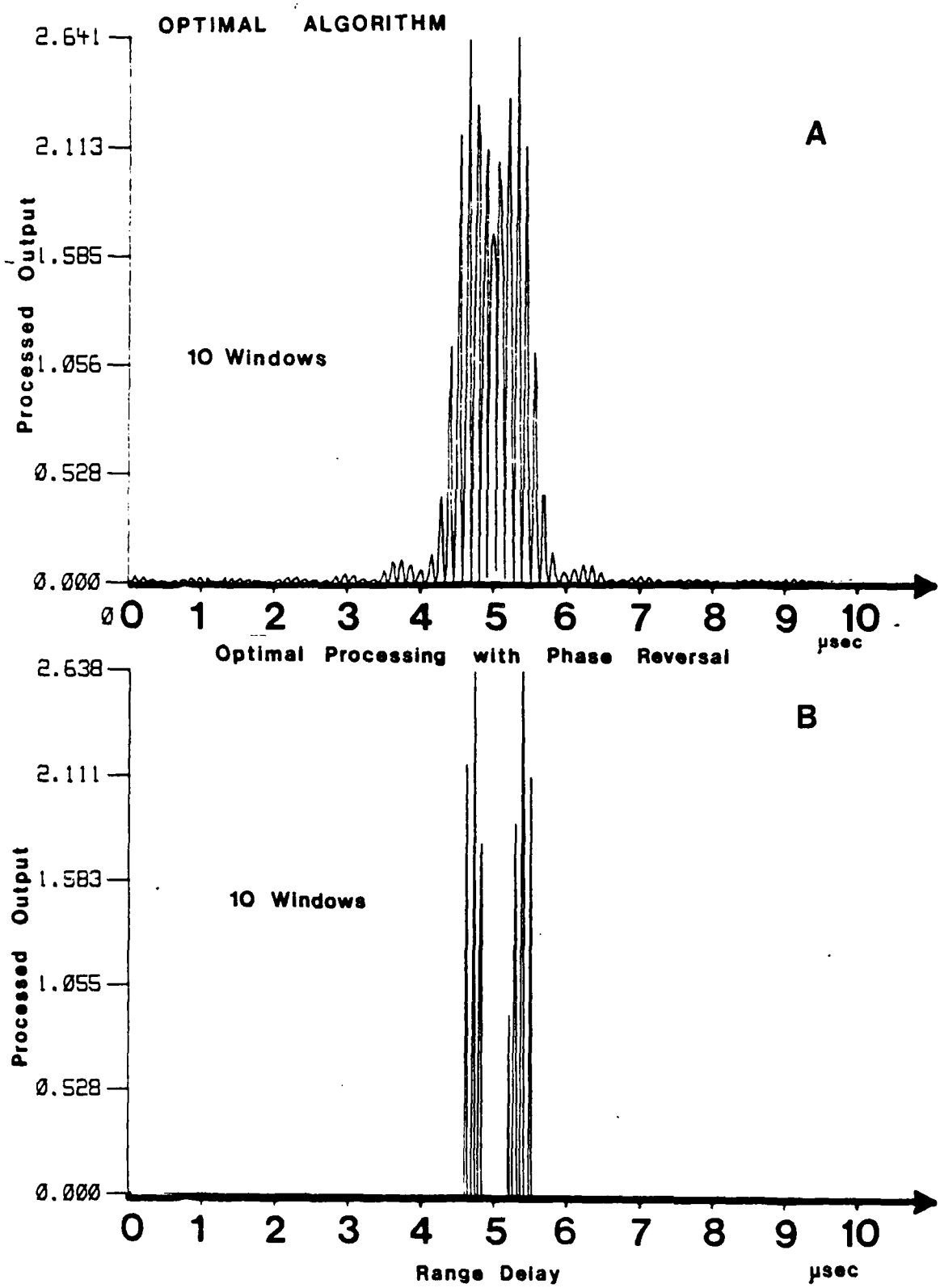

Figure 5.4 Processed output for two signals separated by 1/2 a wavelength (see Fig. 4.7(A)) for Optimal Processing, with (B) and without (A) phase reversal.

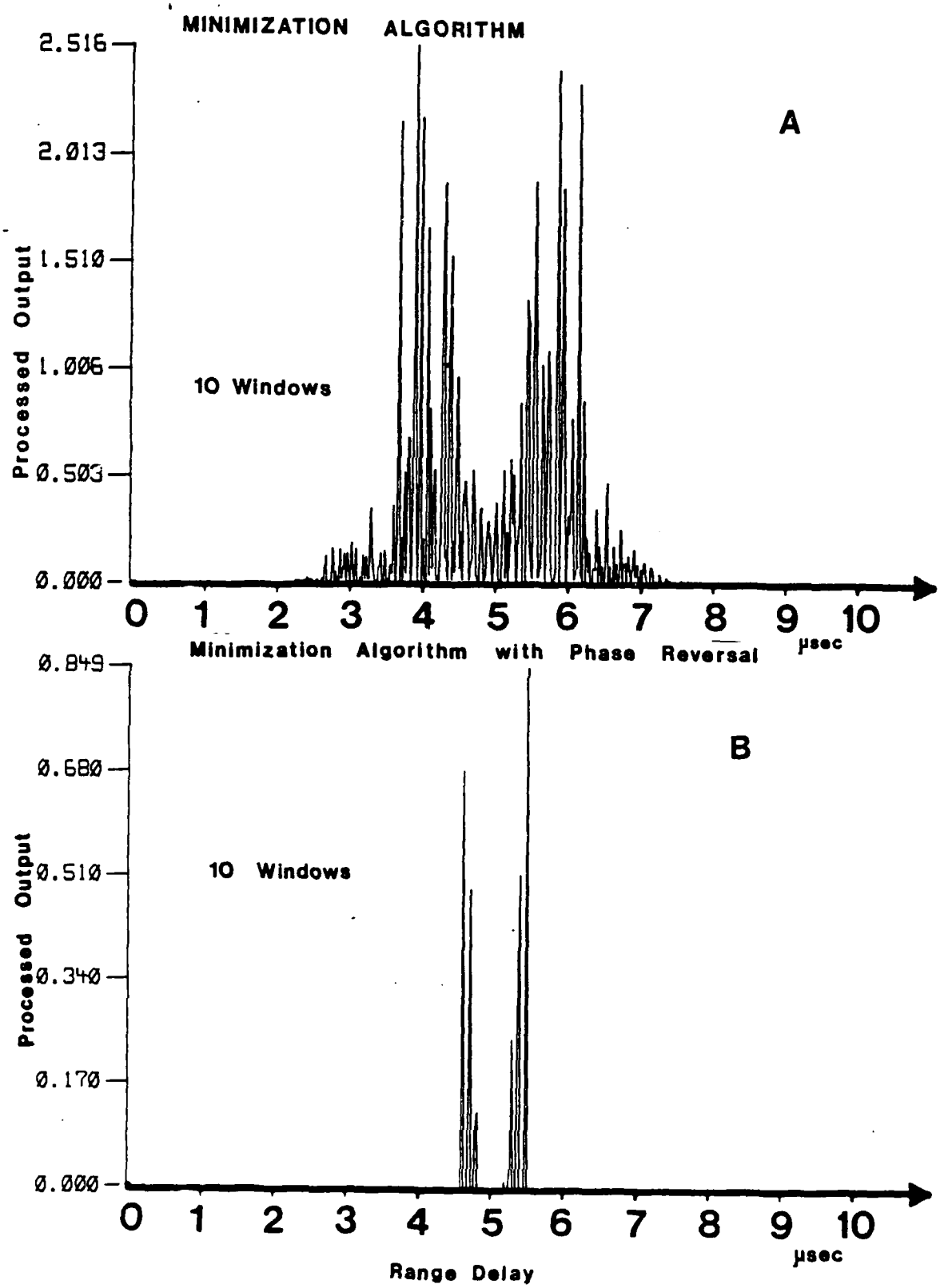

Figure 5.5 Processed output for two signals separated by 1/2 a wavelength (see Fig. 4.7(A)) for the Minimization Algorithm, with (B) and without (A) phase reversal.

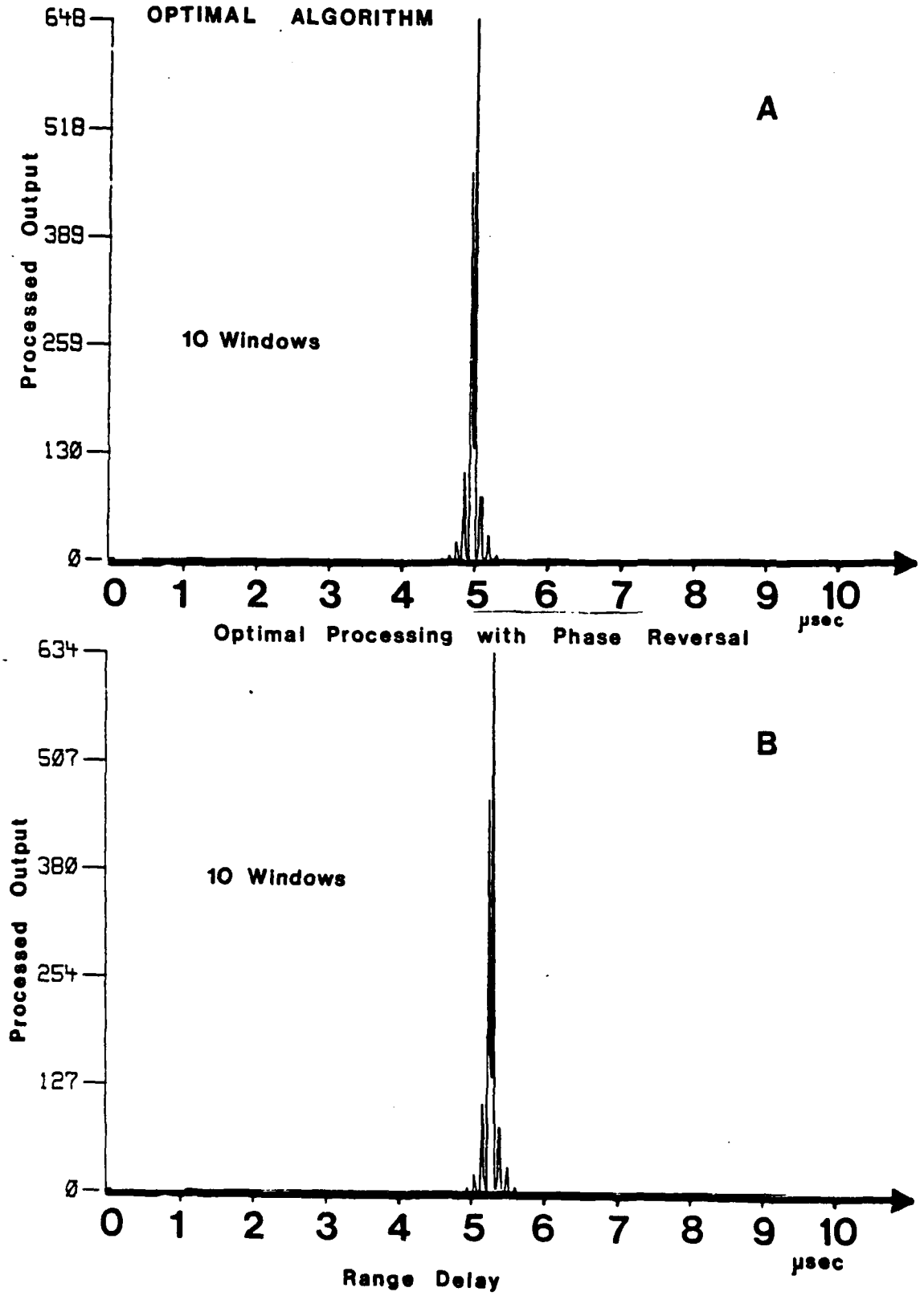

Figure 5.6 Processed output for two signals separated by a full wavelength (see Fig. 4.8(A)) for Optimal Processing, with (B) and without (A) phase reversal.

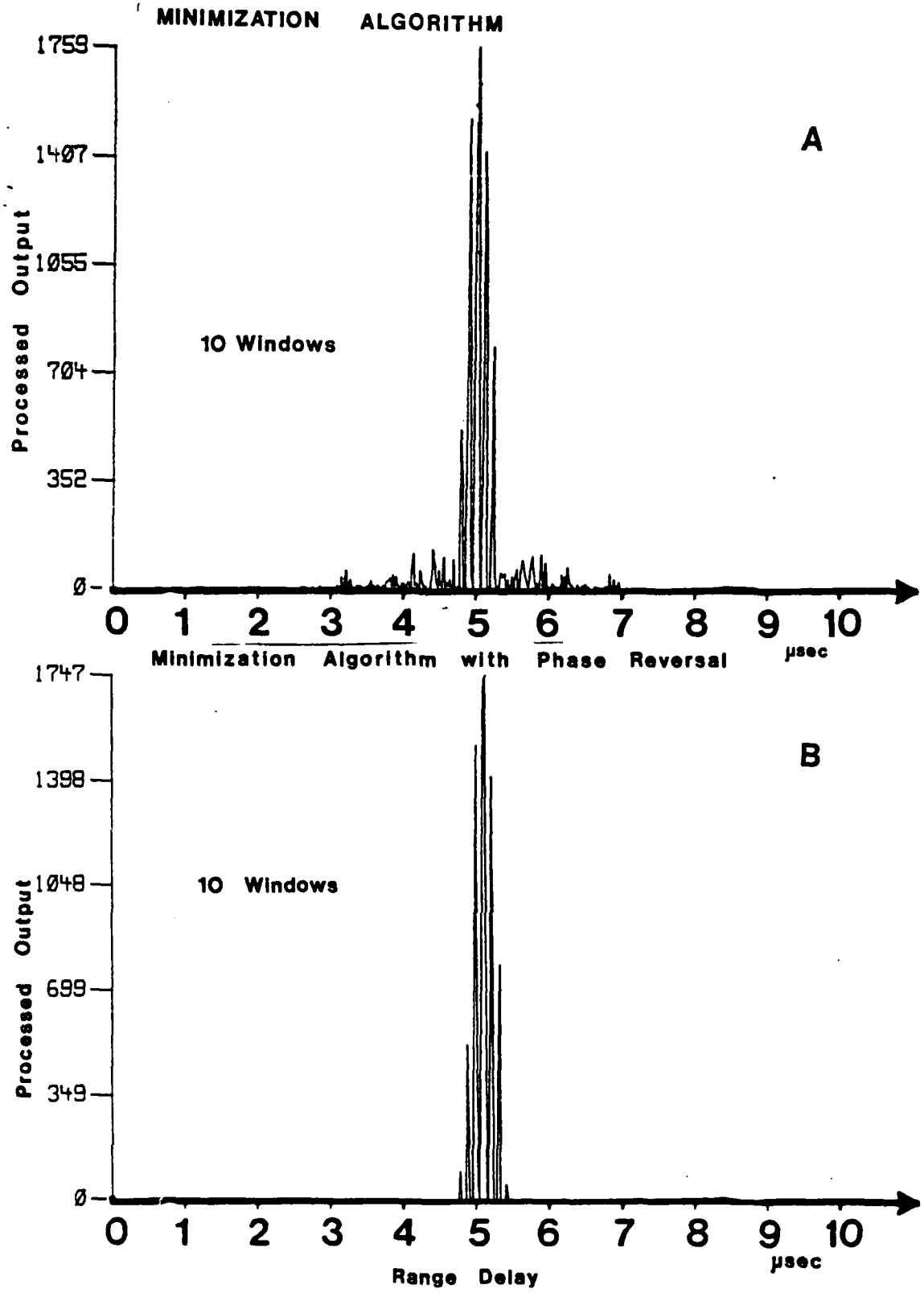

Figure 5.7 Processed output for two signals separated by a full wavelength (see Fig. 4.8(A)) for the Minimization Algorithm, with (B) and without (A) phase reversal.

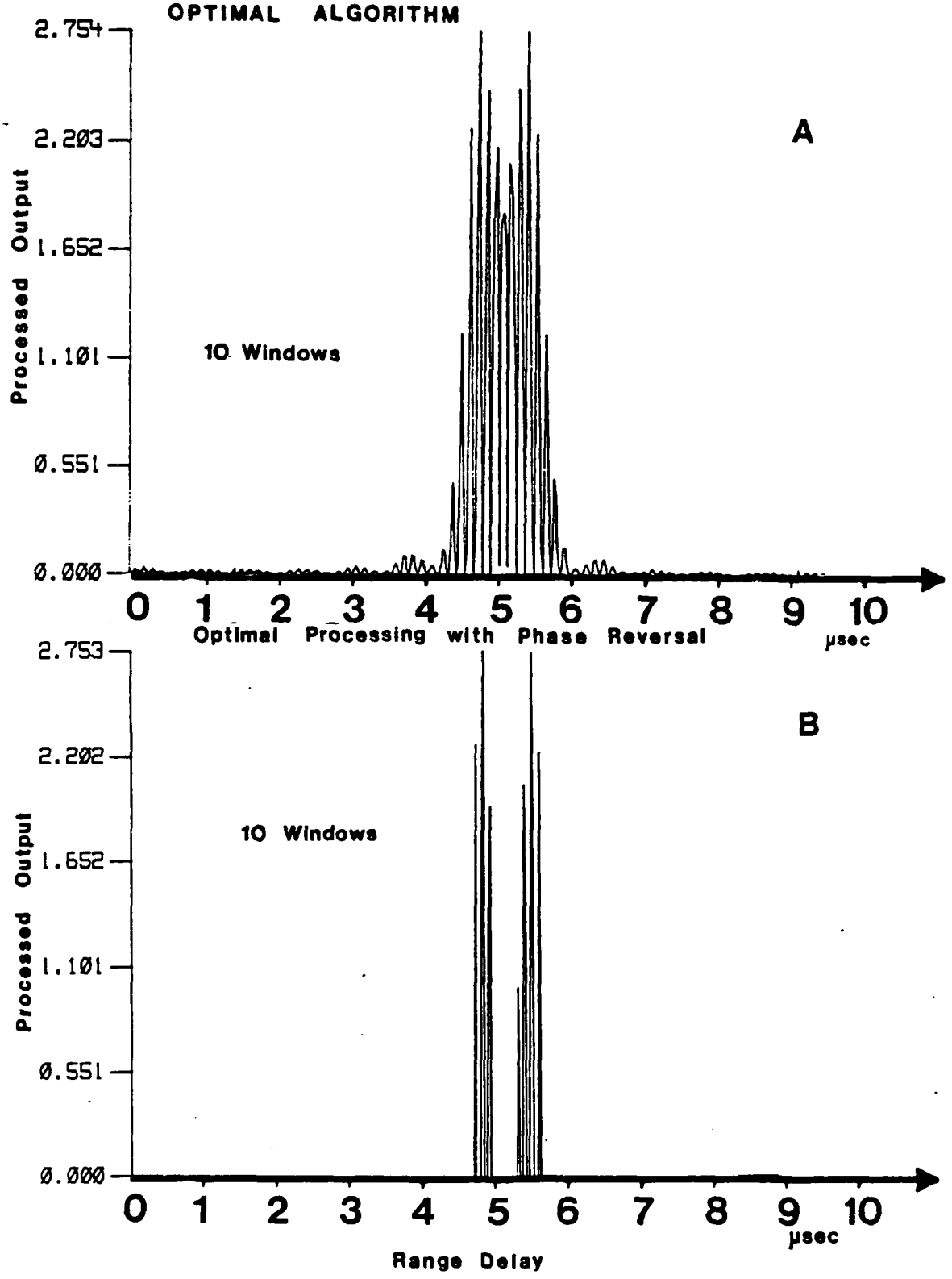

Figure 5.8 Processed output for two signals separated by 3/2 wavelengths (see Fig. 4.9(A)) for Optimal Processing, with (B) and without (A) phase reversal.

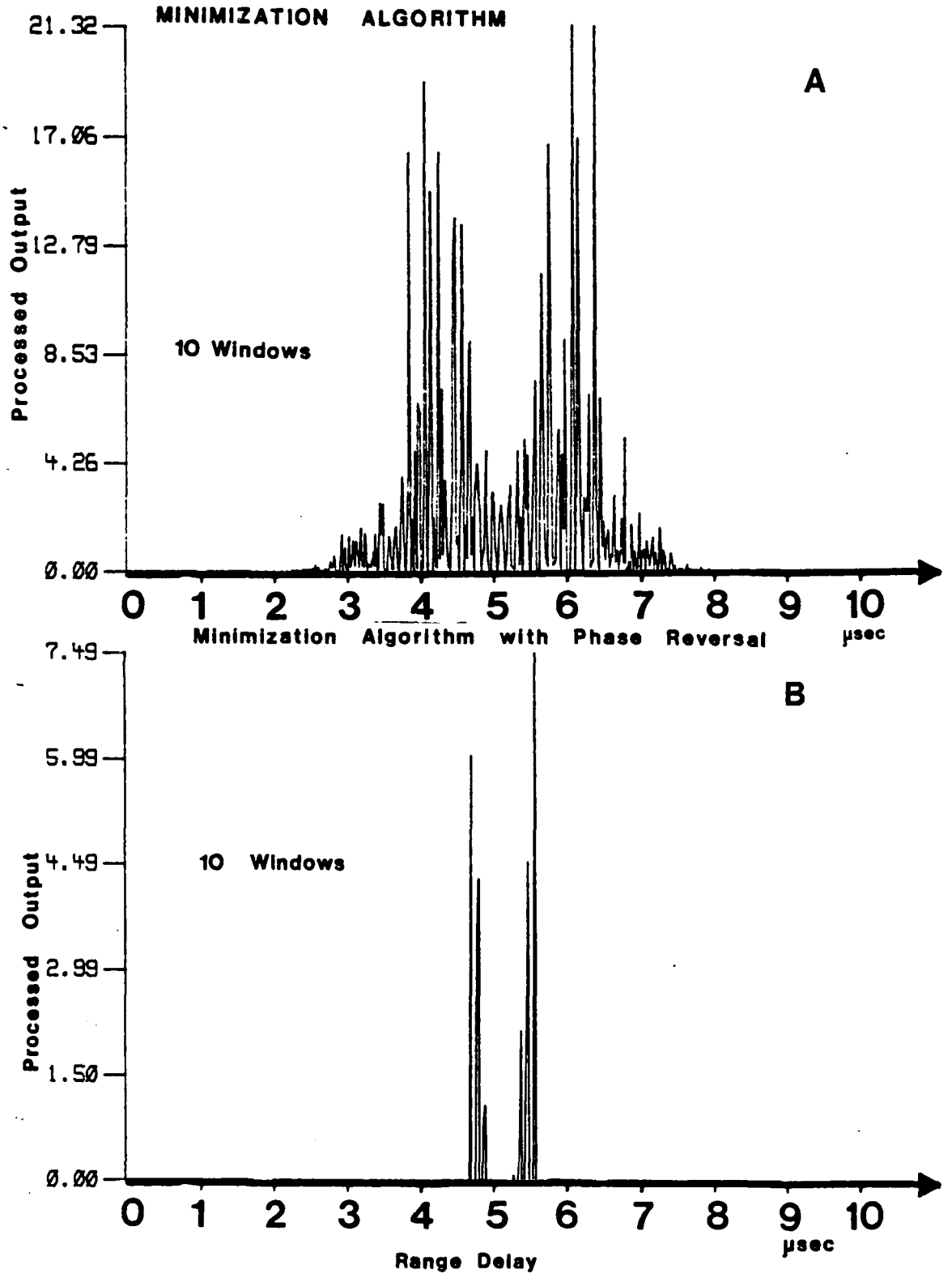

Figure 5.9 Processed output for two signals separated by 3/2 wavelengths (see Fig. 4.9(A)) for the Minimization Algorithm, with (B) and without (A) phase reversal.

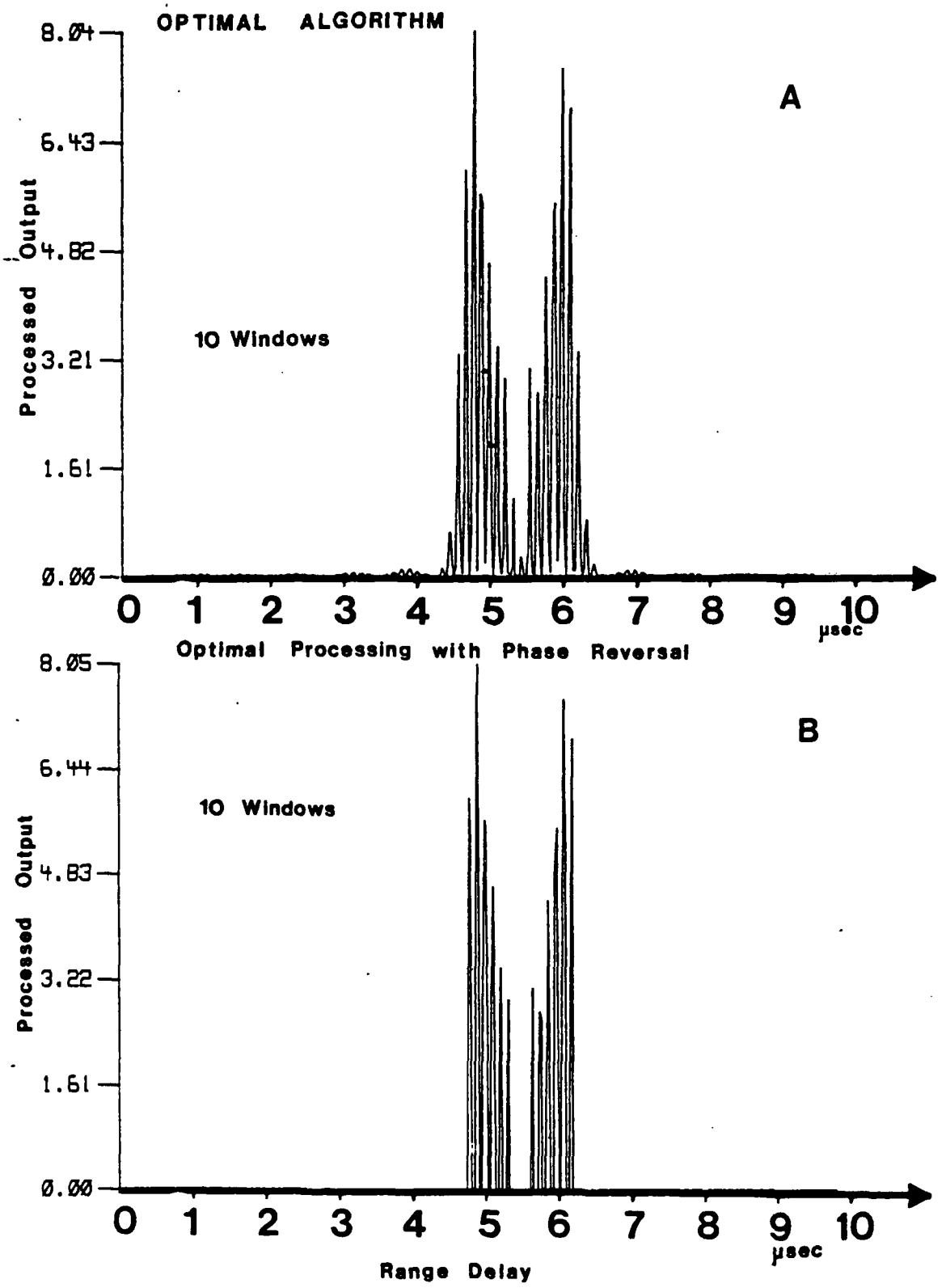

Figure 5.10 Processed output for two signals separated by 4 wavelengths (see Fig. 4.10(A)) for Optimal Processing, with (B) and without (A) phase reversal.

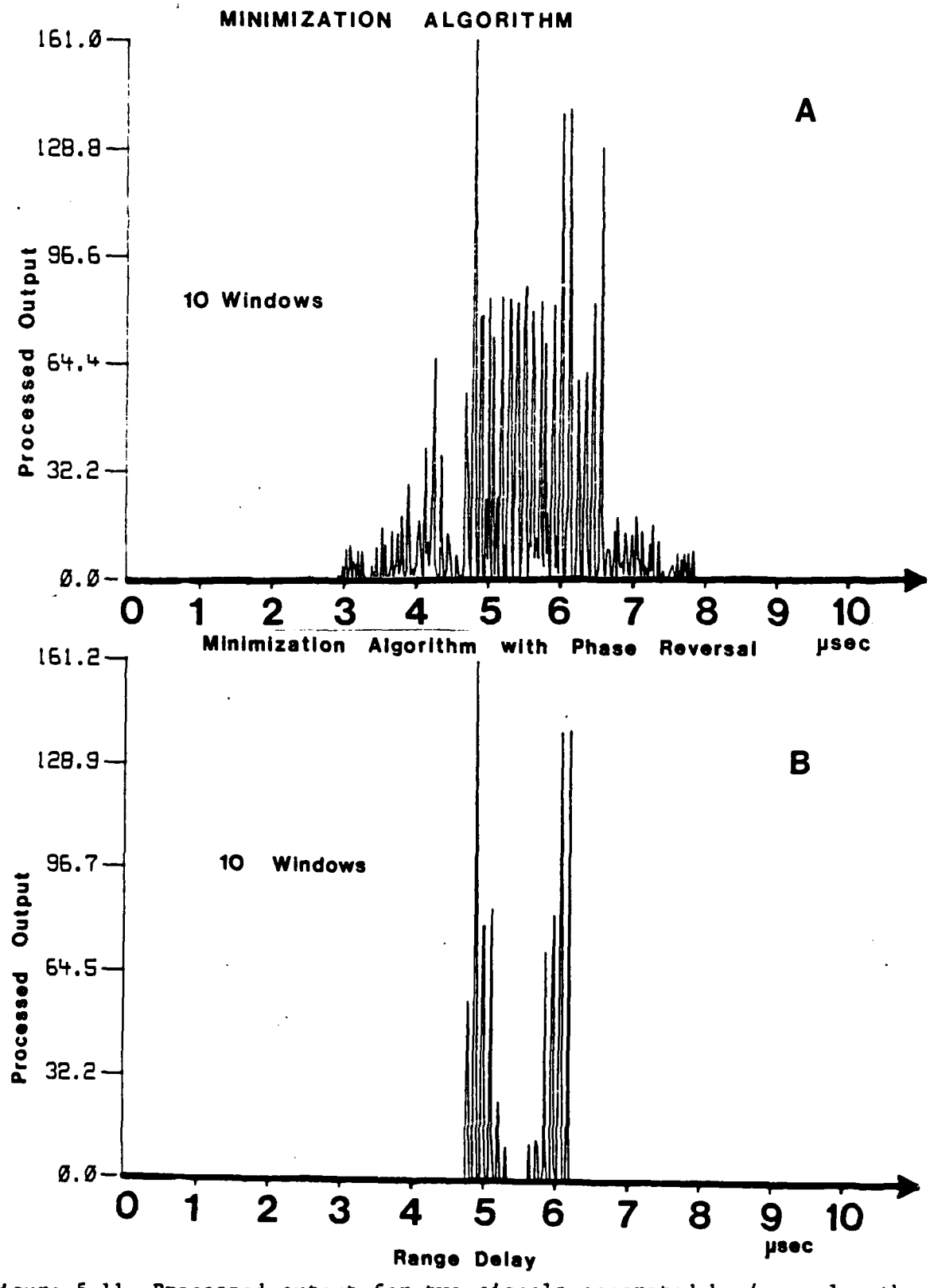

Figure 5.11 Processed output for two signals separated by 4 wavelengths (see Fig. 4.10(A)) for the Minimization Algorithm, with (B) and without (A) phase reversal.

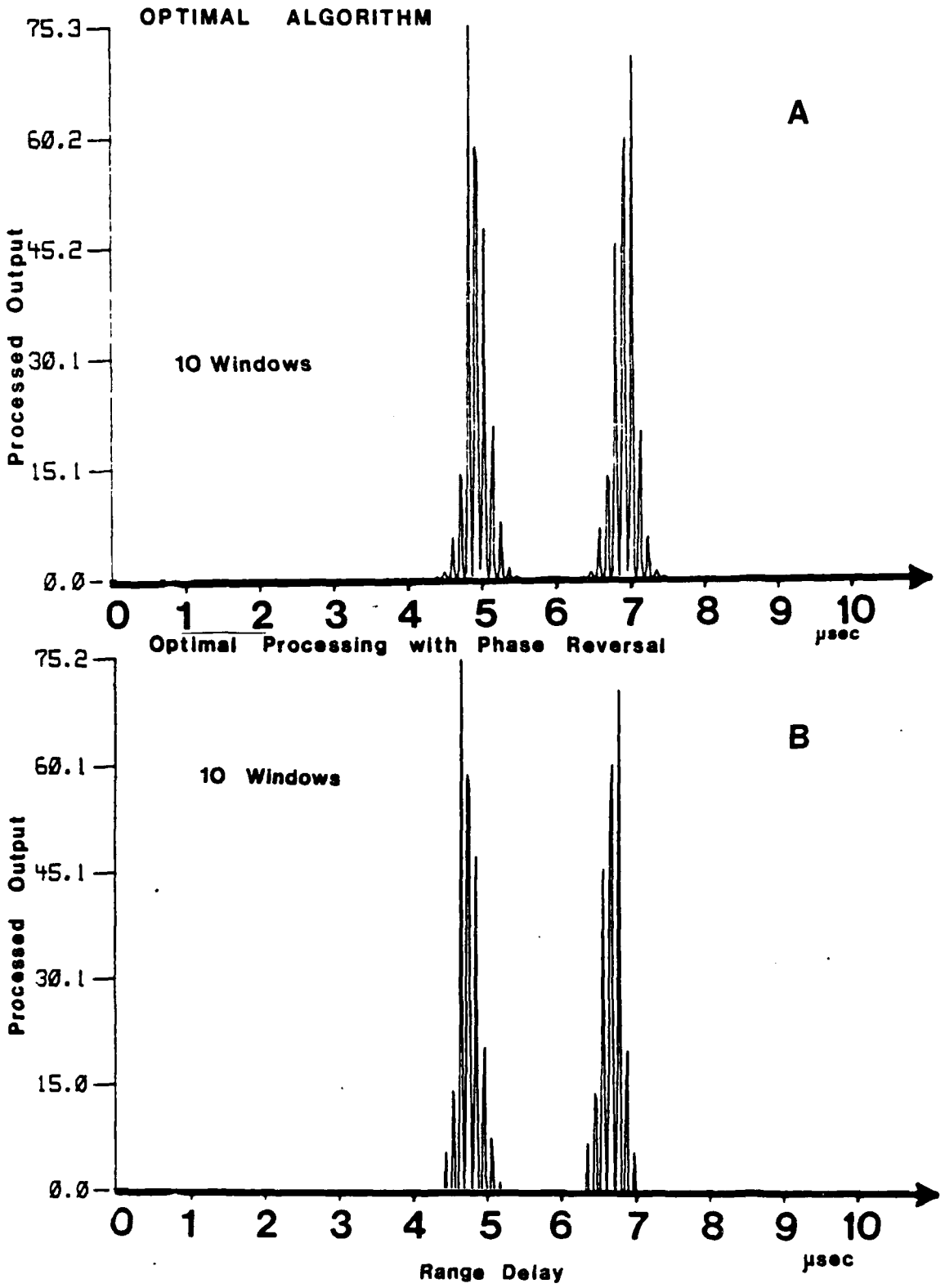

Figure 5.12 Processed output for two signals separated by 8 wavelengths (see Fig. 4.11(A)) for Optimal Processing, with (B) and without (A) phase reversal.

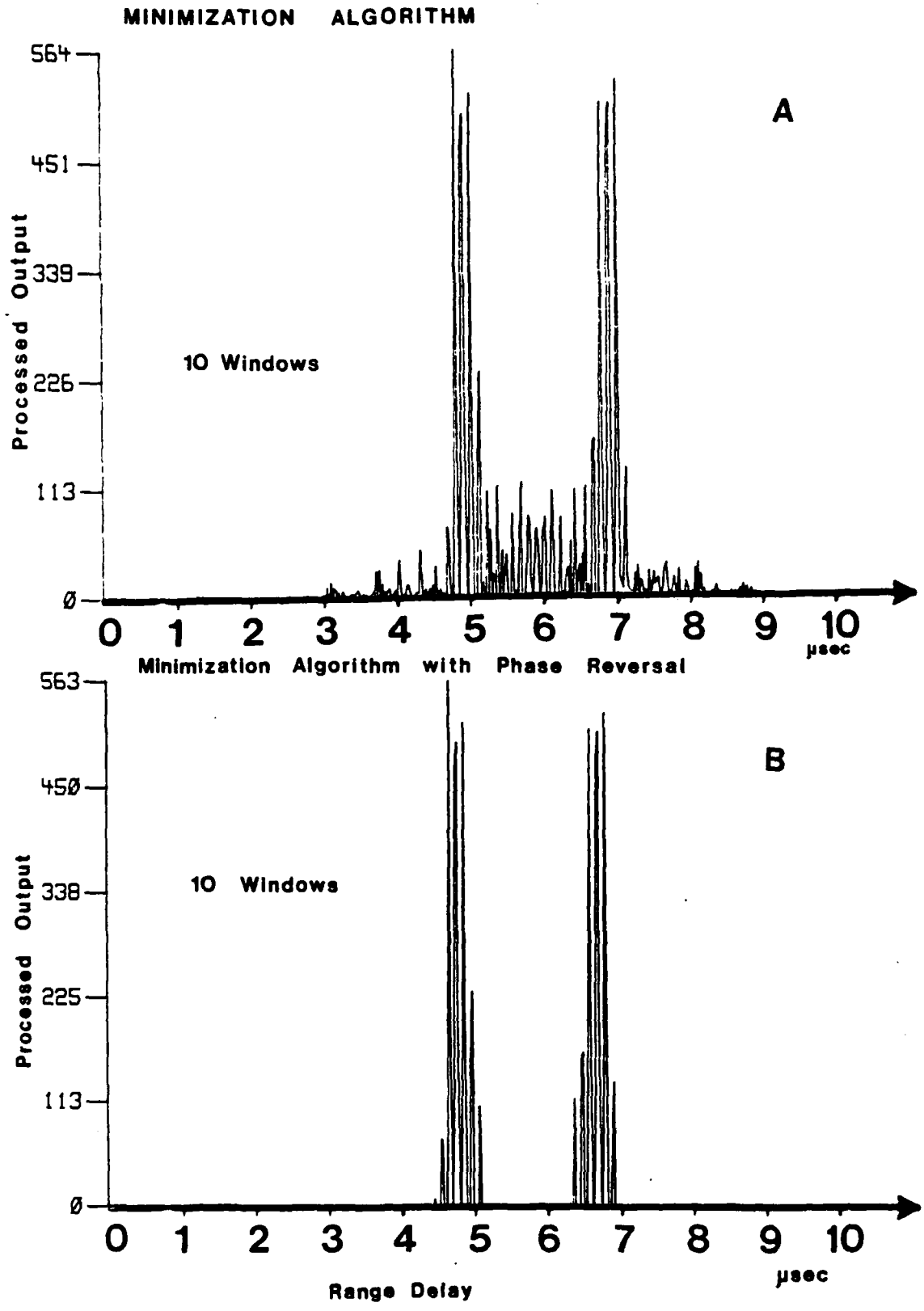

Figure 5.13 Processed output for two signals separated by 8 wavelengths (see Fig. 4.11(A)) for the Minimization Algorithm, with (B) and without (A) phase reversal.

the variances of the two regions. Thus we can treat this problem as a target embedded in fluctuating medium where the standard deviation ratio between the cell containing the target (the boundary) and the cells containing clutter only can take the value of either 2 or 1/2 and the detection performance of the boundary can be evaluated using the type of ROC graphs presented in chapter 4. If we use for example Optimal Processing there will be no difference between the processed output of the signals returned from regions 1 and 2 because m/σ is independent of σ as was shown in chapter 4. Thus for the boundary range delay the processed output will depend on m/σ where m represents the coherent term of the reflected signal. Use of the Minimization Algorithm will result in improved contrast of of the boundary echo with respect to both regions as the SNR of the Minimization Algorithm is much larger than that of any of the other analyzed techniques.

OPTIMUM DYNAMIC RANGE

One of the advantages of the new processors is that they do not require a substantial increase in dynamic range. Though Minimization is a biased estimator of the signal amplitude, for high signal to noise ratios and not too large number of windows this bias is very small and can be considered negligible. Thus there is no need for a substantial increase in amplitude dynamic range of the processed output. The same holds true for the Optimal Processing if the targets are embedded in homogenous type clutter and the number of windows employed is sufficiently high to allow a good estimate of the clutter variance.

If we want to minimize the dynamic range requirements for non-homogenous type clutter and still gain high signal to noise ratio without

a need for a high number of frequency windows to estimate the variance one can use the following scheme: Use the phase reversal scheme to decide if a target exists in the range cell, i.e. if there was a phase change or not. In the event that there is no phase reversal among the n random varibles one can decide to present the original signal instead of the two algorithms suggested in chapter 3 and 4. This scheme will not require any increase in dynamic range of the processed output but will have the clutter reduction properties of the phase reversal scheme.

If one wants to improve the detection properties of this scheme one way to do it is by allowing for example one or two phase reversals without deciding on a zero (i.e. clutter) in the range cell. This way we will increase the probability of detection with a similar increase in probability of false alarm.

REFERENCES

1. V.D. Koryachenko, "Statistical Processing of Flaw Detector Signals to Enhance the Signal to Noise Ratio Associated with Stuctural Reverberation Noise". Translated from Defectoskopiya, No. 1 pp B7-95, 1975.

2. K. Goebbels, "About the Origin of High Frequency Ultrasonic Backscattering Signals", Materials Prufung, Vol. 24, pp. 314-316, 1982.

3. V.L. Newhouse, N.M. Bilgutay, J. Saniie and E.S. Furgason, "Flaw-to-Grain Echo Enhancement by Split Spectrum Processing". Ultrasonics, March, 1982.

4. N.M. Bilgutay, "Split Spectrum Processing for Flaw-to-Grain Echo Enhancement in Ultrasonic Detection", Ph.D Thessis, Purdue University TR-EE 81-20, June 1981.

5. D.E. Robinson and P.C. Knight, "Computer Reconstuction Techniques in Compound Scan Pulse-Echo Imaging", Ultrasonic Imaging 3, 217-234 (1981).

6. D.R. Foster, M. Ardity, F.S. Foster, M.S. Patterson, and J.W. Hunt, "Computer Simulations of Speckle in B-Mode Imaging", Ultrasonic Imaging 5, 308-330 (1983).

7. E.W. Beasley, H.R. Ward, "A Quantitative Analysis of Sea Clutter Decorrelation with Frequency Agility". IEEE Trans. on Aerospace Eng. Vol. AES-4 No. 3, May 1968.

8. P.N. Marinos and W.N. Walters, "A Proposed Coherent Integration Scheme for use in Frequency Agile Radar Systems", IEE 1975, Southeascon, pp. 6E3(1-4).

9. H.M. Finn, R.S. Johnson, "Adaptive Detection Mode with Threshold Control as a Function of Spatially Sampled Clutter-Level Estimates", RCA review, Vol. 29, 414-4, Sept. 1968.

10. G.V. Trunk, "Range Resolution Of Targets using Automatic Detectors", IEEE Trans. AE Sys., Vol. 14, 750-755, Sept. 1978.

11. M. Weiss, "Analysis of Some Modified Cell-Averaging CFAR Processors in Multiple-Target Situations", IEEE Trans. AE Sys., Vol. 18 No. 1, 102-114, Jan. 1982.

12. V.G. Hansen and J.H. Sawyers, "Detectability Loss Due to the Greatest of Selection in a Cell-Averaging CFAR", IEEE Trans. AE Sys., Vol. 16, 115-118, Jan. 1980.

13. A.E. Gibson, "Adaptive Detection Probabilities for Fluctuating Target Models in Non Homogeneous Gaussian Noise", IEEE Trans. AE Sys., Vol. AES-9, 113-115, Jan. 1973.

14. B.G. Gustafson and B.O. As, "System Properties of Jumping Frequency Radars" Philips Telecommunication Review, Vol. 25, No. 1, pp. 70-76, July 1964.

15. J.W. Goodman, "Statistical Properties of Laser Speckle Patterns and Related Phenomena". J.C. Dainty, Ed. Berlin: Springer Verlag, 1975 pp. 9-75.

16. R.F. Wagner, S.W. Smith, J.M. Sandrik and H. Lopez. "Statistics of Speckle in Ultrasound B Scan". IEEE Trans. on Sonics and Ultrasonics, May 1983.

17. S.W. Smith, R.F Wagner, J.M. Sandrik and H. Lopez, "Low Contrast Detectability and Contrast Detail Analysis in Medical Ultrasound", IEEE Trans., Vol. SU-30, pp. 164-173, May 1983.

18. C.B. Burckhardt, Speckle in Ultrasound B-Mode Scans". IEEE Trans. on Sonics and Ultrasonics, Vol. SU-25 No. 1, 1978.

19. J.G. Abott and F.L. Thurstone, "Acoustic Speckle: Theory and Experimental Analysis", Ultrasonic Imaging, Vol. 1, pp. 303-324, 1979.

20. D.L. Parker and T.A. Pryor, "Analysis of B-Scan Speckle Reduction by Resolution Limited Filtering", Ultrasonic Imaging 4, 108-125, (1982).

21. P.N.T. Wells and M. Halliwell, "Speckle in Ultrasonic Imaging", Ultrasonics, Vol. 19, pp. 225-229, 1981.

22. P.A. Magnin, O.T. von Romm, and F.L. Thurstone," Frequency Compounding for Speckle Reduction in Phased Array Imaging", Ultrasonic Imaging, Vol. 4, pp. 267-281, 1982.

23. H.E. Melton, Jr. and P.A. Magnin, "A-Mode Speckle Reduction with Compound Frequencies and Compound Bandwidths.", Ultrasonic Imaging, Vol. 6, pp. 159-173, 1984.

24. M.S. Patterson and F.S. Foster, "The Improvement and Quantitative Assessment of B Mode Images Produced by Annular Array/Cone Hybrid", Ultrasonic Imaging, Vol. 5, pp. 195-213, 1983.

25. D.R. Foster, M. Ardity, F.S. Foster, M.S. Patterson and J.W. Hunt, "Computer Simulations of Speckle in B images", Ultrasonic Imaging, Vol. 5, pp. 308-330, 1983.

26. P.M. Morse and K.U. Ingard: Theoretical Acoustics, McGraw-Hill, 1968.

27. L.A. Chernow, "Wave Propagation in Random Medium", Dover, N.Y., 1960.

28. M.S. Patterson, F.S. Foster and D. Lee, "Sidelobe and Speckle Reduction for an Eight Sector Conical Scanner", IEEE Symposium on Sonics and Ultrasonics, pp. 632-637, 1981.

29. R.C. Chivers, Ultrasound Med. Biol. 4(4), 353-361 (1978).

30. R.C. Chivers, "The Scattering of Ultrasound by Human Tissues-Some Theoretical Models", Ultrasound Med. Biol. 3(1), pp. 1-13, 1977.

31. Ishimaru, "Wave Propagation and Scattering in Random Media", Vol. 1, Academic Press, N.Y. 1978.

32. J.M. Reid, "Scattering of Ultrasound by Tissue", Medical Physics of CT and Ultrasound, G.D. Fullerton and J.A. Zagzebski, eds., Amer. Inst. of Physics, pp. 388-408, 1980.

33. P. Backmann, "Probability in Communication Engineering", Havacourt, Brace and World, Inc. (1967).

34. A.J. Siegert and H. Goldstein, "Coherent and In-Coherent Scattering from Assemblies of Scatterers", App. B, in Propagation of Short Radio Waves (ed. D.E. Kerr), Vol. 13, MIT Radiation Lab Series, McGraw-Hill 1948.

35. V.P. Glotov, "Coherent and Scattering of Plane and Spherical Waves in Deep Sea Layers Containing Discrete Inhomogeneities", Soviet Physics Acoustics, Vol. 7 pp. 211-213, 1962.

36. V.P. Glotov, "Coherent Scattering of Sound from Clusters of Discrete Inhomogeneities in Pulsed Emission", Soviet Physics Acoustics, Vol. 8, pp. 220-222, 1963. Translated from Acousticheskii Zhournal, Vol. 8, No. 3, pp. 281-284, July September, 1962.

37. R. Nitzburg, "Constant False Alarm Rate Signal Processors for Several Types of Interference", IEEE Trans. AE Sys., Vol. 8 No. 1, 27-34, Jan. 1972.

38. V.G. Hansen and H.R. Ward, "Detection Performance of the LOG/CFAR Receiver", IEEE Trans. AE Sys., Vol. 8, 648-652, Sept. 1972.

39. M.W. Long, "Polarization and Statistical Properties of Clutter", Proceedings of the 1984 ISNCR in Radars and Imaging Systems, pp. 25-32.

40. J. Jellins, G. Kossof, T.S. Reeve, B.H. Barraclough, "Ultrasonic Grey Scale Visualization of Breast Disease", Ultrasound in Med. and Biol., Vol. I, pp. 393-404 (1975).

41. W.A. Draheim and E.S. Furgason, "A Two Dimensional Approach to Clutter Rejection in Ultrasonic Images," IEEE Symposium on Sonics and Ultrasonics, October 1983.

42. H.L. Van Trees, "Detection, Estimation and Modulation Theory," Part 1, John Wiley and Sons, New York, 1968.

43. L.L. Scharf and D.W. Lyte, "Signal Detection in Non Gaussian Noise of Unknown Level: an Invariance Application", IEEE Trans. Inf. Theory, Vol. 17, 404-411, July 1971.

44. G.R. Cooper, C.D. McGillem, "Digital Communications and Spread Spectrum", School of Electrical Engineering, Purdue University.

45. S.W. Flax, G.H Glover and N.J. Pelc, "Textural Variations in B Mode Ultrasonography: A Stochastic Model, "Ultrasonic Imaging Vol. 3, pp 235-257, 1981.

46. A. Papoulis, "Probability, Random Variables and Stochastic Processes New York: McGraw-Hill, 1965.

47. M.A. Wright, "Radar Simulation using Ultrasonics in Water". Ultrasonics International 1973 conference proceedings.

48. C. Helstrom, " Statistical Theory of Signal Detection", 1960.

49. A.D. Whalen, "Detection of Signals in Noise", 1971.

50. P. Swerling, "Probability of Detection for Fluctuating Targets" I.R.E. Trans. on Information Theory, Vol. IT6, No. 2, April 1960.

51. W.K. Pratt, "Digital Image Processing". John Wiley and Sons, 1978.

52. A. Rosenfeld, "Picture Processing by Computer, Academic Press, New York, 1969.

53. D.J. Ketcham, "Real Time Image Enhancement Technique", Proceeding SPIE/OSA conference on Image Processing, Pacific Grove, CA, Vol. 74, February 1976, 120-125.

54. E.G. Isherwood, "The Determination of the Detection Probability for a Group- Correlated Target Signal", The Marconi Review, Vol. 39, No. 202, Third Quarter 1976.

55. V.L. Newhouse and Israel Amir, "The Separation Of Coherent and Incoherent Echoes from Sub-Wavelength Scatterers". Presented at AIUM, N.Y. 1983

56. H.E. Melton, Jr., S.M. Collins and D.J. Skorton, "Automatic Real-Time Endocardial Edge Detection in Two-Dimensional Echocardiography", Ultrasonic Imaging Vol. 5, pp. 300-307, 1983.

57. C.M. Sehgal and J.F. Greenleaf, "Scattering of Ultrasound by Tissues", Ultrasonic Imaging, Vol., pp. 60-80 (1984).

58. P.D. Welch, "The Use of Fast Fourier Transform for the Estimation of Power Spectra: A method Based on Time Averaging Over Short, Modified Periodegrams", IEEE Trans. on Audio and Electroacoustics, Vol. AU-15, No. 2, June 1967.

59. N. Senapti, P.P. Lele and A. Woodin, "A study of the Scattering of Sub-Milimiter Ultrasound from Tissues and Organs", in Proc. IEEE Ultrasonics Symp., pp. 59-63, IEEE Cat. No. 72, New-York, 1972.

APPENDICES

APPENDIX A

It can be shown that for many different types of transmitted signal and receiver, the peak of the echo of a point target will not change its delay with respect to the transmit pulse, due to the process of splitting the received echo spectrum. We now demonstrate this for the case of a transmitted signal of Gaussian shape

$$g(t) = e^{-\frac{t^2}{2b^2}} \cos \omega_o t \tag{A1}$$

whose echo from a point target is passed through n filters with a Gaussian transfer function.

It is clear that the peak of g(t) will occur for t=0 (or for t=τ for a delayed version of g(t) for a target located at τ).

The Fourier Transform of g(t) is also Gaussian

$$G(\omega) = \sqrt{2\pi}\, b\left[e^{-\frac{b^2(\omega-\omega_o)^2}{2}} + e^{\frac{-b^2(\omega+\omega_o)^2}{2}}\right] \tag{A2}$$

The transfer function of the n^{th} Gaussian frequency window can be written as follows

$$H_n(\omega) = \sqrt{2\pi}\; b_n\left[e^{-\frac{b_n^2(\omega-\omega_n)^2}{2}} + e^{-\frac{b_n^2(\omega+\omega_n)^2}{2}}\right] \tag{A3}$$

Multiplying eqts. (A2) and (A3), assuming that the cross products are negligible (because the transfer function at zero frequency should be closely zero), we obtain the output spectrum of the n^{th} frequency window

$$G_n(\omega) = G(\omega)\cdot H_n(\omega) = A\left[e^{-\frac{b_n^{*2}}{2}(\omega-\omega_n^*)^2} + e^{-\frac{b_n^{*2}}{2}(\omega+\omega_n^*)^2} \right] \quad \text{(A4)}$$

where

$$b_n^{*2} = b^2 + b_n^2 \quad \text{(A5)}$$

$$\omega_n^* = \frac{\omega_o b^2 + \omega_n b_n^2}{b^2 + b_n^2} \quad \text{(A6)}$$

and A is a proportionality constant which is independent of ω.

As the output of the gaussian filters is Gaussian their inverse Fourier transforms will also be Gaussian with

$$g(t) = e^{-\frac{t^2}{2b_n^{*2}}} \cos \omega_n^* t \quad \text{(A7)}$$

and all the peaks will still be at t=0.

APPENDIX B

The Likelihood Ratio Test of the General Gaussian Problem

In this appendix we derive the Likelihood Ratio Test for the different cases analyzed in chapter 4 and 5. We follow here the derivation given in (19).

Let the set $\vec{r}_1,\ldots.\vec{r}_n$ be jointly Gaussian. If we define

$$\vec{r} = \begin{bmatrix} r_1 \\ \cdot \\ \cdot \\ \cdot \\ r_n \end{bmatrix} \quad E[\vec{r}] = \vec{m} = \begin{bmatrix} m_1 \\ \cdot \\ \cdot \\ \cdot \\ m_n \end{bmatrix} \tag{B1}$$

and

$$\text{cov}[\vec{r}] = E[(\vec{r}-\vec{m})(\vec{r}^T-\vec{m}^T)] = K \tag{B2}$$

Then one can show that

$$P_r(\vec{r}) = [(2\pi)^{\frac{n}{2}}|K|^{1/2}]^{-1} \exp[-\frac{1}{2}(\vec{r}^T-\vec{m}^T)K^{-1}(\vec{r}-\vec{m})] \tag{B3}$$

Under the first hypothesis H_1 we assume that $\vec{r}$ is specified by a mean vector and a covariance matrix. We denote

$$E[\vec{r}|H_1] = m_1 \tag{B4}$$

$$K_1 = E[(\vec{r}-\vec{m}_1)(\vec{r}^T-\vec{m}_1^T)|H_1] \tag{B5}$$

Likewise

$$E[\vec{r}|H_o] = \vec{m}_o \tag{B6}$$

$$K_o = E[(\vec{r}-\vec{m}_o)(\vec{r}^T-\vec{m}_o^T)|H_o] \tag{B7}$$

The likelihood ratio test becomes

$$L(\vec{r}) = \frac{P_r(\vec{r}|H_1)}{P_r(\vec{r}|H_o)} = \frac{|K_o|^{1/2}\exp[-\frac{1}{2}(\vec{r}^T-\vec{m}_1^T)K_1(\vec{r}-\vec{m}_1)]}{|K_o|^{1/2}\exp[-\frac{1}{2}(\vec{r}^T-\vec{m}_o^T)K_1(\vec{r}-\vec{m}_o)]} \underset{H_o}{\overset{H_1}{\gtrless}} \eta \tag{B8}$$

Taking the logarithm we get

$$\frac{1}{2}(\vec{r}^T-\vec{m}_o^T)K_o^{-1}(\vec{r}-\vec{m}_o) - \frac{1}{2}(\vec{r}^T-\vec{m}_o^T)K_1^{-1}(\vec{r}-\vec{m}_1) \underset{H_o}{\overset{H_1}{\gtrless}} \tag{B9}$$

$$\text{Ln } \eta + \frac{1}{2}\text{Ln}|K_1| - \frac{1}{2}\text{Ln}|K_o| = \gamma$$

Now the results used in chapter 4 and 5 can be obtained

1. Eq. 4.22

Corresponds to equal covariance matrices with $K_1=K_o=K$ and $m_o=0$. In this case the LRT becomes

$$L(\vec{r}) = \frac{1}{2}(\vec{r}^T K^{-1}\vec{r}) - \frac{1}{2}(\vec{r}^T-\vec{m}^T)K^{-1}(\vec{r}-\vec{m}_1) =$$

$$= \vec{m}_1^T K^{-1}\vec{r} - \frac{1}{2}\vec{m}_1^T K^{-1}\vec{m}_1 \tag{B10}$$

which becomes

$$\vec{m}_1^T K^{-1}\vec{r} \underset{H_o}{\overset{H_1}{\gtrless}} \gamma \tag{B11}$$

which is eq. 4.22

2. Eq. 4.25

Corresponds to independent components with equal variances. K_1 becomes diagonal and $K_o=kK_1$, $m_o=0$. In this case the LRT becomes

$$L(\vec{r}) = \frac{1}{2}\vec{r}^T k^{-1}K_1^{-1}\vec{r} - \frac{1}{2}(\vec{r}^T-\vec{m}_1^T)K_1(\vec{r}-\vec{m}_1) \tag{B12}$$

but

$$K_1 = \sigma^2 \begin{bmatrix} 1 & & 0 \\ & \ddots & \\ 0 & & 1 \end{bmatrix} \quad K_o = k\,\sigma^2 \begin{bmatrix} 1 & & 0 \\ & \ddots & \\ 0 & & 1 \end{bmatrix} \qquad \vec{m}_1 = m \begin{bmatrix} 1 \\ \vdots \\ 1 \end{bmatrix} \tag{B13}$$

so

$$\begin{aligned} L(\vec{r}) &= \frac{1}{2}r^T k^{-1}K_1^{-1}\vec{r} - \frac{1}{2}\vec{r}^T K_1^{-1}\vec{r} + \vec{m}^T K_1^{-1}\vec{r} \\ &= \frac{\sigma^2}{2k}\sum_{i=1}^{n} r_i^2 - \frac{\sigma^2}{2}\sum_{i=1}^{n} r_i^2 + \sigma^2 m \sum_{i=1}^{n} r_i \underset{H_o}{\overset{H_1}{\gtrless}} \gamma \end{aligned} \tag{B14}$$

σ^2 becomes a constant multiplier. Estimating $m=\frac{1}{n}\sum_{i=1}^{m} r_i$ we get

$$L(r) = \frac{1}{2}\sum_{i=1}^{n} r_i^2(1-K) + \frac{k}{m}\left(\sum_{i=1}^{n} r_i\right)^2 \tag{B15}$$

which is eq, 4.25

3. Eq. 5.3

Corresponds to $m_1=m_o=0$. The LRT becomes

$$L(\vec{r}) = \frac{1}{2}\vec{r}^T K_o^{-1}\vec{r} - \frac{1}{2}\vec{r}^T K_1^{-1}\vec{r} = \frac{1}{2}[\vec{r}^T(K_o^{-1}-K_1^{-1})\vec{r}] \tag{B16}$$

and eq. 5.3 follows

4. Eq. 5.2

Readily can be obtained by using

$$K_1 = \sigma_1^2 \begin{bmatrix} 1 & & 0 \\ & 1 & \\ & \ddots & \\ 0 & & 1 \end{bmatrix} \qquad K_o \sigma_o^2 \begin{bmatrix} 1 & & 0 \\ & 1 & \\ & \ddots & \\ 0 & & 1 \end{bmatrix} \tag{B17}$$

in eq. 5.3.

APPENDIX C

The Use of the Coherent Term for Attenuation Estimation

From chapter 3 the ratio between the coherent and incoherent terms for uniform concentration of scatterers in random media can be shown to be

$$F = \frac{\bar{\rho}^2 N \left| \int_V G(r,t)dv \right|^2}{\overline{\rho^2} \int_V |G(r,t)|^2 dv} \tag{C1}$$

The average power reflected from range delay t taking into account attenuation is

$$\overline{P(t)} = e^{-\alpha t}\left[N\overline{\rho^2}\int_V |G(r,t)|^2 dv + N^2\bar{\rho}^2 \left| \int_V G(r,t)dv \right|^2\right] \tag{C2}$$

The concentration N is calculated through eq. C1 and the evaluation of $\bar{\rho}$ and $\overline{\rho^2}$ is also possible. Measuring P(t) for 2 range delays t_1 and t_2 allows the estimation of the attenuation coefficient α.

$$\frac{\overline{P(t_2)}}{\overline{P(t_2)}} = e^{-\alpha\Delta t} \frac{N\overline{\rho^2}\int_V |G(r,t_1)|^2 dv + N^2\bar{\rho}^2 \left| \int_V G(r,t_1 dv \right|^2]}{N\overline{\rho^2}\int_V |G(r,t_2)|^2 dv + N^2\bar{\rho}^2 \left| \int_V G(r,t_2 dv \right|^2]}$$

$$= e^{-\alpha\Delta t} \cdot K \qquad t_2 - t_1 = \Delta t \tag{C3}$$

and the attenuation coefficient α becomes

$$\alpha = \frac{\mathrm{Ln}K[\overline{P(t_2)}/\overline{P(t_1)}]K}{\Delta t} \tag{C4}$$

For high scattering concentration and sharp field gradients only the second term in the denominator and numerator are left and eq. C4 becomes

$$\alpha = \frac{\mathrm{Ln}\left[\dfrac{\overline{|\int_V G(r,t_1)dv\ |^2}}{\overline{|\int_V G(r,t_2)dv\ |^2}} \cdot \dfrac{\overline{P(t_2)}}{\overline{P(t_1)}}\right]}{\Delta t} \qquad \text{(C5)}$$